Titre: Title:	Mimo Communication Systems with Reconfigurable Antennas
Auteur: Author:	Vida Vakilian
Date:	2014
Type:	Mémoire ou thèse / Dissertation or Thesis
Référence: Citation:	Vakilian, V. (2014). Mimo Communication Systems with Reconfigurable Antennas [Thèse de doctorat, École Polytechnique de Montréal]. PolyPublie. https://publications.polymtl.ca/1498/

URL de PolyPublie: PolyPublie URL:	https://publications.polymtl.ca/1498/
Directeurs de recherche: Advisors:	Jean-François Frigon, & Sébastien Roy
Programme: Program:	génie électrique

UNIVERSITÉ DE MONTRÉAL

MIMO COMMUNICATION SYSTEMS WITH RECONFIGURABLE ANTENNAS

VIDA VAKILIAN
DÉPARTEMENT DE GÉNIE ÉLECTRIQUE
ÉCOLE POLYTECHNIQUE DE MONTRÉAL

THÈSE PRÉSENTÉE EN VUE DE L'OBTENTION
DU DIPLÔME DE PHILOSOPHIÆ DOCTOR
(GÉNIE ÉLECTRIQUE)
JUIN 2014

UNIVERSITÉ DE MONTRÉAL

ÉCOLE POLYTECHNIQUE DE MONTRÉAL

Cette thèse intitulée :

MIMO COMMUNICATION SYSTEMS WITH RECONFIGURABLE ANTENNAS

présentée par : VAKILIAN Vida
en vue de l'obtention du diplôme de : Philosophiæ Doctor
a été dûment acceptée par le jury d'examen constitué de :

M. WU Ke, Ph.D., président
M. FRIGON Jean-François, Ph.D., membre et directeur de recherche
M. ROY Sébastien, Ph.D., membre et codirecteur de recherche
M. CARDINAL Christian, Ph.D., membre
M. SHAYAN Yousef R., Ph.D., membre

ACKNOWLEDGEMENTS

First and foremost, I would like to express my sincere gratitude to my advisor Prof. Jean-François Frigon for his support, guidance and depth of knowledge. His insightful comments and suggestions have helped me to advance my research and improve the quality of this dissertation. I would also like to thank my co-adviser Prof. Sébastien Roy for his valuable feedback and advice throughout this research. My sincere thanks goes to my supervisors at Alcatel-Lucent, Dr. Thorsten Wild and Dr. Stephan Ten Brink who gave me an opportunity to have my internship with their research group and work on diverse exciting projects. I also thank Prof. Zhi Ding, my internship supervisor at University of California, Davis. I especially thank Dr. Shahrokh Nayeb Nazar and Dr. Afshin Haghighat for their support, guidance and supervision during my work at InterDigital Communications. I would also like to express gratitude to the members of my dissertation committee, Prof. Ke Wu, Prof. Yousef R. Shayan and Prof. Christian Cardinal for their valuable time and constructive feedback.

I have also learned from my interactions with some very talented friends, Diego Perea-Vega, Arash Azarfar, Mohammad Torabi, Ali Torabi, Xingliang Li and Mohamed Jihed Gafsi. I am also forever indebted to my parents for their love and support. They have given me everything they could, and they have been encouraging me to make my own decisions throughout my life. Lastly, and most importantly, I would like to thank my husband and best friend, Reza Abdolee. He was always there cheering me up and stood by me through the up's and down's of my life.

Here, I acknowledge that this research would not have been possible without: a) research assistantship from Prof. Jean-François Frigon via Fonds Québécois de la Recherche sur la Nature et les Technologies (FQRNT), b) Supplementary scholarships from Regroupement Stratégique en Microsystème du Québec (ReSMiQ) c) An internship award from Centre de Recherche en Electronique Radiofréquence (CREER), and d) An international Research Internship in Science and Engineering (RISE) award from German Academic Exchange Service (DAAD). I would like to express my gratitude to all those individuals and agencies for their support.

RÉSUMÉ

Les antennes reconfigurables sont capables d'ajuster dynamiquement les caractéristiques de leur diagramme de rayonnement, par exemple, la forme, la direction et la polarisation, en réponse aux conditions environnementales et exigences du système. Ces antennes peuvent aussi être utilisées en conjonction avec des système à entrées multiples sorties multiples (MIMO) pour améliorer davantage la capacité et la fiabilité des systèmes sans fil. Cette thèse étudie certains des problèmes dans les systèmes sans fil équipés d'antennes reconfigurables et propose des solutions pour améliorer la performance du système.

Dans les systèmes sans fil utilisant des antennes reconfigurables, la performance atteignable par le système dépend fortement de la connaissance de la direction d'arrivée (DoA) des signaux souhaités et des interférences. Dans la première partie de cette thèse, nous proposons un nouvel algorithme d'estimation de la DoA pour les système à entrée simple et sortie simple (SISO) qui possèdent un élément d'antenne reconfigurable au niveau du récepteur. Contrairement à un système utilisant un réseau d'antennes conventionnelles à diagramme de rayonnement fixe, où la DoA est estimée en utilisant les signaux reçus par plusieurs éléments, dans le réseau d'antennes avec l'algorithme proposé, la DoA est estimée en utilisant des signaux reçus d'un élément d'antenne unique pendant qu'il balai un ensemble de configurations de diagramme de rayonnement. Nous étudions aussi l'impact des différentes caractéristiques des diagrammes de rayonnement utilisés, tels que la largeur du faisceau de l'antenne et le nombre d'étapes de numérisation, sur l'exactitude de la DoA estimée.

Dans la deuxième partie de cette thèse, nous proposons un système de MIMO faible complexité employant des antennes reconfigurables sur les canaux sélectifs en fréquence pour atténuer les effets de trajets multiples et donc éliminer l'interférence entre symboles sans utiliser la technique de modulation multiplexage orthogonale fréquentiel (OFDM). Nous étudions aussi l'impact de la propagation et de l'antenne angulaire largeur de faisceau sur la performance du système proposé et faire la comparaison avec la performance du système MIMO-OFDM.

Dans la troisième partie de cette thèse, nous fournissons des outils analytiques pour analyser la performance des systèmes sans fil MIMO équipés d'antennes reconfigurables au niveau du récepteur. Nous dérivons d'abord des expressions analytiques pour le calcul de la matrice de covariance des coefficients des signaux reçus empiétant sur un réseau d'antennes reconfigurables en tenant compte de plusieurs caractéristiques de l'antenne tels que la largeur du faisceau, l'espacement d'antenne, l'angle de pointage ainsi que le gain de l'antenne. Dans cette partie, nous considérons un récepteur MIMO reconfigurable où le diagramme de rayonnement

de chaque élément d'antenne dans le réseau peut avoir des caractéristiques différentes. Nous étudions également la capacité d'un système MIMO reconfigurable en utilisant les expressions analytiques dérivées.

Dans la dernière partie de la thèse, nous proposons une nouvelle technique de codage du bloc tri-dimensionelle pour les systèmes reconfigurable MIMO-OFDM qui tirent partie des caractéristiques de l'antenne reconfigurables pour améliorer la diversité de système sans fil et de la performance. Le code en bloc proposé est capable d'extraire de multiple gains de diversité, y compris spatiale, en fréquence et de diagramme de rayonnement. Afin d'obtenir la diversité de diagramme de rayonnement, nous configurons chaque élément d'antenne d'émission pour basculer indépendamment son diagramme de rayonnement dans les directions sélectionnées en fonction de différents critères d'optimisation ; par exemple, la réduction de la corrélation entre les différents états de rayonnement ou l'augmentation de la puissance reçue. Le code en bloc quasi orthogonale proposé, qui est de taux unitaire et qui bénéficie de trois types de diversité, améliore sensiblement les performances d'erreur binaire (BER) des systèmes MIMO.

ABSTRACT

Reconfigurable antennas are able to dynamically adjust their radiation pattern characteristics, e.g., shape, direction and polarization, in response to environmental conditions and system requirements. These antennas can be used in conjunction with multiple-input multiple-output (MIMO) systems to further enhance the capacity and reliability of wireless networks. This dissertation studies some of the issues in wireless cellular systems equipped with reconfigurable antennas and offer solutions to enhance their performance.

In wireless systems employing reconfigurable antennas, the attainable performance improvement highly depends on the knowledge of direction-of-arrival (DoA) of the desired source signals and that of the interferences. In the first part of this dissertation, we propose a novel DoA estimation algorithm for single-input single-output (SISO) system with a reconfigurable antenna element at the receiver. Unlike a conventional antenna array system with fixed radiation pattern where the DoA is estimated using the signals received by multiple elements, in the proposed algorithm, we estimate the DoA using signals collected from a set of radiation pattern states also called scanning steps. We, in addition, investigate the impact of different radiation pattern characteristics such as antenna beamwidth and number of scanning steps on the accuracy of the estimated DoA.

In the second part of this dissertation, we propose a low-complexity MIMO system employing reconfigurable antennas over the frequency-selective channels to mitigate multipath effects and therefore remove inter symbol interference without using orthogonal frequency-division multiplexing (OFDM) modulation. We study the impact of angular spread and antenna beamwidth on the performance of the proposed system and make comparisons with that of MIMO-OFDM system equipped with omnidirectional antennas.

In the third part of this dissertation, we provide an analytical tool to analyze the performance of MIMO wireless systems equipped with reconfigurable antennas at the receiver. We first derive analytical expressions for computing the covariance matrix coefficients of the received signals impinging on a reconfigurable antenna array by taking into account several antenna characteristics such as beamwidth, antenna spacing, antenna pointing angle, and antenna gain. In this part, we consider a reconfigurable MIMO receiver where the radiation pattern of each antenna element in the array can have different characteristics. We, additionally, study the capacity of a reconfigurable MIMO system using the derived analytical expressions.

In the last part of the dissertation, we propose a novel three dimensional block coding technique for reconfigurable MIMO-OFDM systems which takes advantage of the reconfigurable

antenna features to enhance the wireless system diversity and performance. The proposed block code achieves multiple diversity gains, including, spatial, frequency, and state by transmitting a block code over multiple transmit antennas, OFDM tones, and radiation states. To obtain the state diversity, we configure each transmit antenna to independently switch its radiation pattern to a direction that can be selected according to different optimization criteria, e.g., minimization of the correlation among different radiation states. The proposed code is full rate and benefits from three types of diversity, which substanttially improves the bit-error-rate (BER) performance of the MIMO systems.

TABLE OF CONTENTS

LIST OF TABLES

LIST OF FIGURES

LIST OF APPENDICES

LIST OF ACRONYMS

3GPP	Third Generation Partnership Project
BER	Bit-Error Rate
BS	Base Station
AWGN	Additive White Gaussian Noise
IDFT	Inverse Discrete Fourier Transform
IFFT	Inverse Fast Fourier Transform
i.i.d	independent and identically distributed
CCI	Co-Channel Interference
CoMP	Coordinated Multi-Point
CSI	Channel State Information
EVD	Eigenvalue Decomposition
LTE	Long Term Evolution
MIMO	Multiple-Input Multiple-Output
MMSE	Minimum Mean Square Error
RMSE	Root-Mean-Square Error
MSE	Mean Square Error
OFDM	Orthogonal Frequency Division Multiplexing
QoS	Quality-of-Service
RF	Radio Frequency
SER	Symbol-Error Rate
SINR	Signal-to-Interference plus Noise Ratio
SISO	Single-Input Single-Output
SNR	Signal-to-Noise Ratio
SVD	Singular Value Decomposition
WLAN	Wireless Local Area Network
DoA	Direction-of-Arrival
MEMS	Microelectromechanical Systems
FET	Field-Effect transistor
MVDL	Minimum Variance Distortionless Look
MUSIC	MUltiple Signal Classification
ESPAR	Electronically Steerable Passive Array Radiator
ORIOL	Octagonal Recongurable Isolated Orthogonal Element
CRLH-LWA	Composite Right/Left Handed Leaky-Wave Antenna

ULA	Uniform Linear Arrays
PAS	Power Azimuth Spectrum
STS-BC	Space-Time State Block Coding
OSTBC	Orthogonal Space-Time Block Code
QOSTBC	Quasi-Orthogonal Space Time Block Code
PDF	Probability Density Function
w.l.o.g.	without loss of generality
w.r.t.	with respect to

NOTATIONS

$(\cdot)^T$	Transpose
$(\cdot)^*$	Conjugate
$(\cdot)^H$	Conjugate transpose
$\det(\cdot)$	Determinant operation
$\lfloor \cdot \rfloor$	Floor operation
$\mathbf{I}_N$	Identity matrix of dimensions N
$\otimes$	Kronecker product of two matrices
$\text{diag}\{\mathbf{A}_1, \cdots, \mathbf{A}_n\}$	The block diagonal matrix with diagonal blocks $\mathbf{A}_1, \cdots, \mathbf{A}_n$
$\text{col}\{\cdot\}$	stacks up the matrices on top of each other

CHAPTER 1

Introduction

The next generation of wireless communication systems are expected to provide higher data rates and better quality of services to a large number of users in response to their growing demand for voice, data, and multimedia applications. To fulfill these demands, multiple-input multiple-output (MIMO) antenna systems have been proposed, where multiple data streams or codewords can be transmitted simultaneously. Although MIMO systems are capable of providing the expected data rates theoretically, due to spatial correlation between antennas this is not always achievable in practice. Over the past few years, studies have revealed that reconfigurable antennas offer a promising solution to overcome this problem [1–11]. In a reconfigurable antenna system, the characteristics of each antenna radiation pattern (e.g., shape, direction and polarization) can be changed by placing switching devices such as microelectromechanical systems (MEMS), varactor diodes, or field-effect transistor (FET) within the antenna structure [12–14]. As a result, a system employing reconfigurable antennas is able to alter the propagation characteristics of the wireless channel into a form that leads to signal decorrelation and hence the better system performance. Moreover, by designing a proper coding technique, reconfigurable antenna systems are able to achieve an additional diversity gain that can further improve the performance of wireless communication systems. This type of antennas can have different applications in communication field, including mobile and cellular systems, radar, and satellite communication. As an example, these antennas can be used in the 802.11ad standard for 60 GHz wireless gigabit networks, where a directional multi-gigabit beamforming protocol enables the transmitter and receiver to configure the antenna radiation patterns in real-time [15]. In communication systems, an array of antenna elements can be replaced by a single reconfigurable antenna for beamforming and beam steering purposes. Thereby overall size, cost, and complexity of the system can be significantly reduced.

1.1 Objectives and Contributions

The overall objective of this dissertation is to evaluate the performance of wireless systems equipped with reconfigurable antennas and propose new methods and algorithms to improve their performance. To be more specific, in this dissertation, we first aim to develop a DoA estimation algorithm that is able to estimate the DoA of the signals arriving at a

single reconfigurable antenna. We then use the estimated DoA to configure the antenna radiation pattern and compute the covariance matrix coefficients of the impinging signals at the reconfigurable antenna array for this configuration. Considering the computed received covariance coefficients, we select the optimal configuration for the antenna elements in the array at the receiver side in order to maximize the system capacity. Finally, we propose a new space-frequency-state block codes that can extract the maximum diversity gain for a system equipped with reconfigurable antennas in frequency selective fading channels. Fig. 1.1 shows the flow of the works in this dissertation and describe the connection between the aforementioned objectives.

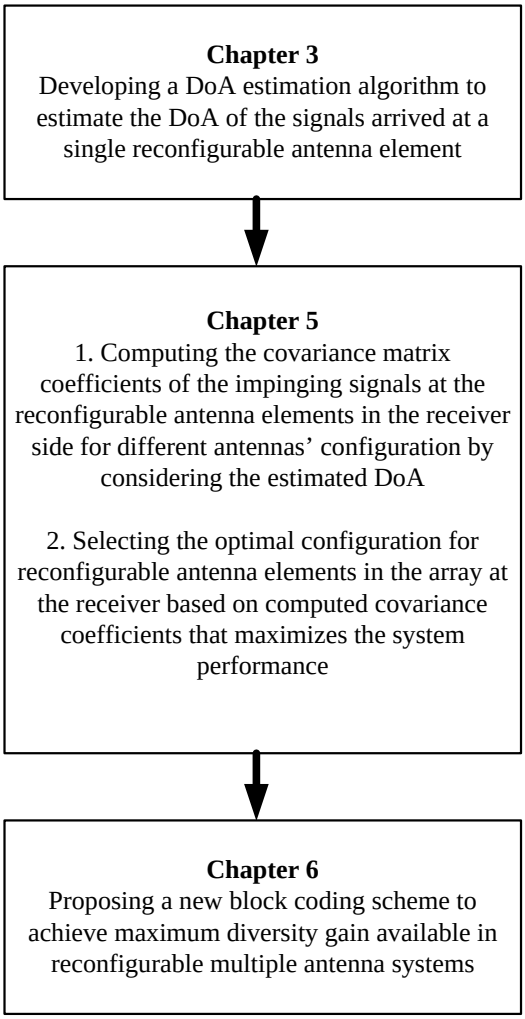

Figure 1.1 Flow of the main works of this dissertation

Below, we discuss the main contributions of this dissertation.

- **DoA estimation algorithm for a single-element reconfigurable antenna system:**
  We develop a DoA estimation algorithm that estimates the DoA using the signal samples collected at different scanning steps corresponding to different radiation angles. We measure the performance of the developed algorithm using an actual reconfigurable antenna called CRLH-LWA in an anechoic chamber. Moreover, we evaluate the performance of the DoA estimation algorithm in a clustered channel model. We also study the impact of DoA estimation error on the BER performance of reconfigurable SISO systems. This contribution has appeard in [16–18].
- **Performance evaluation of reconfigurable MIMO systems in spatially correlated frequency-selective fading channels:**
  We propose to use reconfigurable antennas in MIMO systems over frequency-selective channels in order to mitigate multipath effects and therefore remove inter symbol interference (ISI) without using OFDM modulation technique. In the reconfigurable MIMO system, each element in the MIMO array is able to dynamically change its beam direction in a continuous manner. By integrating of these elements into an array, we can have a system in which the elements steer their beams toward the selected clusters and mitigate the signals coming from the undesired ones. As a result, the ISI can be effectively suppressed. This contribution has appeared in [11].
- **Closed-form expressions of covariance matrix coefficients of the signals impinged at a reconfigurable antenna array:**
  We derive analytical expressions of the covariance matrix coefficients by taking into account several antenna characteristics such as beamwidth, antenna spacing, antenna pointing angle, and antenna gain. Unlike computing intensive numerical integrations to directly evaluate the covariance matrix coefficients, the derived analytical expressions converge rapidly and can be used, for example, in real-time wireless system implementations to quickly choose the optimal configuration for each reconfigurable antenna element in the array, leading to significant performance improvement. Using the derived expressions for covariance coefficients, we analyze the capacity of reconfigurable MIMO systems and discuss its relation with the antennas radiation pattern configuration and channel power angular spectrum characteristics. This contribution has appeared in [19].
- **Space-Frequency-State block coding scheme for reconfigurable MIMO-OFDM communication systems.**
  We propose a novel coding scheme for reconfigurable MIMO-OFDM systems that achieves multiple diversity gains, including, space, frequency, and state. We construct our proposed code based on the fundamental concept of rotated quasi-orthogonal space-

time block codes (QOSTBC). By using the rotated QOSTBC, the proposed coding structure provides rate-one transmission (i.e., one symbol per frequency subcarrier per radiation state) and leads to a simpler maximum likelihood (ML) decoder. In order to obtain state diversity, we configure each transmit antenna element to independently switch its radiation pattern to a direction that can be selected according to different optimization criteria, e.g., to minimize the correlation among different radiation states. Moreover, we derive the maximum achievable level of diversity offered by reconfigurable MIMO-OFDM systems with reconfigurable antennas at the transmitter. We also discuss about the optimal rotation angles for the proposed coding scheme that guarantee full-diversity and maximum coding gain. This contribution has appeared in [20] and a journal paper on this topic has been submitted to IEEE Transactions on Wireless Communications.

1.2 Outline of the Dissertation

In the following, we introduces the basic organization of the dissertation.

In Chapter 2, we provide a synthesis review of the literature on the work related to the thesis's objectives. We also present some related background material that will be used throughout this dissertation, including reconfigurable antennas, different diversity techniques, reconfigurable channel model, space-time block coding, space-frequency coding for MIMO-OFDM systems and space-switching schemes for transmitter-reconfigurable MIMO systems.

In Chapter 3, we introduce a direction-of-arrival (DoA) estimation algorithm for a single-element reconfigurable antenna system. We also study the impact of DoA estimation error on the error rate performance of reconfigurable antenna systems.

In Chapter 4, we propose to use reconfigurable antennas in MIMO systems over frequency-selective fading channels in order to mitigate multipath effects and therefore remove inter symbol interference without using OFDM modulation technique. We also compare the performance of the reconfigurable MIMO system with conventional MIMO-OFDM system in the spatial clustered channel model that takes into account the impact of the physical parameters of wireless channels.

In Chapter 5, we derive closed-form expressions for computing covariance matrix coefficients of reconfigurable MIMO systems, which can be used in real-time wireless implementation to quickly choose the optimal configuration for each reconfigurable antenna element in the MIMO array. Moreover, in Chapter 5, we analyze the capacity of reconfigurable MIMO system using the derived close-form expressions.

In Chapter 6, we first present a system model for reconfigurable MIMO-OFDM systems in

frequency-selective wireless channels. Then, we introduce space-frequency-state block codes for reconfigurable MIMO-OFDM systems that enables the system to transmit codewords across three dimensions. We also derive the maximum diversity and coding gains offered by the proposed codes in reconfigurable MIMO-OFDM systems. Finally, we compare the performance of the proposed coding scheme with the existing space-frequency codes for MIMO-OFDM systems.

CHAPTER 2

Literature review

In this chapter, we first provide a synthesis review of the work available in the literature related to the thesis's objectives. We then present some related background material that will be used throughout this dissertation, including reconfigurable antennas, different diversity techniques, coding techniques for MIMO systems, reconfigurable MIMO systems and coding techniques for reconfigurable MIMO systems.

2.1 Related Works

One way to improve the system performance in a reconfigurable antenna system is to steer the antennas' radiation pattern toward the desired users and place nulls toward the interferences. In such systems, the attainable performance improvement of the system highly depends on the knowledge of the direction-of-arrival (DoA) of the desired source signal and the interference signals. Therefore, DoA estimation plays a key role in wireless communication systems equipped with reconfigurable antennas.

DoA estimation problem in conventional antenna array systems with fixed radiation pattern has been extensively studied in the literature. One of the most well-known DoA estimation technique is the multiple signal classification (MUSIC) algorithm that works based on the eigenvalue decomposition of the signal covariance matrix [21]. The performance of this algorithm is significantly impacted by different array characteristics, such as number of elements, array geometry, and mutual coupling between the elements [22]. These issues can be avoided if a single reconfigurable antenna element capable of beam-forming/steering is employed instead of an array. Nevertheless, the classical MUSIC algorithm developed for antenna array systems is not immediately applicable for this type of antenna. Several modified MUSIC DoA estimation algorithms have been proposed for reconfigurable antennas. In [23], the reactance-domain MUSIC algorithm was proposed for the electronically steerable passive array radiator (ESPAR) antenna which utilizes a single central radiator surrounded with parasitic elements. A similar work for DoA estimation has been also reported in [24] that uses a modified MUSIC algorithm for a two-port composite right/left handed (CRLH) leaky-wave antenna (LWA) [25]. In the first part of this dissertation, we focus on developing a DoA estimation algorithm for a single port reconfigurable antenna and investigating the effect of different antenna parameters on the performance of the developed algorithm.

Similar to conventional MIMO wireless systems, the performance of reconfigurable MIMO is affected by the correlation between the signals impinging on the antenna elements [26]. The correlation coefficients depend on several factors, including the signal spatial distribution, the antenna array topology and the radiation pattern characteristics of each element in the array. In general, these coefficients are computed using two main approaches, namely, numerical and analytical solutions. Works in the first category focus on finding the signal correlation through numerical schemes (e.g., numerical integrations and Monte-Carlo simulations) which are computationally intensive and need long processing time to obtain the solutions [27–32]. In contrast, analytical expressions are computationally more reliable and require shorter processing time. The authors in [33] derived exact expressions to compute the spatial correlation coefficients for uniform linear arrays (ULA) with different spatial distribution assumptions on signal angles of arrival/departure. A similar work was conducted in [34], where the authors proposed closed-form expressions of the spatial correlation matrix in clustered MIMO channels. These works have considered omni-directional antenna elements in their derivation and consequently overlooked the antenna radiation pattern characteristics. In [35], the authors derived an analytical correlation expression for directive antennas with a multimodal truncated Laplacian power azimuth spectrum (PAS). In their analysis, however, they have only considered identical fixed directive radiation patterns for all elements. In the second part of this dissertation, we therefore derive analytical expressions for computing the covariance matrix coefficients of the received signals impinging on a reconfigurable antenna array where the radiation pattern of each antenna element in the array can have different characteristics. We also use those results to analyze the performance of MIMO wireless systems equipped with reconfigurable antennas.

There are several works in the literature on designing efficient codes for reconfigurable MIMO systems in order to take advantage of the antenna reconfigurability. In [6], authors have proposed a MIMO system equipped with reconfigurable antennas at the receiver that can achieve a diversity order equal to the product of the number of transmit antennas, the number of receive antennas and the number of reconfigurable states of the receive antennas. They have shown that this diversity gain is achievable only under certain channel propagation conditions and using an appropriate coding technique. Later on, in [36] the authors extended the concept by using reconfigurable elements at both transmitter and receiver sides. In their work, they have introduced a state-switching transmission scheme, called space-time-state block coding (STS-BC), to further utilize the available diversity in the system over flat fading wireless channels. However, their coding scheme does not exploit the frequency diversity offered by the multipath propagation channels between each transmit and receive antenna pair. To obtain frequency diversity in multipath environment, a space-frequency (SF) block

code was first proposed by the authors in [37], where they used the existing space-time (ST) coding concept and constructed the code in frequency domain. Later works [38–43] also used similar strategies to develop SF codes for MIMO-orthogonal frequency division multiplexing (MIMO-OFDM) systems. However, the resulting SF codes achieved only spatial diversity, and they were not able to obtain both spatial and frequency diversities. To address this problem, a subcarrier grouping method has been proposed in [44] to further enhance the diversity gain while reducing the receiver complexity. In [45], a repetition mapping technique has been proposed that obtains full-diversity in frequency-selective fading channels. Although their proposed technique achieves full-diversity order, it does not guarantee full coding rate. Subsequently, a block coding technique that offers full-diversity and full coding rate was derived [46,47]. However, the SF codes proposed in the above studies and other similar works on the topic are not able to exploit the state diversity available in reconfigurable multiple antenna systems. In the last part of the dissertation, we propose a novel three dimensional block coding scheme for reconfigurable MIMO-OFDM systems which is full rate and benefits from three types of diversity, including, spatial, frequency, and state.

2.2 Background Study

2.2.1 Fading

Multipath causes fading due to constructive and destructive interference of the transmitted waves through different reflexions. In a fading channel, typical errors are mostly due to the channel being in deep fade rather than the noise being large. If no line-of-sight (LOS) component exists, the envelope of the received signal follows a Rayleigh distribution given by [48]

$$f_R(r) = \frac{r}{\sigma^2}\exp\big(\frac{-r^2}{2\sigma^2}\big),\ r \geq 0 \tag{2.1}$$

On the other hand, if a LOS between the transmitter and the receiver exists, then the distribution of the envelope is given by a Ricean distribution [49],

$$f_R(r) = \frac{r}{\sigma^2}\exp\big(\frac{-(r^2+D^2)}{2\sigma^2}\big)I_0\big(\frac{Dr}{\sigma^2}\big),\ r, D \geq 0 \tag{2.2}$$

where D is the amplitude of the dominant LOS component and I_0 is the modified Bessel function of the first kind of order zero.

2.2.2 Diversity Gain

In wireless communication systems, to combat the effects of fading and thereby improve link reliability, various diversity techniques have been proposed [50–52]. Wireless communication channels offer various diversity resources such as: spatial diversity, time diversity, frequency diversity, polarization diversity and pattern diversity.

- **Spatial Diversity**
  Spatial diversity is the most widely implemented form of diversity technique which can be used to mitigate the effects of fading by providing the receiver several replicas of the transmitted signal received at different antenna positions experiencing different fading conditions. Therefore, the probability that all paths will undergo the same amount of fading, or even deep-fades, is reduced to a great extent.
- **Time Diversity**
  In time diversity, multiple versions of the signal are transmitted at different time instants which are experiencing different fading conditions. Time diversity can be achieved by interleaving and coding over different time slots that are separated by the coherence time of the channel.
- **Frequency Diversity**
  Frequency diversity offered by the frequency selective multipath fading channel and can be obtained by spreading the code symbols across multiple frequency carriers that are separated by the coherence bandwidth of the channel.
- **Polarization Diversity**
  Polarization diversity is achieved by receiving the signals on orthogonally polarized waves. The benefits of polarization diversity include the ability to locate the antennas in the same place, unlike spatial diversity.
- **Pattern Diversity**
  Pattern diversity exploits the difference in radiation pattern between the array elements to decorrelate the sub-channels of the communication link [53–55]. This technique helps to achieve independent fading by transmitting/receiving over different signal paths at each antenna depending on the selected radiation pattern. Pattern diversity is a promising solution for systems such as laptops and handsets where the array size is a constraint.

2.2.3 Coding Techniques for MIMO Systems

In this section, we give an overview of the various emerging coding techniques developed for MIMO communication systems, including orthogonal and quasi-orthogonal space-time

block coding techniques.

Orthogonal Space-Time Block Codes

Space-time block code (STBC) is a technique used in wireless communications to transmit a copy of a data stream in a number of antennas and over multiple time slots. STBC was first introduced by Alamouti [50]. It provides rate-one and full-diversity and also has a simple maximum-likelihood decoder structure, where the transmitted symbols can be decoded independently of one another. Thus, the decoding complexity increases linearly, not exponentially, with the code size. The Alamouti structure for two transmit antennas is given by

$$\mathbf{A}\big(x_1, x_2\big) = \begin{bmatrix} x_1 & x_2 \\ -x_2^* & x_1^* \end{bmatrix}, \tag{2.3}$$

where x_1 and x_2 are indeterminate variables representing the signals to transmit. The Alamouti code was generalized to orthogonal designs by Tarokh [56]. The orthogonal space-time block codes (OSTBC) for more than two transmit antennas, can provide full-diversity transmission with linear decoding complexity but are not able to provide rate-one coding due to their orthogonal structure constraint.

Quasi-Orthogonal Space-Time Block Codes

For more than two transmit antennas, OSTBC can not provide rate-one transmission. To achieve rate one transmission, a new class of STBC's referred to as quasi-orthogonal space-time block codes structures were first introduced in [57]. Quasi-orthogonal designs provide rate-one codes and pairwise ML decoding but fail to achieve full-diversity. The full-diversity gain can however be achieved through appropriate constellation rotation [58–60]. A rotated QOSTBC provides both full diversity and rate-one transmission and performs better compared to OSTBC. In [57], the following QOSTBC structure has been proposed for the indeterminate variables x_1 , x_2 , x_3 and x_4

$$\mathbf{C}_4\big(x_1, x_2, x_3, x_4\big) = \begin{bmatrix} \mathbf{A}\big(x_1, x_2\big) & \mathbf{A}\big(x_3, x_4\big) \\ -\mathbf{A}^*\big(x_3, x_4\big) & \mathbf{A}^*\big(x_1, x_2\big) \end{bmatrix}, \tag{2.4}$$

where $\mathbf{A}\big(x_i, x_j\big)$ is given in (2.3). In a rotated QOSTBC, half the symbols are chosen from a rotated constellation to provide full-diversity. The rotation angle is chosen such that the coding gain is maximized. The optimal rotation angle for BPSK, QPSK, 8-PSK and QAM are $\pi/2, \pi/4, \pi/8$ and $\pi/4$, respectively. In general, the ML decoding for rotated QOSTBC's

is performed for two complex symbols (pair-wise ML decoding).

2.2.4 Reconfigurable MIMO Systems

MIMO communication systems can significantly improve the wireless communication performance in rich scattering environments, however, in practice, placing multiple antennas in handset or portable wireless devices may not be possible due to space and cost constraints. To overcome this limitation, reconfigurable antennas can be a promising solution to improve the performance of MIMO communication systems, especially in environments where it is difficult to obtain enough signal decorrelation with conventional means (spatial separation of antennas, polarization, etc.). Unlike conventional antenna elements in MIMO systems, which have a fixed radiation characteristic, the reconfigurable antenna element in reconfigurable MIMO systems has the capability of changing its characteristics such as operating frequency, polarization and radiation patterns. Therefore, using this type of antenna in wireless communication systems can enhance their performance by adding an additional degree of freedom which can be obtained by changing the characteristics of the wireless propagation channels. Generally, reconfigurable antennas are divided into three categories including frequency, polarization and radiation pattern reconfigurable antennas. Many innovative reconfigurable antennas have been proposed in recent years such as composite right/left-handed leaky-wave antenna, electronically steerable parasitic array radiator [61], switchable MEMS antennas such as PIXEL antenna [62], octagonal reconfigurable isolated orthogonal element (ORIOL) antenna [63]. Reconfigurable antennas have been used to yield diversity gain in SISO systems [64], [12] and also have been suggested for MIMO systems [1, 2, 4].

2.2.5 Coding Techniques for Reconfigurable MIMO Systems

In this section, we introduce a block coding technique proposed in [36] for reconfigurable MIMO systems which is capable of achieving maximum spatial and state diversity gains by coding across three dimensions: space, time and channel propagation state.

Space-Time-State Block Code

Consider a reconfigurable MIMO system with M_t transmit antennas and M_r receive antennas. In this system, in each channel propagation state, the input bit stream is mapped to the baseband modulation symbol matrices, $\mathbf{C}_p \in \mathcal{C}^{T \times M_t}$, where T denotes the duration of each constellation matrix in time. The overall space-time-state (STS) codeword for all P

channel propagation states, $\mathbf{C} \in \mathcal{C}^{PT \times PM_t}$, is given by

$$\mathbf{C} = \begin{bmatrix} \mathbf{C}_1 & \mathbf{0} & \cdots & \mathbf{0} \\ \mathbf{0} & \mathbf{C}_2 & \cdots & \mathbf{0} \\ \vdots & \vdots & \ddots & \vdots \\ \mathbf{0} & \mathbf{0} & \cdots & \mathbf{C}_P \end{bmatrix}, \tag{2.5}$$

where $\mathbf{C}_p \in \mathcal{C}^{T \times M_t}$ is the codeword transmitted during the p-th channel propagation state. Then, the received signal, $\mathbf{Y}_p \in \mathcal{C}^{T \times M_r}$, during the p-th channel propagation states can be written as

$$\mathbf{Y}_p = \mathbf{C}_p \mathbf{H}_p + \mathbf{N}_p, \tag{2.6}$$

where $\mathbf{H}_p \in \mathcal{C}^{M_t \times M_r}$ is the channel matrix and $\mathbf{N}_p \in \mathcal{C}^{T \times M_r}$ is a zero-mean Gaussian noise matrix during the p-th state. The received signal matrix, $\mathbf{Y} \in \mathcal{C}^{PT \times M_r}$, over all radiation states is given by

$$\mathbf{Y} = \mathbf{C}\mathbf{H} + \mathbf{N}, \tag{2.7}$$

where

$$\begin{aligned} \mathbf{Y} &= \begin{bmatrix} \mathbf{Y}_1^T & \mathbf{Y}_2^T & \cdots & \mathbf{Y}_P^T \end{bmatrix}^T, \\ \mathbf{H} &= \begin{bmatrix} \mathbf{H}_1^T & \mathbf{H}_2^T & \cdots & \mathbf{H}_P^T \end{bmatrix}^T, \\ \mathbf{N} &= \begin{bmatrix} \mathbf{N}_1^T & \mathbf{N}_2^T & \cdots & \mathbf{N}_P^T \end{bmatrix}^T, \end{aligned}$$

For $M_t = 2$, the STS codeword defined in 2.5 can be written as

$$\mathbf{C} = \frac{1}{\sqrt{2P}} \begin{bmatrix} \mathbf{A}\big(\mathcal{S}_1, \mathcal{S}_2\big) & \mathbf{0} & \cdots & \mathbf{0} \\ \mathbf{0} & \mathbf{A}\big(\mathcal{S}_3, \mathcal{S}_4\big) & \cdots & \mathbf{0} \\ \vdots & \vdots & \ddots & \vdots \\ \mathbf{0} & \mathbf{0} & \cdots & \mathbf{A}\big(\mathcal{S}_{2P-1}, \mathcal{S}_{2P}\big) \end{bmatrix}, \tag{2.8}$$

where, $\mathbf{A}\big(\mathcal{S}_{2p-1}, \mathcal{S}_{2p}\big)$ for $p \in \{1, 2, \cdots, P\}$ is

$$\mathbf{A}\big(x_1, x_2\big) = \begin{bmatrix} x_1 & x_2 \\ -x_2^* & x_1^* \end{bmatrix}, \tag{2.9}$$

and

$$\begin{bmatrix} \mathcal{S}_1 & \mathcal{S}_3 & \cdots & \mathcal{S}_{2P-1} \end{bmatrix}^T = \Theta \begin{bmatrix} s_1 & s_3 & \cdots & s_{2P-1} \end{bmatrix}^T, \tag{2.10}$$

$$\begin{bmatrix} \mathcal{S}_2 & \mathcal{S}_4 & \cdots & \mathcal{S}_{2P} \end{bmatrix}^T = \Theta \begin{bmatrix} s_2 & s_4 & \cdots & s_{2P} \end{bmatrix}^T, \tag{2.11}$$

where $\Theta = \mathbf{U} \times \text{diag}\{1, e^{j\theta_1}, \ldots, e^{j\theta_{P-1}}\}$ and $\mathbf{U}$ is a $P \times P$ Hadamard matrix. The θ_i's are the rotation angles which are chosen to maximize the coding gain.

Now, as an example, let us consider $P = 2$ radiation states and $M_t = 2$ transmit antennas. Then, the codeword $\mathbf{C}$ can be written as

$$\mathbf{C} = \frac{1}{2} \begin{bmatrix} \mathbf{C}_1 & \mathbf{0} \\ \mathbf{0} & \mathbf{C}_2 \end{bmatrix},$$

where $\mathbf{C}_1$ and $\mathbf{C}_2$ are given by

$$\mathbf{C}_1 = \frac{1}{2} \begin{bmatrix} s_1 + \tilde{s}_3 & s_2 + \tilde{s}_4 \\ -s_2^* - \tilde{s}_4^* & s_1^* + \tilde{s}_3^* \end{bmatrix}, \tag{2.12}$$

$$\mathbf{C}_2 = \frac{1}{2} \begin{bmatrix} s_1 - \tilde{s}_3 & s_2 - \tilde{s}_4 \\ -s_2^* + \tilde{s}_4^* & s_1^* - \tilde{s}_3^* \end{bmatrix}, \tag{2.13}$$

and $\tilde{s}_i = e^{j\theta_1} s_i$.

CHAPTER 3

DoA Estimation for Reconfigurable Antenna Systems [1]

DoA estimation algorithms in general can be classified into two main categories, namely the conventional algorithms and the subspace algorithms [65]. The conventional algorithms, e.g. the delay-and-sum method and the minimum variance distortionless look (MVDL) method, generally estimate the DoA based on the largest output power in the region of interest. The subspace algorithms, e.g. the MUSIC, root-MUSIC, MIN-NORM (minimum-norm), and ESPRIT (estimation of signal parameters via rotational invariance techniques) algorithms, estimate the DoA based on the signal and noise subspace decomposition principle. Technically, the subspace algorithms have superior performance in terms of precision and resolution compared to conventional algorithms. Various subspace-based DoA estimation techniques have been proposed over the years. One of the most well-known DoA estimation technique is the MUSIC algorithm that works based on the eigenvalue decomposition of the signal covariance matrix [21]. The performance of this algorithm is significantly impacted by different array characteristics, such as number of elements, array geometry, and the mutual coupling between the elements [22]. These issues can be avoided if a single reconfigurable antenna element capable of beam-forming/steering is employed instead of an array. For example, phase synchronization which is one of the most important factor in the accuracy of the MUSIC algorithm in conventional arrays will not be an issue with a reconfigurable antenna [23], [66]. Nevertheless, the classical MUSIC algorithm developed for antenna array systems is not immediately applicable for this type of antenna.

Several modified MUSIC DoA estimation algorithms have been proposed for reconfigurable antennas. In [23], the reactance-domain MUSIC algorithm was proposed for the ESPAR antenna which utilizes a single central radiator with surrounding parasitic elements.

1. Part of the work presented in this chapter was published in:
   - V. Vakilian, J.-F. Frigon, and S. Roy, "Direction-of-Arrival Estimation in a Clustered Channel Model", *Proc. IEEE Int. New Circuits and Systems Conf. (NEWCAS)*, Montreal, QC, Canada, June 2012. pp. 313–316.
   - V. Vakilian, J.-F. Frigon, and S. Roy, "Effects of Angle-of-Arrival Estimation Errors, Angular Spread and Antenna Beamwidth on the Performance of Reconfigurable SISO Systems", in *Proc. IIEEE Pacific Rim Conf. on Commun., Computers and Signal Process. (PacRim)*, Victoria, B.C., Canada, Aug. 2011. pp. 515–519.
   - V. Vakilian, H.V. Nguyen, S. Abielmona, S. Roy, and J.-F. Frigon, "Experimental Study of Direction-of-Arrival Estimation Using Reconfigurable Antennas", *Accepted for publication in proc. IEEE Canadian Conf. on Elect. and Computer Eng. (CCECE)*, Toronto, ON, Canada, May 2014.

A similar work for DoA estimation has been also reported in [24] that uses a modified MUSIC algorithm for a two-port CRLH-LWA [25]. However, no further evaluation was carried out on how configuring the antenna radiation patterns for signal observations can impact the algorithm performance. In this chapter, we address the problem of DoA estimation using a single reconfigurable antenna element and present simulation results of the developed algorithm for different cases. Moreover, we investigate the impact of DoA estimation errors on the performance of reconfigurable SISO systems. We also study the effect of angular spread and antenna beamwidth on the reconfigurable antenna system performance.

3.1 Signal Model

Consider a single reconfigurable antenna element that is capable of changing its radiation pattern direction for P different cases, where each radiation pattern case is called a radiation state as shown in Fig. 3.1. Let $g(\theta, \psi)$ denote the antenna gain at incoming signal direction $\theta \in [-\pi, \pi)$ and pointing angle $\psi \in [-\pi, \pi)$ (the pointing angle is a reconfigurable parameter). Suppose that this antenna element receives signals from K uncorrelated narrowband sources $s_1(t), s_2(t), \cdots, s_K(t)$ with the directions $\theta_1, \cdots, \theta_K$. The received signal during the p-th radiation state, for $p \in \{1, 2, ..., P\}$, can be expressed as,

$$x_p(t) = \sum_{k=1}^{K} g(\theta_k, \psi_p) s_k(t) + n_p(t), \tag{3.1}$$

where $g(\theta_k, \psi_p)$ denotes the antenna gain at direction θ_k and pointing angle of the p-th radiation state set to ψ_p, and $n_p(t)$ is the zero-mean complex Gaussian noise at the receiver with variance of σ^2.

$g(\theta_k, \psi_p)$ depends on the structure of reconfigurable antennas. For ESPAR antenna, it can be written as [23]

$$g(\theta_k, \psi_p) = i^T \mathbf{a}(\theta_k), \tag{3.2}$$

where $\mathbf{a}(\theta_k) = [1, e^{j\frac{\pi}{2}cos(\theta_k - \phi_1)}, \cdots, e^{j\frac{\pi}{2}cos(\theta_k - \phi_M)}]$ is the steering vector for M parasitic radiators elements, $\phi_m = (2\pi/M)(m-1)(m = 1, \cdots, M)$ corresponds to the m-th element position, and i is the RF current vector. For CRLH-LWA, $g(\theta_k, \psi_p)$ can be expressed as [67]

$$g(\theta_k, \psi_p) = \sum_{n=1}^{N_c} I_0 e^{-\alpha(n-1)d + j(n-1)k_o d[sin(\theta_k) - sin(\psi_p)]}, \tag{3.3}$$

where N_c is the number of cell in the CRLH-LWA structure which corresponds to the antenna length, α is the leakage factor, d is the period of the structure, k_0 is the free space wavenumber,

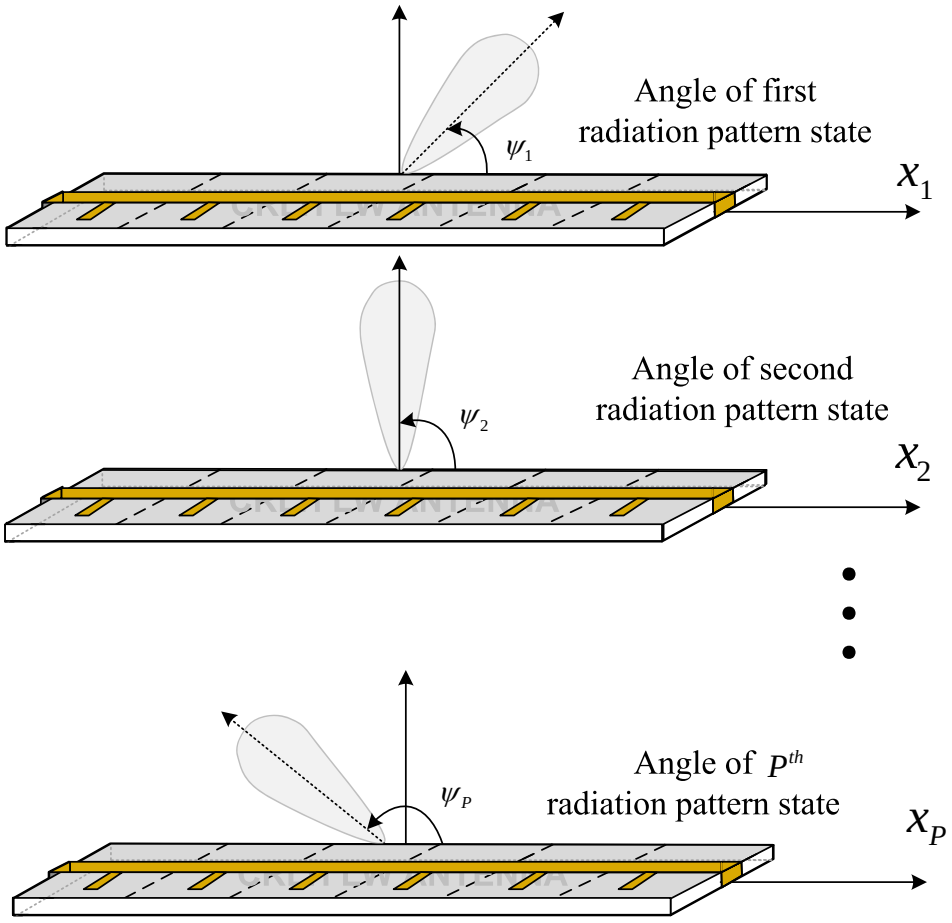

Figure 3.1 Single reconfigurable antenna with P radiation pattern states

and ψ_p is the radiation angle of the unit cells. The radiation pattern of the CRLH-LWA for four different radiation pattern states is shown in Fig. 3.2.

The received data vector over all possible P radiation pattern states $\mathbf{x}(t) \in \mathbb{C}^{P\times 1}$ for a single antenna element can be written as follows

$$\mathbf{x}(t) = \mathbf{G}\mathbf{s}(t) + \mathbf{n}(t), \tag{3.4}$$

where, $\mathbf{s}(t) \in \mathbb{C}^{K\times 1}$ is the transmitted signal vector from the K sources, $\mathbf{n}(t) \in \mathbb{C}^{P\times 1}$ is the noise vector at the receiver for the P measurements, and $\mathbf{G} \in \mathbb{C}^{P\times K}$ is the antenna gain matrix which can be defined as

$$\mathbf{G} = \Big[\mathbf{g}(\theta_1, \psi), \mathbf{g}(\theta_2, \psi) \cdots, \mathbf{g}(\theta_K, \psi)\Big] \tag{3.5}$$

$$\mathbf{g}(\theta_k, \psi) = \Big[g(\theta_k, \psi_1), g(\theta_k, \psi_2), \cdots, g(\theta_k, \psi_P)\Big]^T, \tag{3.6}$$

where $g(\theta_k, \psi_p)$ is the radiation pattern of the reconfigurable antenna. We assume that N snapshots of data samples are collected at $t = 1, 2, \cdots, N$. We also consider that $\mathbf{s}(t)$ and $\mathbf{n}(t)$ are uncorrelated and $\mathbf{n}(t)$ is a Gaussian noise vector with zero mean and correlation matrix $\sigma^2\mathbf{I}$.

3.2 DoA Algorithm for a Single Reconfigurable Antenna Element

In this section, we propose a radiation pattern scan-MUSIC (RPS-MUSIC) algorithm which is able to estimate the DoAs of multiple signals impinging on a single reconfigurable antenna element. In the proposed algorithm, the signals are received by the reconfigurable antenna while it switches over a set of radiation pattern configurations. Then, the receive covariance matrix is calculated as a function of antenna radiation patterns. Once the data covariance matrix is formed, the eigenvalue decomposition (EVD) is performed to decompose the matrix to the signal and noise subspaces. We find the DoAs by searching for the incident angles where the noise and signal subspaces are orthogonal to each other. Moreover, we propose another DoA estimation technique based on the cross-correlation between the received signal power and power radiation pattern proposed in [68].

3.2.1 Radiation Pattern Scan-MUSIC Algorithm

In general, DoA estimation algorithms utilize the received signal on each element of an antenna array to create the required correlation matrix. This method of creating correlation

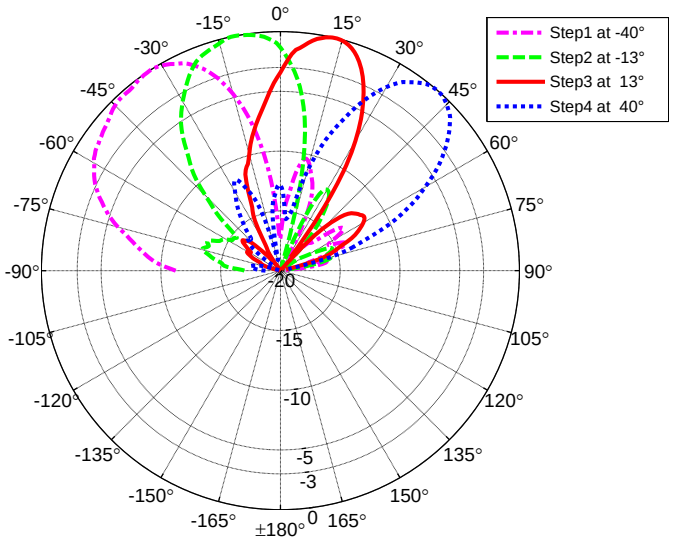

Figure 3.2 Radiation pattern of a reconfigurable antenna for four different radiation state

matrix is not applicable for a communication system with a single antenna element. To solve this problem, the correlation can be created using the signal received by a single antenna element from multiple radiation states. Fig. 3.2 shows the measured radiation pattern of a reconfigurable antenna for four radiation states. Therefore, instead of observing signals from different elements of an antenna array, signals are obtained from different antenna radiation patterns. Hence, we are able to create a correlation matrix with only a single reconfigurable antenna element. For the signal model in (3.4), the $P \times P$ covariance matrix can be written in the following form

$$\begin{aligned}\mathbf{R}_{xx} &= \mathbb{E}\big[\mathbf{x}(t)\mathbf{x}^H(t)\big] = \mathbb{E}\big[(\mathbf{G}\mathbf{s}(t)+\mathbf{n}(t))(\mathbf{G}\mathbf{s}(t)+\mathbf{n}(t))^H\big] \\ &= \mathbf{G}\mathbb{E}\big[\mathbf{s}(t)\mathbf{s}^H(t)\big]\mathbf{G}^H + \mathbb{E}\big[\mathbf{n}(t)\mathbf{n}^H(t)\big] \\ &= \mathbf{G}\mathbf{R}_{ss}\mathbf{G}^H + \sigma^2\mathbf{I}, \end{aligned} \tag{3.7}$$

where $\mathbf{R}_{ss} = \mathbb{E}[\mathbf{s}(t)\mathbf{s}^H(t)]$ is the $K \times K$ covariance matrix of input signals, and $\mathbb{E}[\cdot]$ and $(\cdot)^H$ denote the statistical expectation and complex conjugate transpose, respectively. Both the signal and noise subspaces can be obtained by EVD of (3.7), where the decomposed signal and noise subspaces can be denoted as

$$\mathbf{R}_{xx} = \mathbf{Q}\mathbf{D}\mathbf{Q}^{\mathbf{H}} = \begin{bmatrix}\mathbf{Q_s} & \mathbf{Q_n}\end{bmatrix}\begin{bmatrix}\mathbf{D_s} & 0 \\ 0 & \sigma^2\mathbf{I}\end{bmatrix}\begin{bmatrix}\mathbf{Q_s} & \mathbf{Q_n}\end{bmatrix}^H. \tag{3.8}$$

The matrix $\mathbf{Q}$ is partitioned into signal and noise subspaces denoted by $\mathbf{Q_s}$ and $\mathbf{Q_n}$, respectively. $\mathbf{Q_s}$ is a $P \times K$ matrix whose columns are the K eigenvectors corresponding to the signal subspace and $\mathbf{Q_n}$ is a $P \times (P-K)$ matrix composed of the noise eigenvectors. The matrix $\mathbf{D}$ is also partitioned into a $K \times K$ diagonal matrix $\mathbf{D_s}$ whose diagonal elements are the signal eigenvalues and a $(P-K) \times (P-K)$ scaled identity matrix $\sigma^2\mathbf{I}$ whose diagonal elements are the $P \times K$ noise eigenvalues. After EVD of the received signal correlation matrix, the RPS-MUSIC spectrum for a single reconfigurable antenna element can be computed as follows,

$$P_{RPS-MUSIC}(\theta) = \frac{\mathbf{g}^H(\theta,\psi)\mathbf{g}(\theta,\psi)}{\mathbf{g}^H(\theta,\psi)\mathbf{Q_n}\mathbf{Q_n}^H\mathbf{g}(\theta,\psi)}. \tag{3.9}$$

where $\mathbf{g}^H(\theta,\psi)$ is defined in (3.6). Note that the noise subspace is orthogonal to the antenna gain vector $\mathbf{g}(\theta)$ at the DoA's of the received signals and the RPS-MUSIC algorithm employs this property by searching over θ for these incident angles of orthogonality.

3.2.2 Power Pattern Cross-Correlation Approach

As proposed in [68], the DoAs of the signals can be estimated by computing the cross-correlation between the received signal power and power radiation pattern and then finding the largest cross-correlation coefficient as an estimated DoA. In this section, we generalize this algorithm to any reconfigurable antenna. For given P radiation pattern configurations, the cross-correlation coefficient can be define as [68]

$$\Gamma(\theta) = \frac{\sum_{p=1}^{P} P_{\psi_p}(\theta) P_{\psi_p}^R}{\sqrt{\sum_{p=1}^{P} P_{\psi_p}(\theta)^2}\sqrt{\sum_{p=1}^{P}(P_{\psi_p}^R)^2}}, \tag{3.10}$$

where $P_{\psi_p}(\theta)$ is the power pattern of a reconfigurable antenna and $P_{\psi_p}^R$ is the average received signal power over N number of observations in the p radiation state and it can be expressed as

$$P_{\psi_p}^R = \frac{1}{N}\sum_{t=1}^{N} |x_{\psi_p}(t)|^2. \tag{3.11}$$

Then, the DoA can be estimated as follow

$$\hat{\theta} = \arg\max_{\theta} \Gamma(\theta). \tag{3.12}$$

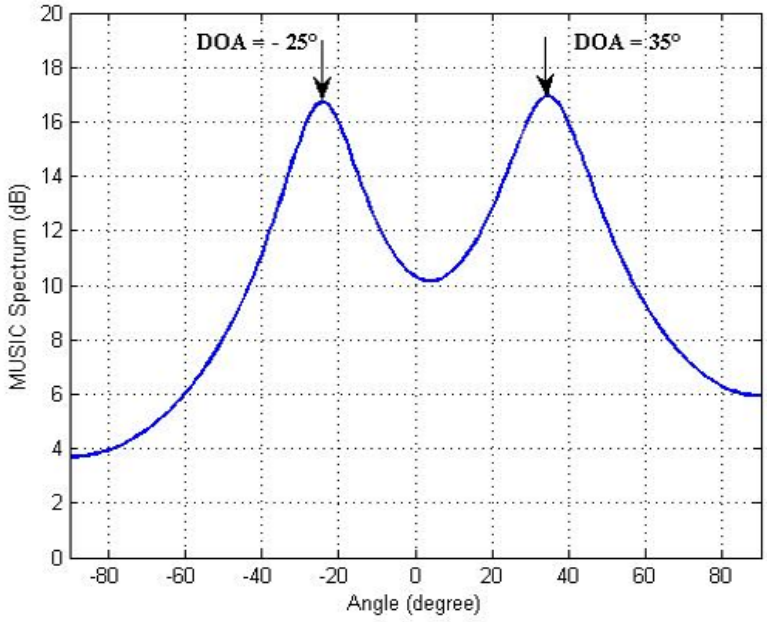

Figure 3.3 RPS-MUSIC spectrum for two sources with $\theta_1 = -25°$ and $\theta_2 = 35°$.

3.2.3 Numerical Results

In this section, we perform several simulations to numerically evaluate the performance of the proposed RPS-MUSIC and power pattern cross correlation algorithms. In all the simulations, we consider a single reconfigurable antenna at the transmitter with four radiation states, where the pointing angles of these states are set to $\psi_1 = -40°, \psi_2 = -13°, \psi_3 = 13°$, and $\psi_4 = 40°$.

Fig. 3.3 shows the RPS-MUSIC spectrum and the values of the estimated DoAs for incident signals at $\theta_1 = -25°$ and $\theta_2 = 35°$. The spectrum calculated by using equation (3.9) was averaged for 100 independent trials at the signal to noise ratio (SNR) of 20 dB and 10 snapshots ($N = 10$). From Fig. 3.3, it can be seen that the RPS-MUSIC algorithm performs reasonably well and it is observed that the proposed algorithm is capable of resolving the two sources.

In Fig. 3.4, the RMSE of DoA estimation versus the SNR for different number of snapshots N is plotted in which, for each SNR, 1000 Monte Carlo trials are conducted. The radiation patterns of these four states is shown in Fig. 3.2. We can observe from Fig. 3.4 that, as expected, as the SNR increases, the RMSE decreases and also the performance of the estimator improves as the number of observation increases.

Fig. 3.5 shows the RMSE of the DoA estimation for different number of snapshots N as a function of the number of radiation pattern states P. In this simulation, we investigate the

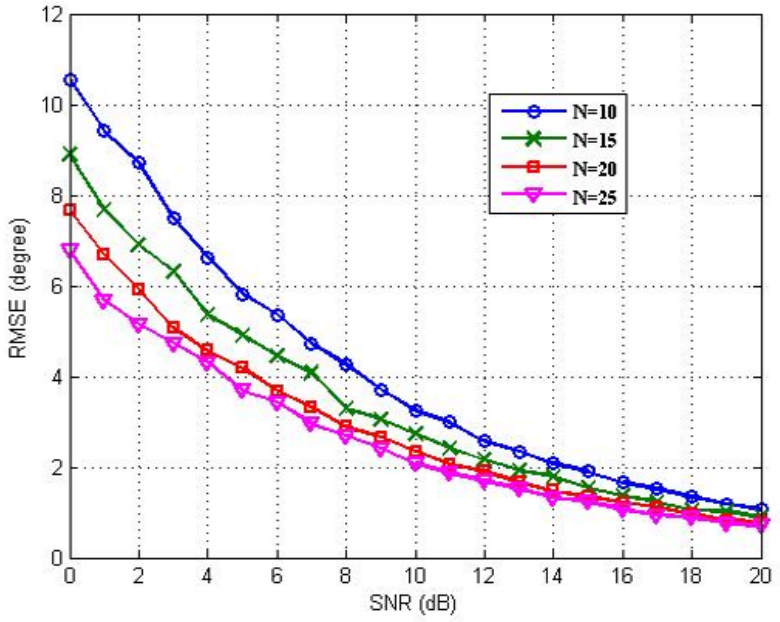

Figure 3.4 RMSE of RPS-MUSIC for different number of snapshots

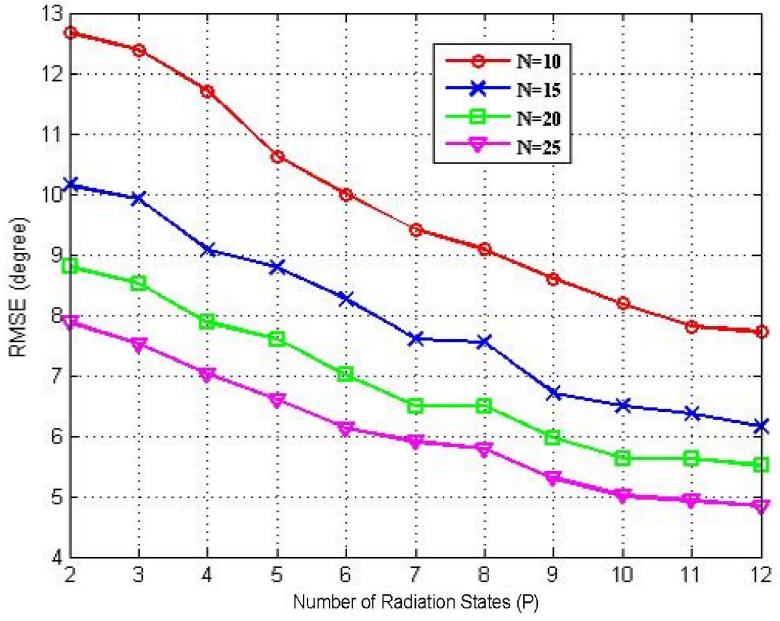

Figure 3.5 RMSE of RPS-MUSIC versus different number of radiation states for different number of snapshots

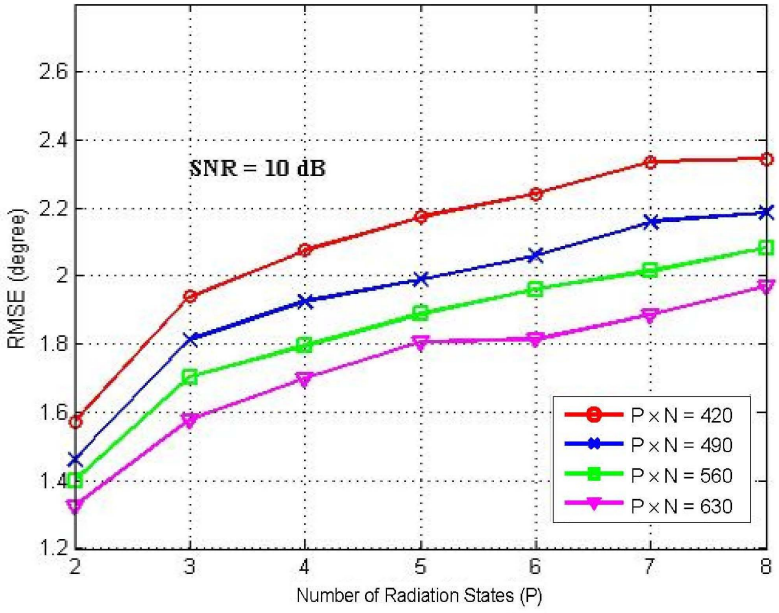

Figure 3.6 RMSE of RPS-MUSIC for different number of radiation states and same amount of information for all the states

DoA estimation performance versus the number of radiation states when the SNR is fixed at 10 dB and the antenna beamwidth is assumed to be 45°. It can be noted that the RMSE decreases with the increase in the number of radiation states. This is because increasing P for the fixed number of snapshots, increases the total observing information used for estimating the DoA.

Fig. 3.6 illustrates the RMSE of the DoA estimation versus the number of radiation states P for different amount of measurements PN. In this simulation, the SNR is fixed at 10 dB and the antenna beamwidth is assumed to be 45°. Obviously, by increasing the amount of information used for estimation, we can achieve better accuracy. However it is interesting to observe that for a fixed total amount of measurements, it is better to increase the number of radiation pattern states P than increasing the number of measurements done for a radiation pattern state N. This comes from the added signal diversity obtained by using different radiation patterns.

Fig. 3.7 illustrates the power spectrum of estimated DoA for a signal source at $\theta_1 = 10°$ obtained using the power pattern cross correlation method. The spectrum calculated using (3.12) at SNR = 10 dB with 10 samples. It can be observed that the spectrum is not as sharp as the RPS-MUSIC. However, it's measurement complexity is much lower since no tight synchronization is required for power measurement.

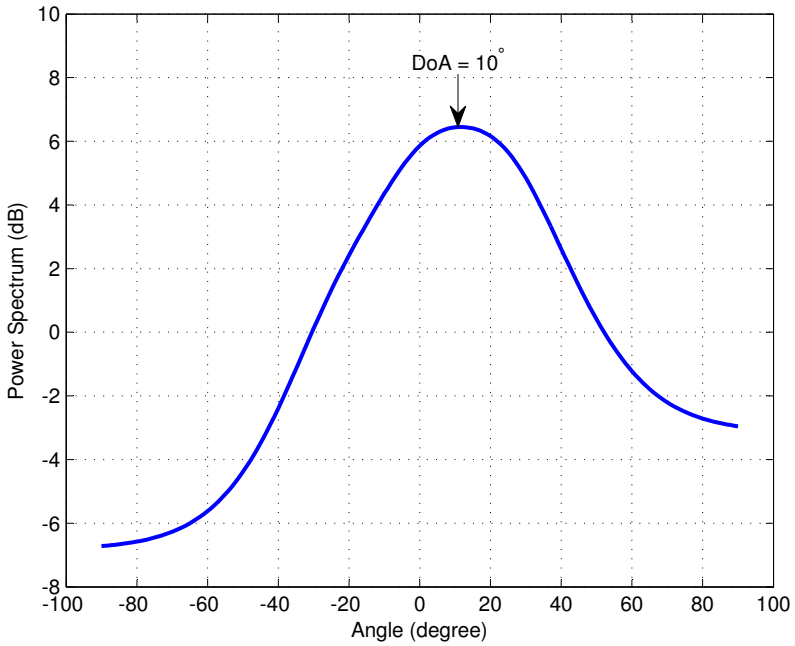

Figure 3.7 Power spectrum for one sources with $\theta_1 = 10^\circ$

3.3 Impact of DoA Estimation Errors on the BER Performance of Reconfigurable SISO Systems

In reconfigurable antenna systems, DoA estimation errors can significantly affect the performance of the system. The impact of DoA estimation errors on the outage probability of a wireless system has been investigated in [69]. In this reference, the authors have used an antenna array beamformer to examine the impact of beamforming impairments, such as DoA estimation errors, signal spatial spreads, antenna array perturbation, and mutual coupling. It was then demonstrated that the outage probability increases due to the DoA estimation errors. However, they considered the impact of DoA estimation errors on the outage probability using a ULA.

In this section, we analyze the effect of DoA estimation errors on the BER performance of systems, employing a single reconfigurable antenna at the receiver and an omni-directional antenna at the transmitter. As a first step, we assume perfect knowledge of the direction-of-arrival at the receiver. Then, we compute the average BER performance of the system based on this information. Next, we investigate the BER of the system when the DoA is estimated with an error. Moreover, we evaluate the effect of angular spread and antenna beamwidth on the system performance. We use the practical clustered channel model, validated in [70], which currently is being utilized in different wireless standards such as the IEEE 802.11n

Technical Group (TG) [71] and 3GPP Technical Specification Group (TSG) [72]. In this model, groups of scatterers are modeled as clusters around transmit and receive antennas.

3.3.1 BER Analysis for a Reconfigurable SISO System

Consider a SISO system equipped with an omni-directional antenna at the transmitter, and a reconfigurable antenna at the receiver as shown in Fig. 3.8. Let $h^n(t)$ be the channel between transmitter and receiver for the n-th cluster where each cluster has M multipaths. Then, the impulse response for the n-th cluster can be given by [73]

$$\begin{aligned} h^n(t) &= \frac{1}{\sqrt{M}} \sum_{m=1}^{M} \sqrt{g_r(\theta_m^n)} \alpha_m^n(t) \delta(t-\tau_n) \\ &= \sum_{m=1}^{M} h_m^n(t) \delta(t-\tau_n), \end{aligned} \tag{3.13}$$

where $h_m^n(t) = \frac{1}{\sqrt{M}} \sqrt{g_r(\theta_m^n)} \alpha_m^n(t)$, M is the number of paths per cluster, $\alpha_m^n(t)$ is the complex gain of the m-th multipath (the $\alpha_m^n(t)$ are zero mean unit variance independent identically-distributed (i.i.d.) complex random variables), and $g_r(\theta_m^n)$ is the reconfigurable antenna gain at the direction $\theta_m^n = \theta_{DoA}^n + \vartheta_m^n$ where θ_{DoA}^n is the mean direction-of-arrival of the n^{th} cluster and ϑ_m^n is the deviation of the paths from mean DoA. The ϑ_m^n are modeled as i.i.d. Gaussian random variables, with zero mean and variance σ_{DoA}^2. Furthermore, the $\alpha_m^n(t)$ and ϑ_m^n are independent. For the analysis presented in this section, we approximate the radiation pattern of reconfigurable antennas, $g_r(\theta)$, by a parabolic function which can be expressed as [74]

$$g_r(\theta) = \frac{2\pi}{B_{3dB}} 10^{0.1A(\theta)}, \tag{3.14}$$

where $A(\theta) = -\eta \left(\frac{\theta - \theta_p}{B_{3dB}} \right)^2$ in dB, η is a constant (set to 12 in [74]), B_{3dB} is the 3dB reconfigurable antenna beamwidth in radians, and θ_p is the antenna pointing angle. For the ideal case considered in this section we have $\theta_p = \theta_{DoA}$.

The received signal can be written as

$$\begin{aligned} y &= hx + z \\ &= \frac{1}{\sqrt{M}} \sum_{m=1}^{M} \sqrt{g_r(\theta_m)} \alpha_m x + z \\ &= \sum_{m=1}^{M} h_m x + z \end{aligned} \tag{3.15}$$

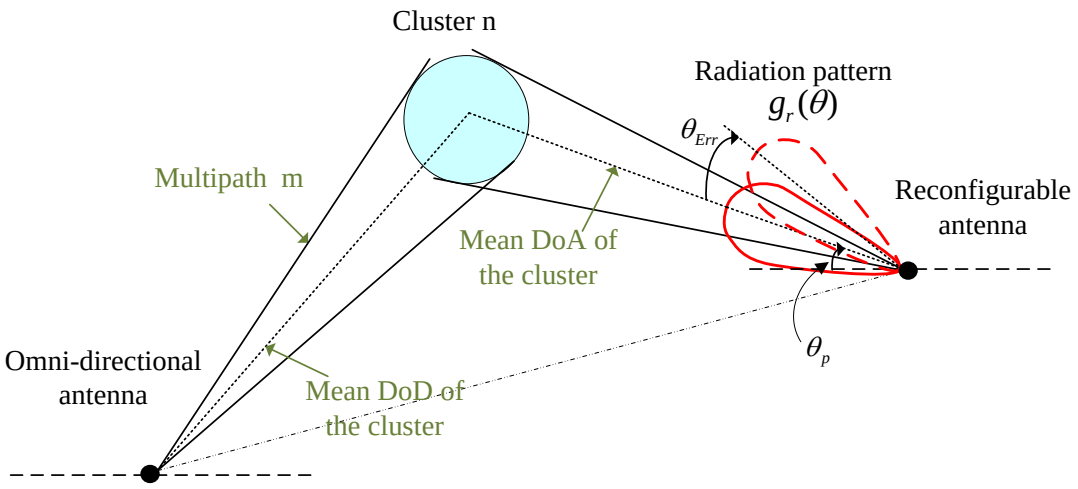

Figure 3.8 System model for the RE-SISO system with a reconfigurable antenna at the receiver

where y is the received signal, x is the transmitted signal, z is a zero mean complex AWGN with unit variance, and $h_m = \frac{1}{\sqrt{M}}\sqrt{g_r(\theta_m)}\alpha_m$ are i.i.d. complex random variables.

Since $h = \sum_{m=1}^{M} h_m$ is a sum of independent random variables, based on the the central limit theorem (CLT) for a large number of multipaths, h can reasonably be modeled as a zero-mean Gaussian random variable with variance $\sigma_h^2 = M\text{var}[h_m]$, where $\text{var}[h_m]$ can be computed as follows

$$\begin{aligned} \text{var}[h_m] &= \frac{1}{M}(\mathbb{E}[(\sqrt{g_r(\theta_m)}\alpha_m)^2] - \mathbb{E}[\sqrt{g_r(\theta_m)}\alpha_m]^2) \\ &= \frac{1}{M}(\mathbb{E}[g_r(\theta_m)]) = \frac{2\pi}{MB_{3dB}\sqrt{2c\sigma^2+1}}, \end{aligned} \tag{3.16}$$

where $c = \ln 10$ is a constant and $\sigma^2 = \frac{0.1\eta\sigma_{DoA}^2}{B_{3dB}^2}$ (see Appendix A). Using (3.16), the variance of h can be defined as follows:

$$\sigma_h^2 = \frac{2\pi}{\sqrt{0.2c\eta\sigma_{DoA}^2 + B_{3dB}}}. \tag{3.17}$$

Note that the variance of the channel coefficient is a function of the variance of the DoA and the antenna beamwidth.

Now, let us define the average error probability for a BPSK modulation with respect to the channel statistics as follows

$$\bar{p}_e = \mathbb{E}_h\left[Q\left(\sqrt{2|h|^2\text{SNR}}\right)\right], \tag{3.18}$$

where SNR is the average received signal-to-noise ratio, $Q(x)$ denotes the Gaussian-Q function $Q(x) = \frac{1}{\sqrt{2\pi}} \int_x^\infty \exp(-t^2/2)dt$ and $|h|^2$ is exponentially distributed. Therefore, direct integration of (3.18) yields

$$\bar{p}_e = \frac{1}{2}\left(1 - \sqrt{\frac{\sigma_h^2 \mathrm{SNR}}{1+\sigma_h^2 \mathrm{SNR}}}\right). \tag{3.19}$$

3.3.2 BER Analysis for a Reconfigurable SISO System with DoA Estimation Error

The received signal in (3.15) with taking DoA estimation errors into consideration becomes as follows

$$\begin{aligned} y &= \widetilde{h}x + z \\ &= \frac{1}{\sqrt{M}} \sum_{m=1}^{M} \sqrt{\widetilde{g_r}(\theta_m)}\alpha_m x + z \\ &= \sum_{m=1}^{M} \widetilde{h}_m x + z, \end{aligned} \tag{3.20}$$

where $\widetilde{h}$ is the channel coefficient when the DoA is estimated with a fixed error of θ_{Err} and $\widetilde{g_r}(\theta)$ is the antenna gain which can be written as

$$\widetilde{g_r}(\theta) = \frac{2\pi}{B_{3dB}} 10^{-0.1\eta\left(\frac{\theta-\hat{\theta}_p}{B_{3dB}}\right)^2}, \tag{3.21}$$

where $\hat{\theta}_p = \theta_{DoA} + \theta_{Err}$. By expanding $\hat{\theta}_p$ in the above expression, we get

$$\begin{aligned} \widetilde{g_r}(\theta) &= \frac{2\pi}{B_{3dB}} 10^{-0.1\eta\left(\frac{\theta-(\theta_{DoA}+\theta_{Err})}{B_{3dB}}\right)^2} \\ &= \beta g_r(\theta), \end{aligned} \tag{3.22}$$

where $\beta = 10^{-0.1\eta\left[\left(\frac{\theta_{Err}}{B_{3dB}}\right)^2 - 2\frac{(\theta-\theta_{DoA})\theta_{Err}}{B_{3dB}^2}\right]}$. Therefore, the variance of $\widetilde{h}_m$ can be computed as follows,

$$\begin{aligned} \mathrm{var}[\widetilde{h}_m] &= \frac{1}{M}(\mathbb{E}[(\sqrt{\widetilde{g_r}(\theta_m)}\alpha_m)^2] - \mathbb{E}[\sqrt{\widetilde{g_r}(\theta_m)}\alpha_m]^2) \\ &= \frac{1}{M}(\mathbb{E}[\widetilde{g_r}(\theta_m)]) \\ &= \frac{2\pi}{MB_{3dB}\sqrt{2c\sigma^2+1}} e^{\frac{(\frac{\mu}{\sigma^2})^2}{4(\ln 10 + 1/2\sigma^2)} - \frac{\mu^2}{2\sigma^2}}, \end{aligned} \tag{3.23}$$

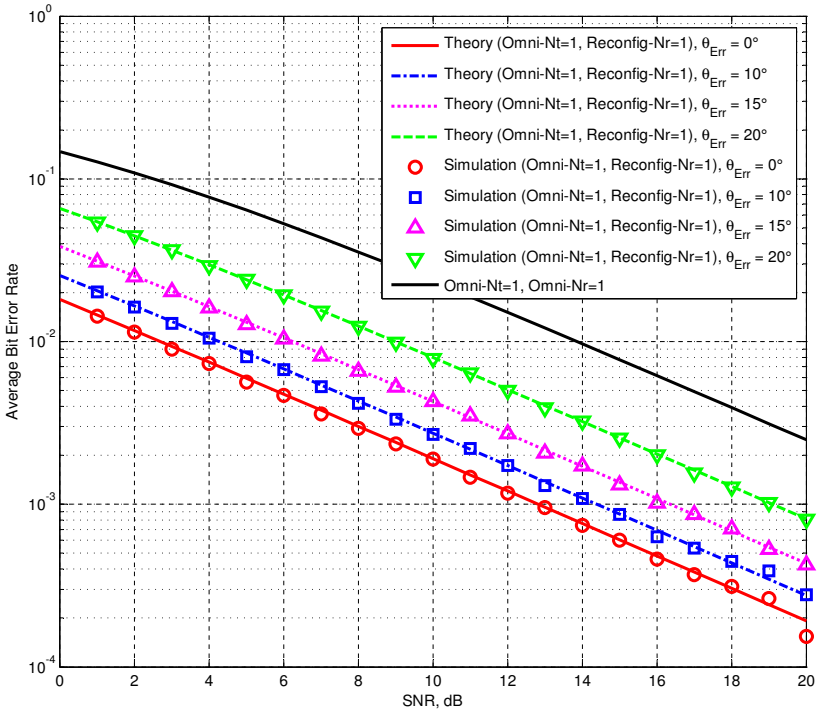

Figure 3.9 Effect of DoA estimation errors on the average bit error rate

where $\mu = -\frac{\sqrt{0.1\eta}\theta_{Err}}{B_{3dB}}$ and $\sigma^2 = \frac{0.1\eta\sigma_{DoA}^2}{B_{3dB}^2}$. Therefore, the variance of $\widetilde{h}$ can be defined as

$$\sigma_{\widetilde{h}}^2 \quad = \quad M\text{var}[\widetilde{h}_m]. \tag{3.24}$$

Then, by using (3.19) the average BER for BPSK modulation is given by

$$\bar{p}_e = \frac{1}{2}\left(1 - \sqrt{\frac{\sigma_{\widetilde{h}}^2 \text{SNR}}{1 + \sigma_{\widetilde{h}}^2 \text{SNR}}}\right). \tag{3.25}$$

3.3.3 Simulation Results

In this section, we perform several simulations to investigate the impact of DoA estimation errors on the performance of reconfigurable SISO systems. We also study the effect of angular spread and antenna beamwidth on the system performance.

Fig. 3.9 illustrates the BER versus signal to noise ratio (SNR). In this simulation, we set the antenna beamwidth at $B_{3dB} = 20°$ and angular spread at $\sigma_{DoA} = 5°$. From this figure, we can observe that the theoretical results exactly match the Monte-Carlo simulations with 1000 trials per simulation, validating the analysis. It also can be observed that the BER increases as the DoA estimation error increases. It is interesting to note that even though

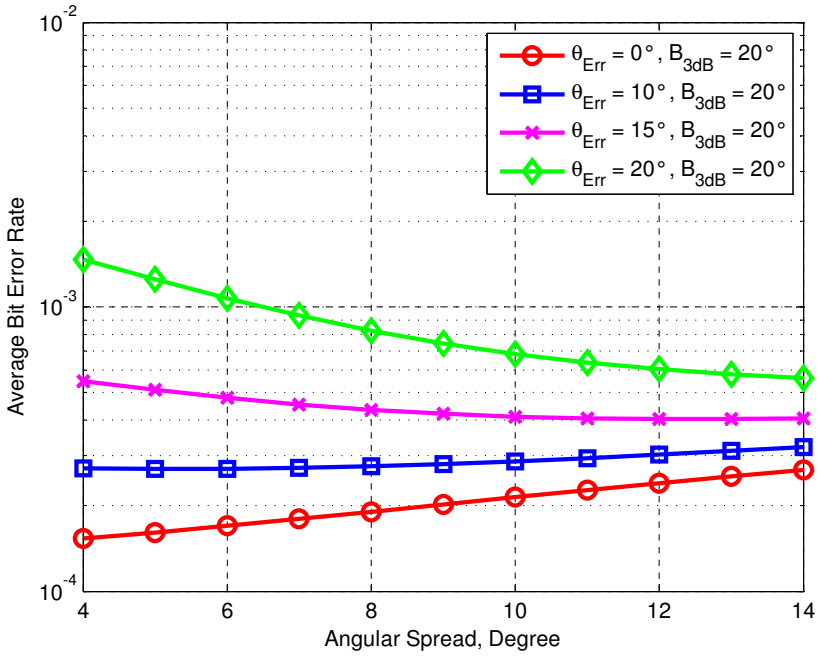

Figure 3.10 Average bit error rate performance of the RE-SISO system versus angular spread for different amounts of DoA estimation errors at SNR= 20dB

the DoA estimation error is as large as the half beamwidth of the radiation pattern, the BER performance of the reconfigurable systems still outperforms a traditional system with a fixed omni-directional antenna.

Fig. 3.10 depicts the BER performance of the reconfigurable SISO (RE-SISO) system versus angular spread (AS) for different DoA errors and fixed antenna beamwidth. We observe that in the case of perfect DoA estimation ($\theta_{Err} = 0$), the average BER increases as the angular spread increases. This is expected since as the angular spread increases we are receiving fewer multipaths in the middle of the radiation pattern where the gain is the largest. On the other hand, in the presence of a significant estimation error, the average BER initially decreases as a function of the angular spread. This is due to the fact that the number of multipaths impinging in the misaligned radiation pattern increases as a function of the angular spread.

Fig. 3.11 also illustrates the impact of direction-of-arrival estimation error on the performance of the reconfigurable antenna system. As shown in the figure, for all AS values, the performance loss increases as the DoA errors increase. It can be observed that the BER performance of the system with smaller AS is better than the BER of the system with greater AS in the case of small DoA error. This is due to the fact that the antenna receives almost all the multipaths from scatterers near to its maximum gain when the AS is small. However, as the figure illustrates, the situation is reversed for large DoA error since most of the mul-

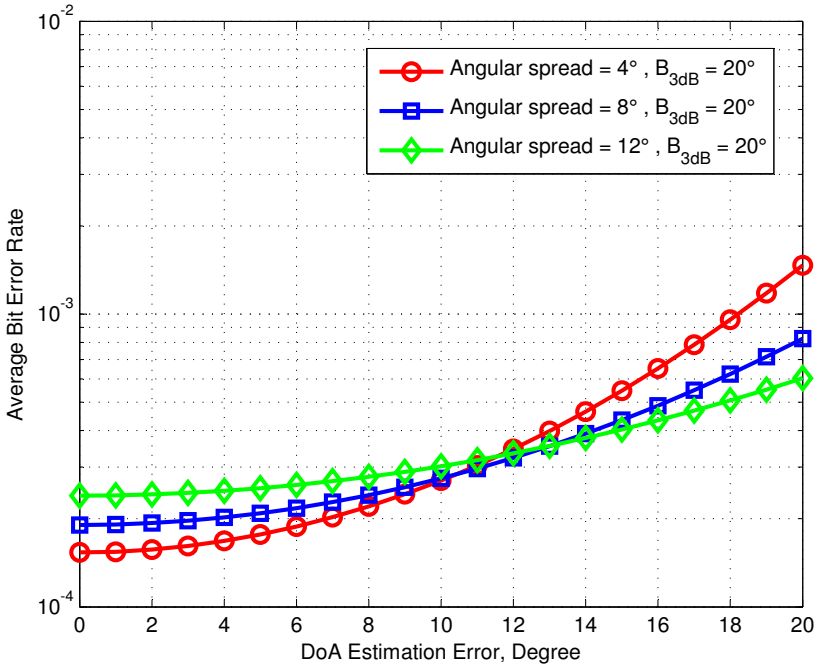

Figure 3.11 Effect of DoA estimation errors on the average bit error rate for different values of angular spread at SNR= 20dB (AS)

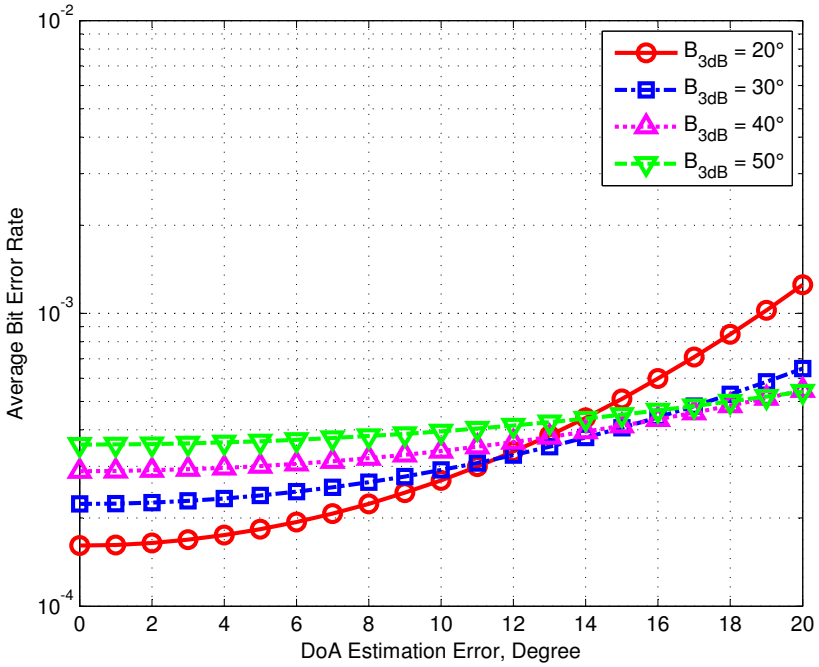

Figure 3.12 Effect of antenna beamwidth on the average bit error rate for different amounts of DoA estimation errors

tuipaths are tightly clustered and imping on the low gain sides of the misaligned radiation pattern. Therefore, it is important to improve the direction-of-arrival estimation error for channel with small angular spread.

The impact of antenna beamwidth is examined in Fig. 3.12 when the angular spread is fixed at 5° and the DoA estimation error is varied from 0 to 20 degrees. As expected, for small values of DoA estimation error, the most directive antenna yields the lowest BER, profiting directly from the higher antenna gain. However, for large DoA error, the antenna with wider beamwidth has a better BER performance due to the higher received signal energy as compared to a narrow misaligned beam which will miss most of the energy. In fact it can be observed that a system with a narrow beam is much more sensitive to estimation errors than for a system with a large beamwidth antenna.

3.4 Experimental Study of DoA Estimation Using Reconfigurable Antennas

In this section, we present the DoA estimation experiment for the RPS-MUSIC algorithm done in an anechoic chamber.

3.4.1 Measurement Setup

The measurement setup is illustrated in Fig. 3.13, where the antenna at the transmitter is a horn antenna and at the receiver the antenna is a single element CRLH-LWA which provides electronically controllable radiation patterns. Furthermore, we use a Lyrtech MIMO advanced development system which is a baseband-to-RF solution and consists of several signal processing platforms, such as the VHS-ADC for analog-to-digital conversion (ADC), the VHS-DAC for digital-to-analog conversion (DAC), the SignalMaster Quad for baseband signal processing, and the Quad Dual Band RF Transceiver for up and down conversion [75].

At the transmitter, the data is first generated using an Agilent signal generator, and then the resulting baseband signal is split into in-phase (I) and quadrature (Q) components. These components are then converted to analog using the Lyrtech VHS-DAC. Next, using the Quad

Table 3.1 Experimental parameters

Parameters	Value
RF frequency	2.4 GHz
Modulation	QAM
Tx antenna	Horn antenna
Rx antenna	CRLH-LW antenna

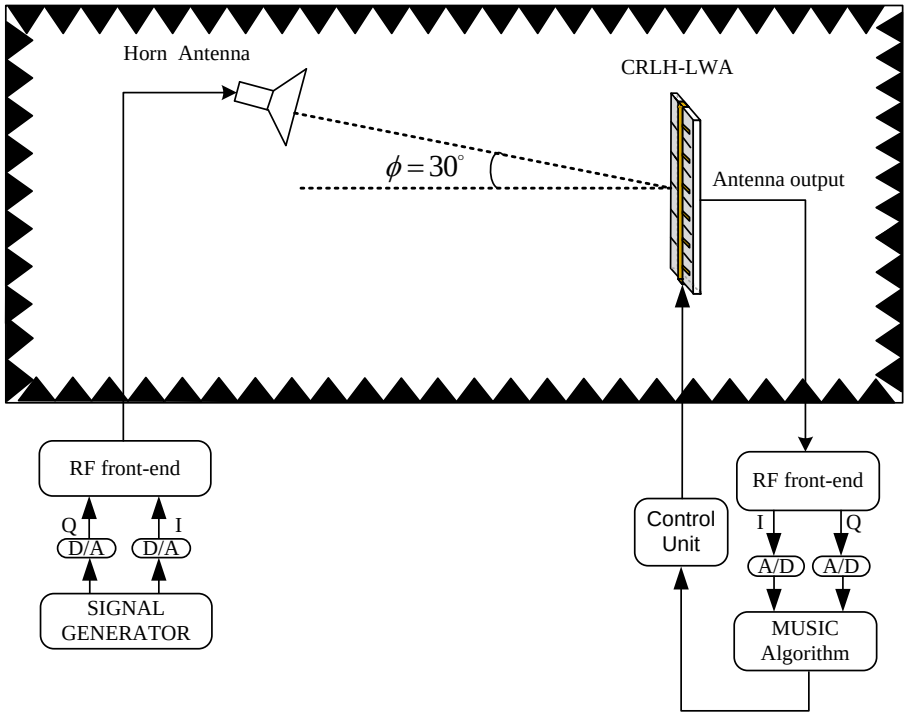

Figure 3.13 The measurement setup for one-source DoA estimation in an anechoic chamber.

Table 3.2 Different cases for radiation states

Case \ ψ_p	-50	-40	-20	-15	-5	+5	+15	+20	+40	+50
1					×	×				
2	×									×
3		×		×			×		×	
4	×			×			×			×
5		×	×					×	×	
6	×		×					×		×

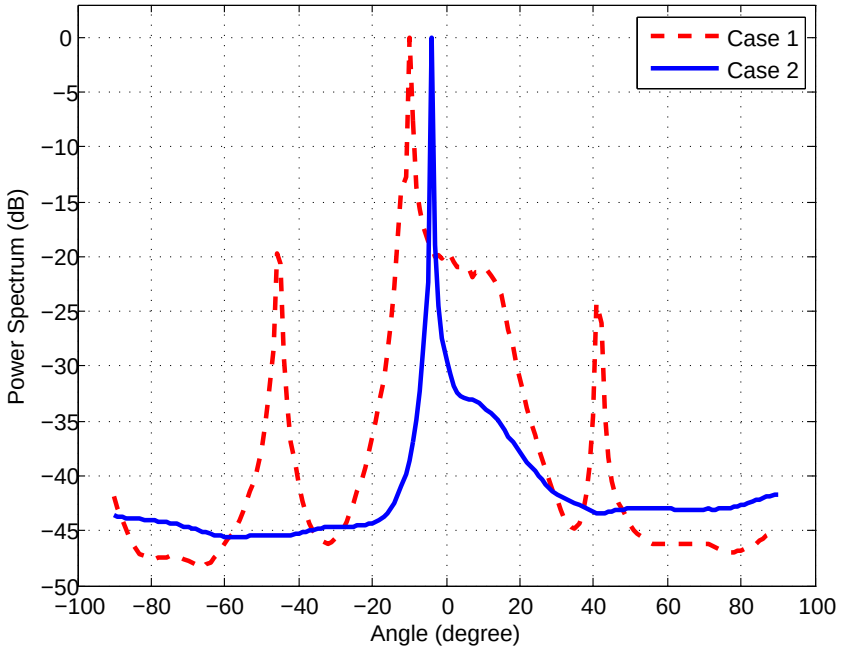

Figure 3.14 Power spectrum for DoA of 0° with $P = 2$

Dual Band RF Transceiver which is a four-channel RF analog front-end, the analog signal is upconverted to the carrier frequency of 2.4 GHz and transmitted over the air. At the receiver, the signal is captured by the CRLH-LW antenna at different radiation states and sent to the RF front-end to down-convert the RF signal to baseband. Then, the baseband analog signal is sampled by the Lyrtech VHS-ADC. The resulting sampled streams are stored in real time on memory boards and transferred offline to a PC for estimating the DoA. The experimental parameters are shown in Table 3.1.

3.4.2 Experimental Results

To validate the performance of the introduced DoA estimation algorithm for the reconfigurable antenna, we conducted several experiments in an anechoic chamber. Figs. 3.14 and 3.15 show the power spectrum for DoAs of 0°, and 30°, respectively. The results illustrated in these figures are obtained using $P = 2$ radiation states which have been chosen from Table 3.2. The first column in this table shows cases 1 to 6, that correspond to different choices for number of radiation states and their pointing angles. For each case, we estimates the DoA using only the radiation states which are identified by cross-marks. Figs. 3.14 and 3.15 illustrate the results of the DoA estimation for case 1 and 2. From these figures, it can be observed that the DoA can be estimated accurately if the two chosen radiation states are

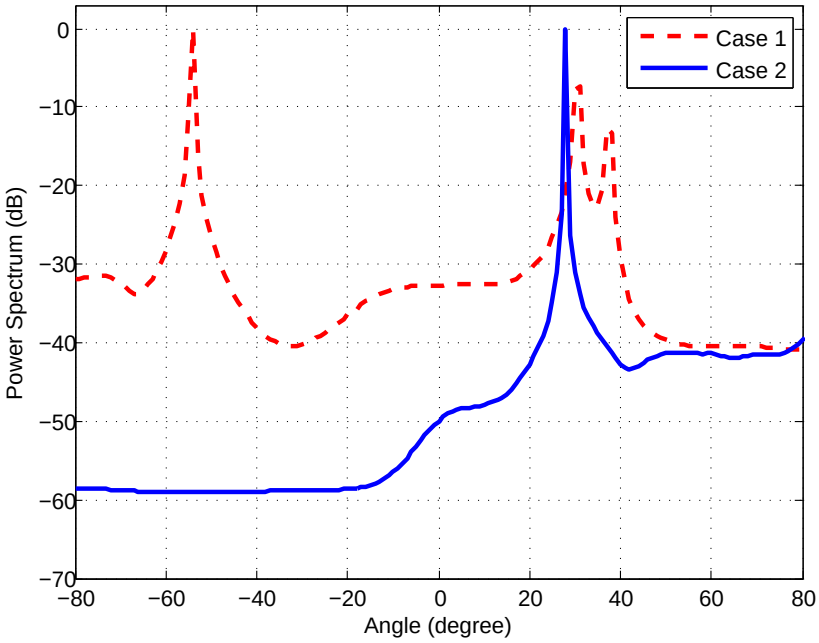

Figure 3.15 Power spectrum for DoA of 30° with $P = 2$

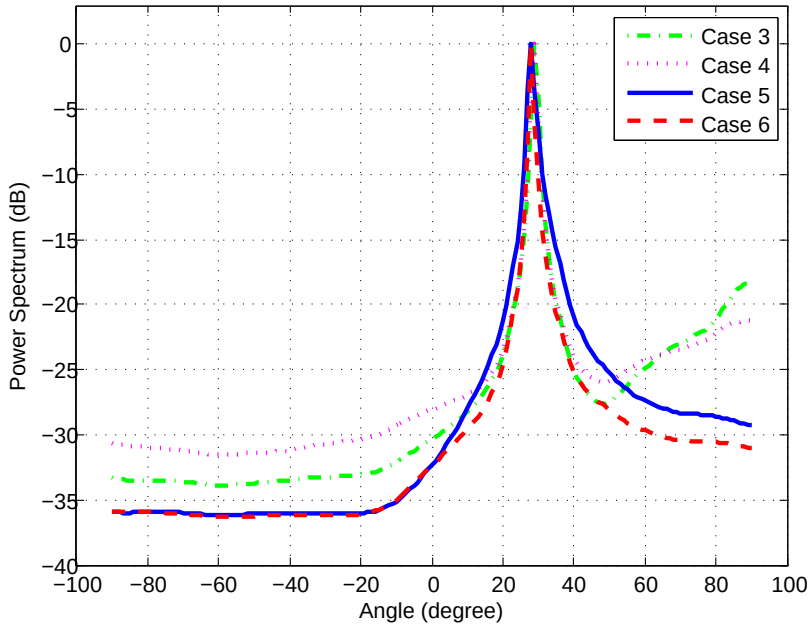

Figure 3.16 Power spectrum for DoA of 30° with $P = 4$

sufficiently far apart. For case 1, the two radiation states are very close and there is a large overlap in their radiation patterns. Consequently, the algorithm fails to estimate the DoA properly and creates large fluctuations in the power spectrum. We also observe similar results for other two-radiation state cases. The conclusion is that as the angular distance between the radiation states increases, the estimation accuracy increases.

Fig. 3.16 depicts the power spectrum obtained using $P = 4$ radiation states. The DoA to be estimated is 30°. In this experiment, we consider two scenarios to investigate the impact of antenna radiation states on the estimated DoA. In the first scenario, we fix the two radiation states' pointing angles at -15 and $+15$ and change the other two. In the second scenario, we fix the two radiation states' pointing angles at -20 and $+20$ and change the other two radiation states. In terms of power fluctuation over the spectrum, the later scenario performs better because the overlapping radiation patterns between the radiation states is smaller than the first scenario.

3.5 Conclusion

In this chapter, we studied the DoA estimation problem in a single-element reconfigurable antenna system and experimentally evaluated its performance using MUSIC algorithm. We examined the effect of number of radiation states on the accuracy of the estimated DoA. We particularly considered different choices of the radiation states for estimating the DoA. We found out that as the angular distance between the radiation states increases, the estimation accuracy increases. Furthermore, we analyzed the BER performance of a reconfigurable SISO system employing an omnidirectional antenna at the transmitter and a reconfigurable antenna at the receiver. The impact of different parameters, including the DoA estimation error, angular spread and antenna beamwidth, on the BER of the reconfigurable SISO system was examined. Simulation results showed that the BER of the reconfigurable SISO system with fixed antenna beamwidth and angular spread increases due to error in DoA estimation. Moreover, it was shown that with small DoA estimation error, the system with smaller angular spread has a better performance than that with larger angular spread. However, for large DoA estimation error, this relationship is reversed. We also examined the BER performance of the system for different values of antenna beamwidth. While the BER of the system with narrower beamwidth has a better performance with small DoA estimation error, it is observed that with large DoA estimation error the system with wider beamwidth outperforms the system with narrow beamwidth.

CHAPTER 4

Performance Evaluation of Reconfigurable MIMO Systems in Spatially Correlated Frequency-Selective Fading Channels [1]

In the reconfigurable MIMO system, antennas at the transmitter and/or receiver are capable of changing their radiation properties such as frequency, polarization, and radiation pattern. In [6], it has been shown that the maximum achievable diversity offered by RE-MIMO systems employing reconfigurable antennas at the receiver only over flat fading channels, is equal to the product of number of transmit antennas, number of receive antennas and the number of states that the reconfigurable antennas can be configured. Moreover, in [36], a novel transmission scheme called space-time-state block code was proposed to exploit maximum diversity gain offered by a RE-MIMO system. However, these previous works have not addressed the frequency-selectivity problem of fading channels in a MIMO system equipped with reconfigurable antennas.

One conventional solution to frequency-selectivity problem of the wireless channel in MIMO systems is to use OFDM modulation which transforms the frequency-selective channel into a set of flat-fading channels. However, OFDM modulation generally requires an accurate synchronization, has high peak-to-average power ratio (PAPR), and demands high computational power due to multiple inverse fast Fourier transform and fast Fourier transform operations.

In this chapter, we propose a lower complexity MIMO system employing reconfigurable antennas at the receiver side with electronically controllable radiation patterns over the frequency-selective channels to mitigate multipath effects and therefore remove inter symbol interference without using OFDM modulation technique. In the proposed system, we assume that each element in the MIMO array is able to dynamically change its beam direction in a continuous manner from backfire to endfire. As an example of such element, we can refer to the CRLH-LWA which can provide electronically controllable dynamic radiation patterns with high directivity [76]. By integration of these elements in an array, we can have a system in which the elements steer their beams toward the selected clusters and attenuate the signals coming from the undesired clusters. As a result, the ISI can be effectively sup-

1. Part of the work presented in this chapter was published in:
   - V. Vakilian, J.-F. Frigon, and S. Roy, "Performance Evaluation of Reconfigurable MIMO Systems in Spatially Correlated Frequency-Selective Fading Channels", *Proc. IEEE Veh. Technol. Conf.*, Quebec City, QC, Canada, Sept. 2012. pp. 1–5.

pressed. Moreover, the STS-BC transmission scheme can be used in the RE-MIMO systems to achieve the same diversity order as space-time block coded MIMO-OFDM systems. To show the superiority of the proposed system, the bit-error rate performance of the coded RE-MIMO is compared with the performance of STBC-MIMO-OFDM system in the spatial clustered channel model that takes into account the impact of most of the physical parameters of wireless channels.

4.1 Spatial Channel Model

In this chapter, we consider a spatial channel model (SCM) which is a statistical-based model developed by 3GPP for evaluating MIMO system performance in urban micro-cell, urban macro-cell and suburban macro-cell fading environments [74]. This model takes into account the impact of several physical parameters of wireless channels such as direction-of-arrival, direction-of-departure (DoD), path power, antenna radiation patterns, angular and delay spread. The channel coefficient between transmitter antenna i and receiver antenna j for the l-th cluster, $l \in \{1, 2, \cdots, L\}$, is given by

$$\begin{aligned} h_{i,j}(l) &= \sqrt{\frac{P_l}{M}} \sum_{m=1}^{M} \alpha_l^m \sqrt{g_i^t(\theta_l^m)} e^{\jmath k_0 d_t (i-1) \sin(\theta_l^m)} \\ &\times \sqrt{g_j^r(\phi_l^m)} e^{\jmath k_0 d_r (j-1) \sin(\phi_l^m)}, \end{aligned} \tag{4.1}$$

where $\jmath = \sqrt{-1}$ is the imaginary unit, P_l is the power of the l-th cluster which is normalized so that the total average power for all clusters is equal to one, M is the number of unresolvable multipaths per cluster that have similar characteristics, $k_0 = 2\pi/\lambda$ is the free space wavenumber, where λ is the free-space wavelength, d_t and d_r are the antenna spacing between two elements at the transmitter and receiver side, respectively, α_l^m is the complex gain of the m-th multipath of the l-th path (the α_l^m are zero mean unit variance independent identically-distributed (i.i.d) complex random variables), $g_i^t(\theta_l^m)$ is the gains of i-th transmit antenna, and $g_j^r(\phi_l^m)$ is the gain of j-th receive antenna. θ_l^m and ϕ_l^m are the DoD and DoA for the m-th multipath of the l-th cluster, respectively, and can be given by

$$\theta_l^m = \theta_{l,DoD} + \vartheta_{l,DoD}^m, \tag{4.2}$$

$$\phi_l^m = \phi_{l,DoA} + \vartheta_{l,DoA}^m, \tag{4.3}$$

where $\theta_{l,DoD}$ and $\phi_{l,DoA}$ are the mean DoD and the mean DoA of the l^{th} cluster, respectively. The $\vartheta^m_{l,DoD}$ and $\vartheta^m_{l,DoA}$ are the deviation of the paths from mean DoD and DoA, respectively. The $\vartheta^m_{l,DoD}$ and $\vartheta^m_{l,DoA}$ are modeled as i.i.d. Gaussian random variables, with zero mean and variance σ^2_{DoD} and σ^2_{DoA}, respectively.

The channel impulse response between transmit antenna i and receive antenna j can then be modeled as

$$h_{i,j}(\tau) = \sum_{l=1}^{L} h_{i,j}(l)\delta(\tau - \tau_l), \tag{4.4}$$

where τ_l is the l-th cluster delay, and $h_{i,j}(l)$ is the complex amplitude of the l-th cluster defined in (4.1).

4.2 Space-Time-State coded RE-MIMO System in Frequency-Selective Channels

In this section, we consider a RE-MIMO system equipped with M_t omni-directional antenna elements at the transmitter and M_r directive reconfigurable antenna elements with P radiation pattern scan-step at the receiver. We assume that the mean DoA of the clusters are known at the receiver and in each radiation pattern scan-step, the reconfigurable antenna element steers toward a cluster as shown in Fig.4.1.

In the RE-MIMO system, the radiation pattern of received reconfigurable antenna at p-th scan-step is approximated in this section by a parabolic function that can be expressed as [17]

$$g^r_j(\phi^m_l, \psi^p_j) = \frac{2\pi}{B_{3dB}} 10^{0.1A(\phi^m_l, \psi^p_j)}, \tag{4.5}$$

where $A(\phi^m_l, \psi^p_j) = -\eta \left(\frac{\phi^m_l - \psi^p_j}{B_{3dB}}\right)^2$ in dB, η is a constant (set to 12 in [74]), B_{3dB} is the 3dB reconfigurable antenna beamwidth in radians, and ψ^p_j is the j-th received antenna pointing angle during p-th step. Therefore, the channel coefficient defined in (4.1) becomes a function of the antenna pointing angle and can be rewritten as

$$\begin{aligned} h^p_{i,j}(l, \psi^p_j) = \sqrt{\frac{P_l}{M}} \sum_{m=1}^{M} \alpha^m_l \sqrt{g^t_i(\theta^m_l)} e^{\jmath k_0 d_t (i-1)\sin(\theta^m_l)} \\ \times \sqrt{g^r_j(\phi^m_l, \psi^p_j)} e^{\jmath k_0 d_r (j-1)\sin(\phi^m_l)}. \end{aligned} \tag{4.6}$$

We assume a block fading channel, where the fading coefficients are time-invariant over each scan-step, and change independently from one scan-step to another. Each scan-step is

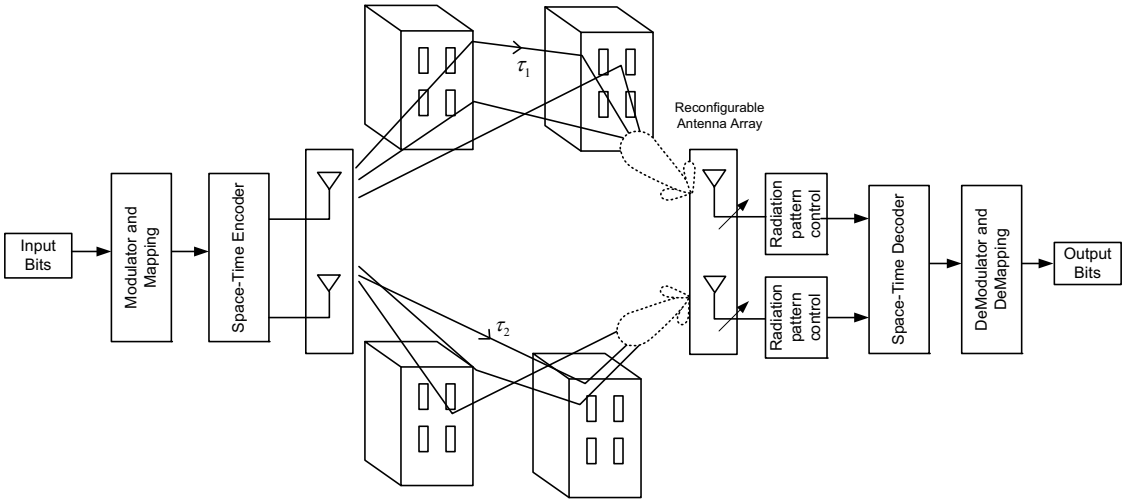

Figure 4.1 RE-MIMO system with $M_t = 2$, $M_r = 2$ and $L = 2$ clusters.

composed of K blocks of T time slots. To have a fair comparison with MIMO-OFDM, we consider $K = N_c/T$, where N_c is the number of OFDM subcarriers. At each scan-step p and time slots t in the k-th data block, the transmit codeword vector for the M_t antennas can be defined as,

$$\mathbf{c}^p(t,k) = [\mathbf{c}_1^p(t,k), \mathbf{c}_2^p(t,k), \cdots, \mathbf{c}_{M_t}^p(t,k)] \in \mathcal{C}^{1\times M_t} \tag{4.7}$$

where, $\mathbf{c}_i^p(t,k)$, for $i = 1, \cdots, M_t$, is the transmitted symbol at the p-th scan-step from i-th transmit antenna during t-th time slot of k-th block. At time t and scan-step p, the received antenna j is pointing to the mean DoA of a cluster such that $\psi_j^p = \phi_{l',DoA}$, where $l' \in \{1, 2, \cdots, L\}$. In this scenario, the received signal by antenna j within k-th block is given by

$$\begin{aligned} y_j^p(t,k) = & \overbrace{\sqrt{E_s}\mathbf{c}^p(t,k)\ \mathbf{h}_j^p(l',\psi_j^p)}^{\text{mainlobe}} \\ & + \underbrace{\sum_{l\neq l'} \sqrt{E_s}\mathbf{c}^p(t,k)\ \mathbf{h}_j^p(l,\psi_j^p)}_{\text{sidelobe}} + z_j^p(t,k), \end{aligned} \tag{4.8}$$

where E_s is the average energy per symbol at each transmit antenna, $z_j(t,k)$ is a zero mean complex AWGN at receive antenna j and time instant t with variance $\sigma_n^2/2$ per dimension.

In (4.8), $\mathbf{h}_j^p(l,\psi_j^p) \in \mathcal{C}^{M_t \times 1}$ is the channel vector given by

$$\mathbf{h}_j^p(l,\psi_j^p) \triangleq [h_{1,j}^p(l,\psi_j^p), h_{2,j}^p(l,\psi_j^p), \cdots, h_{M_t,j}^p(l,\psi_j^p)]^T. \tag{4.9}$$

After T time slots, the overall received signal during p-th scan-step and k-th block can be defined as $T \times M_r$ matrix, as below

$$\mathbf{Y}^p(k) \triangleq [\mathbf{y}_1^p(k), \mathbf{y}_2^p(k), \cdots, \mathbf{y}_{M_r}^p(k)], \tag{4.10}$$

where

$$\mathbf{y}_j^p(k) \triangleq [y_j^p(1,k), y_j^p(2,k), \cdots, y_j^p(T,k)]^T. \tag{4.11}$$

(4.10) can be computed as

$$\mathbf{Y}^p(k) = \sum_{l=1}^{L} \sqrt{E_s}\mathbf{C}^p(k)\ \mathbf{H}^p(l,\boldsymbol{\psi}^p) + \mathbf{Z}^p(k), \tag{4.12}$$

where

$$\mathbf{H}^p(l,\boldsymbol{\psi}^p) \triangleq [\mathbf{h}_1^p(l,\psi_1^p), \mathbf{h}_2^p(l,\psi_2^p), \cdots, \mathbf{h}_{M_r}^p(l,\psi_{M_r}^p)], \tag{4.13}$$

$$\boldsymbol{\psi}^p \triangleq [\psi_1^p, \psi_2^p, \cdots, \psi_{M_r}^p], \tag{4.14}$$

$$\mathbf{C}^p(k) \triangleq [\mathbf{c}(1,k)^T, \mathbf{c}(2,k)^T, \cdots, \mathbf{c}(T,k)^T]^T, \tag{4.15}$$

$$\mathbf{Z}^p(k) \triangleq [\mathbf{z}_1^p(k), \mathbf{z}_2^p(k), \cdots, \mathbf{z}_{M_r}^p(k)]. \tag{4.16}$$

The codeword transmitted over all P scan-steps can be expressed as

$$\mathbf{C} \triangleq \mathrm{diag}\{\mathbf{C}^1, \mathbf{C}^2, \cdots, \mathbf{C}^P\}, \tag{4.17}$$

where $\mathbf{C}^p \triangleq [\mathbf{C}^{p^T}(1), \mathbf{C}^{p^T}(2), \cdots, \mathbf{C}^{p^T}(K)]^T$ is the transmitted codeword during one scan-step. In this case, the received signal over over all P scan-steps $\mathbf{Y} \in \mathcal{C}^{PKT \times M_r}$ is given by

$$\mathbf{Y} = \sum_{l=1}^{L} \sqrt{E_s}\mathbf{C}\ \mathbf{H}(l,\boldsymbol{\psi}) + \mathbf{Z}, \tag{4.18}$$

where

$$\mathbf{H}(l,\boldsymbol{\psi}) \triangleq [\mathbf{H}^1(l,\boldsymbol{\psi}^1)^T, \mathbf{H}^2(l,\boldsymbol{\psi}^2)^T, \cdots, \mathbf{H}^P(l,\boldsymbol{\psi}^P)^T]^T, \tag{4.19}$$

$$\boldsymbol{\psi} \triangleq [\boldsymbol{\psi}^1, \boldsymbol{\psi}^2, \cdots, \boldsymbol{\psi}^P], \tag{4.20}$$

$$\mathbf{Z} \triangleq [\mathbf{Z}^1, \mathbf{Z}^2, \cdots, \mathbf{Z}^P]. \tag{4.21}$$

Now, as an example, consider a 2×2 RE-MIMO system in a two-cluster channel model with STS-BC scheme at the transmitter and reconfigurable antennas with $P = 2$ scan-steps at the receiver which is equal to the number of the clusters. In this scenario, in the first scan-step, the pointing angle of the first and second reconfigurable antenna elements at the receiver are $\psi_1^1 = \phi_{1,DoA}$ and $\psi_2^1 = \phi_{2,DoA}$, respectively, and in the next step, they will be $\psi_1^2 = \phi_{2,DoA}$ and $\psi_2^2 = \phi_{1,DoA}$. In this case, we define a vector containing the received signals at two consecutive scan-steps over the k-th block that can be expressed as

$$\begin{bmatrix} \mathbf{Y}^1(k) \\ \mathbf{Y}^2(k) \end{bmatrix} = \begin{bmatrix} \mathbf{C}^1(k) & \mathbf{0} \\ \mathbf{0} & \mathbf{C}^2(k) \end{bmatrix} \begin{bmatrix} \mathbf{H}^1(l,\boldsymbol{\psi}^1) \\ \mathbf{H}^2(l,\boldsymbol{\psi}^2) \end{bmatrix} + \begin{bmatrix} \mathbf{Z}^1(k) \\ \mathbf{Z}^2(k) \end{bmatrix}, \tag{4.22}$$

where $\mathbf{C}^p(k)$ is a quasi-orthogonal space-time-state block code given by [36] which can be represented as

$$\mathbf{C}^1(k) = \begin{bmatrix} s_1^k + \tilde{s}_3^k & s_2^k + \tilde{s}_4^k \\ -\left(s_2^k + \tilde{s}_4^k\right)^* & \left(s_1^k + \tilde{s}_3^k\right)^* \end{bmatrix},$$

$$\mathbf{C}^2(k) = \begin{bmatrix} s_1^k - \tilde{s}_3^k & s_2^k - \tilde{s}_4^k \\ -\left(s_2^k - \tilde{s}_4^k\right)^* & \left(s_1^k - \tilde{s}_3^k\right)^* \end{bmatrix}, \tag{4.23}$$

where s_1^k and s_2^k belong to a constellation $\mathcal{A}$ and $\tilde{s}_3^k$ and $\tilde{s}_4^k$ belong to the rotated constellation $e^{\jmath\theta}\mathcal{A}$, where θ is the optimal rotation angle and is equal to $\pi/2$ for BPSK. (4.22) can be decoupled into received signals from mainlobe and sidelobe. If we have more than two clusters and we to use the codeword built based on two scan-steps, then at the receiver, we configure the antenna to receive the signal from the two strongest clusters.

At the receiver, due to the independence of different blocks of data corresponding to different values of k, the ML decoding is reduced into independent ML decoding per block. In this case, ML decoding is performed to estimate the transmitted symbol by solving the following optimization problem

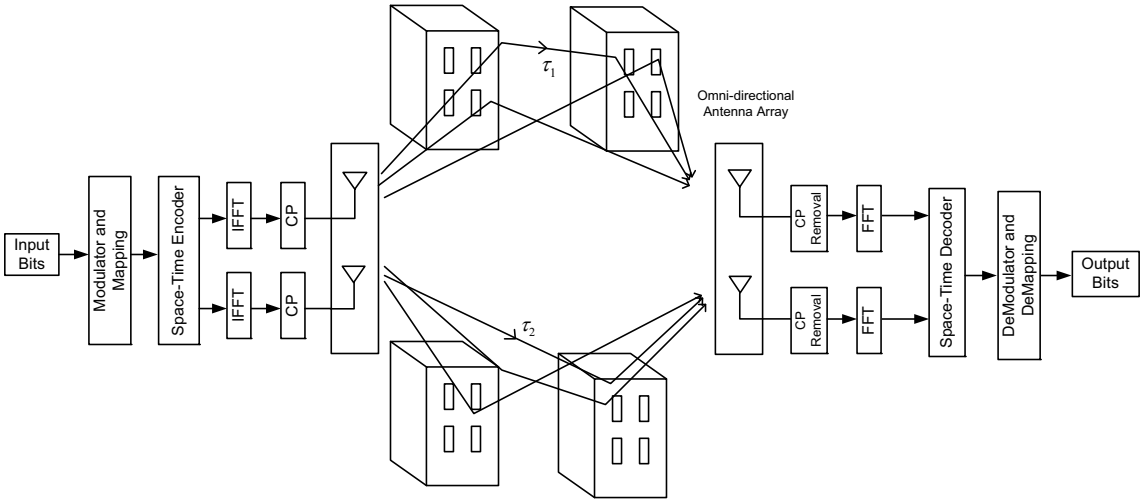

Figure 4.2 MIMO-OFDM system with $M_t = 2$, $M_r = 2$ and $L = 2$ clusters.

$$\arg\min \sum_{p=1}^{P} ||\mathbf{Y}^p(k) - \mathbf{C}^p(k)\mathbf{H}^p(l, \boldsymbol{\psi})||_F^2, \tag{4.24}$$

where $||.||_F$ denotes the Frobenius norm.

4.3 Space-Time Coded MIMO-OFDM System

In this section, we consider the MIMO-OFDM system with M_t omni-directional transmit antennas, M_r omni-directional receive antennas, and N_c subcarriers illustrated in Fig. 4.2. The frequency response of the channel impulse response defined in (4.4), is given

$$H_{i,j}(e^{\jmath \frac{2\pi}{N_c} n}) = \sum_{l=1}^{L} h_{i,j}(l) e^{-\jmath \frac{2\pi}{N_c} \tau_l n}, n = 0, 1, \cdots, N_c - 1 \tag{4.25}$$

At the transmitter, we consider STBC scheme to encode information and produce the codeword $\mathbf{c}^b(n) \triangleq [c_1^b(n), c_2^b(n), \cdots, c_{M_t}^b(n)]$, where $c_i^b(n)$ is the coded symbol transmitted from the i-th antenna on the b-th OFDM symbols and n-th subchannel. At the receiver, after the cyclic prefix removal and FFT, the frequency domain of the received signal at the j-th receive antenna and n-th subcarrier, where $n = 0, 1, \cdots, N_c - 1$ and $b = 1, 2, \cdots, B$, can be written as

$$y_j^b(n) = \sum_{i=1}^{M_t} \sqrt{E_s} c_i^b(n) H_{i,j}^b(e^{j\frac{2\pi}{N_c}n}) + z_j^b(n), \tag{4.26}$$

where $z_j^b(n)$ is the additive white Gaussian noise at the n-th subcarrier and the b-th OFDM symbol duration with variance $\sigma_n^2/2$ per dimension. We assume that the channel is quasi-static and remains constant for B OFDM symbols $\mathbf{H}^b(n) = \mathbf{H}(n) \in \mathcal{C}^{M_t \times M_r}$. Therefore, the received signal during b-th OFDM symbol duration $\mathbf{Y}^b \in \mathcal{C}^{N_c \times M_r}$ can be given as

$$\mathbf{Y}^b = \sqrt{E_s}\mathbf{C}^b\mathbf{H} + \mathbf{Z}^b, \tag{4.27}$$

where

$$\mathbf{C}^b \triangleq \text{diag}\{\mathbf{c}^b(0), \mathbf{c}^b(1), \cdots, \mathbf{c}^b(N_c-1)\}, \tag{4.28}$$

$$\mathbf{H} \triangleq [\mathbf{H}^T(0), \mathbf{H}^T(1), \cdots, \mathbf{H}(N_c-1)]^T. \tag{4.29}$$

Using Alamouti code [50], the transmission codeword for $M_t = 2$ transmit antenna and $B = 2$ OFDM symbols can be expressed as

$$\mathbf{C}^1 = \text{diag}\big\{[s_1, s_2], \cdots, [s_{2N_c-1}, s_{2N_c}]\big\}, \tag{4.30}$$

$$\mathbf{C}^2 = \text{diag}\big\{[-s_2^*, s_1^*], \cdots, [-s_{2N_c}^*, s_{2N_c-1}^*]\big\}. \tag{4.31}$$

Now, let $\underline{\mathbf{y}}_j(n) \triangleq [y_j^1(n)\ y_j^2(n)]^T$ be the signal received by j-th antenna during two consecutive OFDM symbols over the n-th subcarrier. Also, assume perfect channel information at the receiver. In this case, the ML decoding can be performed by solving the following minimization problem

$$\arg\min \sum_{j=1}^{M_r} |\underline{\mathbf{y}}_j(n) - \underline{\mathbf{c}}(n)\mathbf{H}_j(n)|^2, \tag{4.32}$$

where

$$\underline{\mathbf{c}}(n) = \begin{bmatrix} s_{2n+1} & s_{2n+2} \\ -s_{2n+2}^* & s_{2n+1}^* \end{bmatrix}, \tag{4.33}$$

is the transmitted codeword during two consecutive OFDM symbols over the n-th subcarrier and $\mathbf{H}_j(n)$ is the j-th column of channel matrix $\mathbf{H}(n)$.

4.4 Simulation Results

In order to compare the performance of RE-MIMO with MIMO-OFDM systems, the BER is computed by Monte Carlo simulations, while the same throughput and transmission power are considered for both systems. For all simulations, BPSK modulation is applied and the maximum likelihood decoding with perfect channel state information at the receiver is implemented. Furthermore, a two-cluster channel model according to (4.1), is considered in which each cluster is composed of $M = 20$ unresolvable multipaths. For RE-MIMO system, we consider two reconfigurable antenna elements at the transmitter where each element has two radiation pattern scan-steps and two omni-directional antennas at the receiver ($M_t = M_r = 2$, $P = 2$). We also perform simulations using the STS-BC given by (4.22). For MIMO-OFDM system, we consider two omni-directional antennas at the transmitter and two omni-directional antennas at the receiver ($M_t = M_r = 2$) and $N_c = 64$ subcarriers. Moreover, we use Alamouti coding scheme at the transmitter. For both RE-MIMO and MIMO-OFDM system, the inter-element spacing at the receiver and transmitter, is equal to $\lambda_c/2$, where $\lambda_c = c/f_c$ is the wavelength of the transmitted signal, f_c is the carrier frequency, and c is the light speed. The simulation parameters are listed in Table 4.1.

Fig. 4.3 shows the BER versus SNR for coded RE-MIMO and MIMO-OFDM system for various value of received angular spread (σ_{DoA}) and reconfigurable antenna beamwidth (B_{3dB}). From this figure, it can be observed that the diversity order is preserved in RE-MIMO system. Moreover, it is evident from the figure that for smaller angular spread at the receiver, the RE-MIMO systems perform extremely well, specially for narrower beamwidth, thanks to the power gain provided by directional reconfigurable antenna. However, for larger angular spread, the performance of the RE-MIMO system degrades due to much stronger contribution of undesired multipath components.

Fig. 4.4 depicts the bit error rate performance of coded RE-MIMO and MIMO-OFDM systems with different received angle spread values. In this simulation, we set the reconfigurable antenna beamwidth at $B_{3dB} = 35^\circ$ and SNR= 10 dB. From this figure, we observe that the BER performance of RE-MIMO system highly depends on the angular spread. When the angle spread is smaller than 18 degree, the RE-MIMO system outperforms the MIMO-OFDM system.

Table 4.1 Simulation parameters for the proposed RE-MIMO and MIMO-OFDM systems

Simulation parameters	
Carrier frequency (f_c)	3.484 GHz
Reconfigurable antenna Beamwidth (B_{3dB})	35&45°
Number of Tx and Rx antennas (N_t,N_r)	(2, 2)
Number of scan-steps (P)	2
Number of subcarriers (N_c)	64
Number of clusters (L)	2
Number of multipaths per cluster (M)	20
Cluster delay (τ_1, τ_2)	$(0.46, 0.89)$ μs
Cluster power (P_1, P_2)	$(0.53, 0.47)$
Cluster direction-of-departure ($\theta_{1,DoD}, \theta_{2,DoD}$)	$(6.6617°, -3.4544°)$
Cluster direction-of-arrival ($\phi_{1,DoA}, \phi_{2,DoA}$)	$(10°, 45°)$

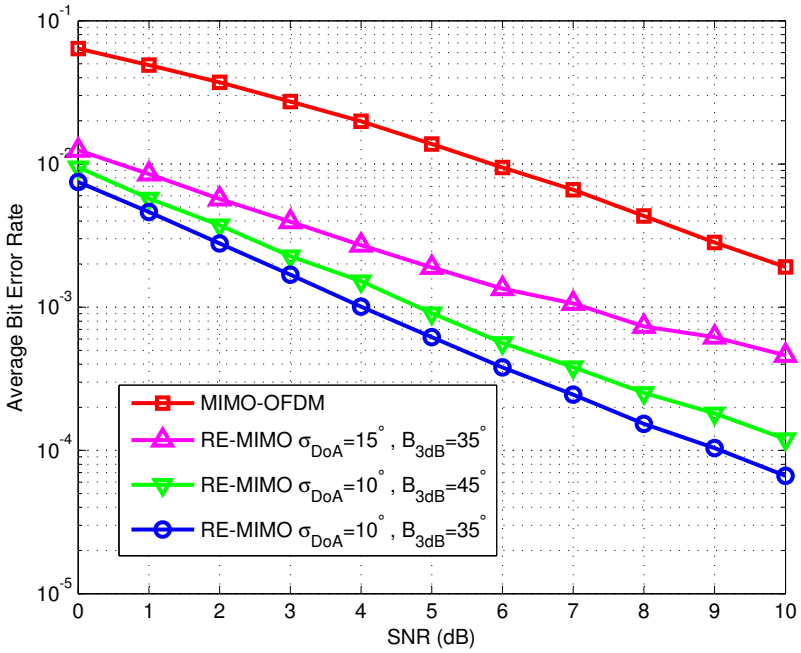

Figure 4.3 Average BER vs. SNR for RE-MIMO and MIMO-OFDM systems with $M_t = 2$, $M_r = 2$, $L = 2$, and angular spread of 10°.

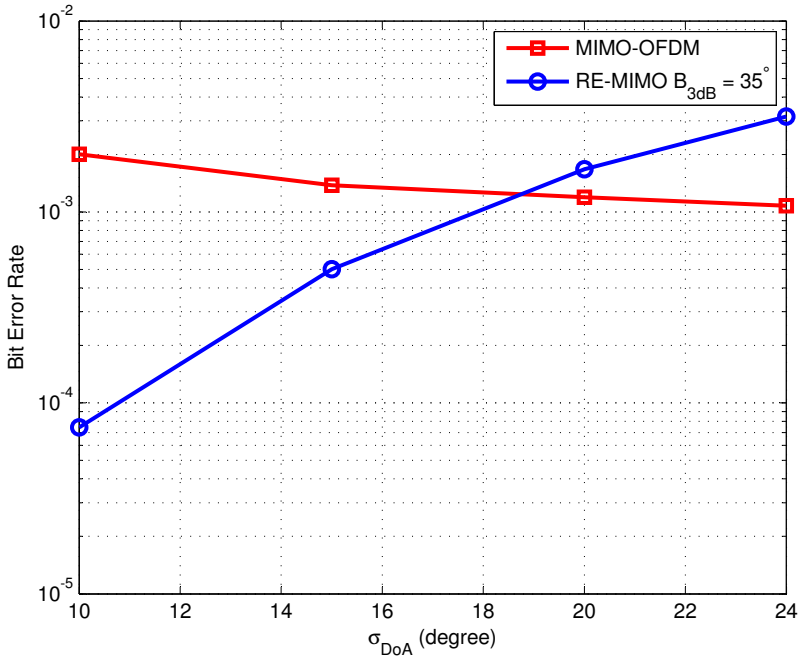

Figure 4.4 Average BER vs. received angular spread for RE-MIMO and MIMO-OFDM systems with $M_t = 2$, $M_r = 2$, and $L = 2$ clusters.

4.5 Conclusion

In this chapter, we evaluated the performance of the space-time-state block-coded RE-MIMO system in the spatially correlated frequency-selective fading channels. We also studied the impact of angular spread and antenna beamwidth on the performance of the system. Moreover, we compared the BER performance of the proposed system with that of MIMO-OFDM system. Simulation results show that as the angular spread decreases, the RE-MIMO system outperforms the MIMO-OFDM system. Furthermore, we observed the same conclusion for the antenna beamwidth, i.e., the performance of the RE-MIMO system improves as the antenna beamwidth decreases. Therefore, the proposed RE-MIMO represents a low complexity alternative to a MIMO-OFDM system and can even outperform it in certain channel environments and system configurations.

CHAPTER 5

Covariance Matrix and Capacity Evaluation of Reconfigurable Antenna Array Systems [1]

Over the past few years, studies have revealed that reconfigurable antennas can be used in conjunction with MIMO technology to further enhance the system capacity and reduce the deleterious effects of interference sources in wireless systems [1,3–11,77]. Unlike a phased array antenna (PAA) where the reconfigurable radiation pattern is created by properly feeding each element in the array, in a reconfigurable antenna array, each element can independently adjust its radiation pattern characteristics [78]. A reconfigurable antenna array, for example, can be used in the 802.11ad standard to replace the PAA for 60 GHz wireless gigabit networks, where a directional multi-gigabit beamforming protocol enables the transmitter and receiver to configure the antenna radiation patterns in real-time [15].

Similar to conventional MIMO wireless systems, the performance of a reconfigurable MIMO wireless system is affected by the correlation between the signals impinging on the antenna elements [26]. The correlation coefficients depend on several factors, including the signal spatial distribution, the antenna array topology and the radiation pattern characteristics of each element in the array. In general, these coefficients are computed using two main approaches, namely, numerical and analytical solutions. Works in the first category focus on finding the signal correlation through numerical schemes (e.g., numerical integrations and Monte-Carlo simulations) which are computationally intensive and need long processing time to obtain the solutions [27–32]. In contrast, analytical expressions are computationally more reliable and require shorter processing time.

The authors in [33] derived exact expressions to compute the spatial correlation coefficients for ULA with different spatial distribution assumptions on signal angles of arrival/departure. A similar work was conducted in [34], where the authors proposed closed-form expressions of the spatial correlation matrix in clustered MIMO channels. These works have considered omni-directional antenna elements in their derivation and consequently overlooked the antenna radiation pattern characteristics. In [35], the authors derived an analytical correlation expression for directive antennas with a multimodal truncated Laplacian power azimuth spectrum (PAS). In their analysis, however, they have only considered identical fixed directive

1. Part of the work presented in this chapter was published in:
   - V. Vakilian, J.-F. Frigon, and S. Roy, "Closed-Form Expressions for the Covariance Matrix of a Reconfigurable Antenna System", *IEEE Trans. Wireless Commun.*, vol. 13, pp. 3452-3463, June 2014.

radiation patterns for all elements.

In this chapter, we derive analytical expressions of the covariance matrix coefficients of the received signals at the antenna array by taking into account several antenna characteristics such as beamwidth, antenna spacing, antenna pointing angle, and antenna gain. In particular, we consider the more realistic and practical scenario where the radiation pattern of each antenna element in the array has different characteristics. This is in contrast with previous works where all antenna elements have the same radiation patterns, which is not applicable for advanced RE-MIMO systems employing independent reconfigurable antennas. Part of the challenge in derivation of analytical expressions comes from the fact that due to the continuous and independent beam steering feature of each antenna element, there are numerous configurations for which the correlation coefficients need to be found. We derive analytical expressions for computing these coefficients for all possible configurations. Unlike computing intensive numerical integrations to directly evaluate the covariance matrix coefficients, the analytical expressions derived in this chapter converge rapidly and can be used, for example, in real-time RE-MIMO wireless system implementations to quickly choose the optimal configuration for each reconfigurable antenna element in the array, leading to the highest system performance. This is a significant gain for practical implementations of communication systems using reconfigurable antenna arrays. We furthermore use the derived analytical expressions to analyze the capacity of RE-MIMO systems equipped with reconfigurable antennas and discuss its relation with the antennas radiation pattern configuration and channel power angular spectrum characteristics.

5.1 Modeling and Problem Formulation

Consider a reconfigurable antenna array with N_r elements, where the radiation pattern of the m-th element can be characterized using the following parabolic function [74]:

$$g_m(\phi, \boldsymbol{\Theta_m}) = \max\left[G_m e^{-\alpha_m(\phi-\psi_m)^2}, g_{c_m}\right]. \tag{5.1}$$

In this model, $\boldsymbol{\Theta}_m = [\psi_m, G_m, B_m]$ is a vector of parameters related to the antenna radiation pattern, ψ_m denotes the pointing angle of the antenna (i.e., the azimuth angle with maximum gain), G_m is the antenna gain, B_m is the 3-dB antenna beamwidth, $\phi \in [\psi_m - \pi, \psi_m + \pi)$ represents the azimuth angle, $\alpha_m = (\eta \ln 10)/(10B_m^2)$ with $\eta = 12$, and g_{c_m} is the constant gain of the antenna sidelobe. To simplify the notation, we use

$$g_{p_m} = G_m e^{-\alpha_m(\phi-\psi_m)^2} \tag{5.2}$$

to refer to the parabolic part of the antenna radiation pattern.

Let $x(k,\phi)$ denote the impinging signal that has a PAS defined as follows:

$$p(\phi) = \mathbb{E}_{k|\phi}\Big[|x(k,\phi)|^2\Big], \tag{5.3}$$

where $p(\phi)$ is a multimodal truncated Laplacian PAS [79]. In the multimodal PAS, each mode represents a resolvable multipath signal reflecting from a given cluster over the space. We express the multimodal truncated Laplacian PAS with L modes as

$$p(\phi) = \sum_{l=1}^{L} p_l(\phi), \tag{5.4}$$

where $p_l(\phi)$ is the truncated Laplacian distribution of the l-th mode, given by

$$p_l(\phi) = \begin{cases} \frac{b_l}{\sqrt{2}\sigma_l} e^{-\sqrt{2}|\phi-\phi_0^l|/\sigma_l}, & \text{for } \phi \in [\phi_0^l - \triangle_l, \phi_0^l + \triangle_l), \\ 0, & \text{otherwise,} \end{cases} \tag{5.5}$$

in which ϕ_0^l is the DoA of the l-th mode, σ_l is the standard deviation of the PAS, $0 \leq \triangle_l \leq \pi$ is the truncation angle, and $b_l = P_l/\big(1 - e^{-\sqrt{2}\triangle_l/\sigma_l}\big)$ is the PAS normalization factor. In this representation, P_l is chosen such that $\sum_{l=1}^{L} P_l = 1$.

Fig. 5.1 illustrates the geometry of a plane wave signal impinging on two reconfigurable elements. The dashed and the solid parabolic curves represent the radiation pattern of the m-th and n-th elements, respectively. The dotted-dashed line shows the PAS of the arriving signal from the l-th mode. As illustrated in this figure, ϕ_{c_i} is the intersect angle, where the parabolic part of the radiation pattern crosses the constant part and can be computed as

$$\phi_{c_i} = B_i \sqrt{\frac{g_{c_i}[\text{dB}]}{\eta}}, \tag{5.6}$$

where $g_{c_i}[\text{dB}]$ is the sidelobe gain in dB.

We assume that the signal received by the m-th antenna at time instant k is expressed by

$$r_m(k, \boldsymbol{\Theta_m}) = x(k,\phi)\sqrt{g_m(\phi, \boldsymbol{\Theta_m})} e^{jk_0 d_r (m-1)\sin(\phi)}, \tag{5.7}$$

where $x(k,\phi)$ is the impinging wave signal with multimodal truncated Laplacian distribution, $k_0 = 2\pi/\lambda$ is the free-space wavenumber, λ is the free-space wavelength, and d_r is the antenna spacing at the receiver sides.

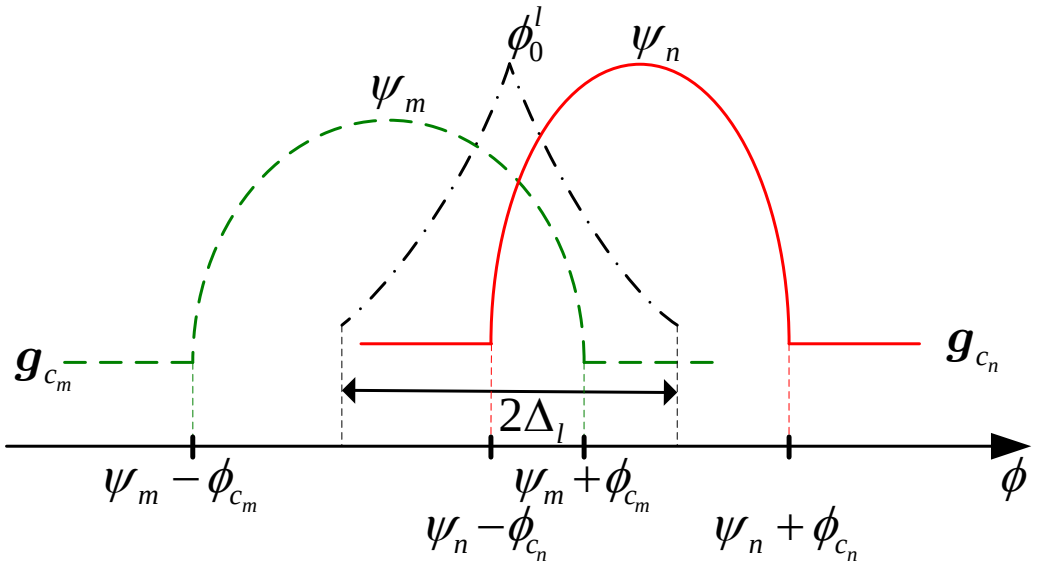

Figure 5.1 PAS and the reconfigurable antenna radiation patterns

5.2 Closed-Form Expressions for Covariance Matrix Coefficients

In this section, we derive analytical expressions to compute the covariance matrix of the signals received by the reconfigurable antenna array. Let us define $\boldsymbol{\Theta} = [\boldsymbol{\Theta}_1 \dots \boldsymbol{\Theta}_{N_r}]$ as the vector of reconfigurable parameters for all receive antennas. Then, the (m,n)-th coefficient of $\mathbf{R}_r(\boldsymbol{\Theta}) \in \mathbb{C}^{N_r \times N_r}$, for $m \neq n$, can be expressed as

$$[\mathbf{R}_r]_{m,n}(\boldsymbol{\Theta}_m, \boldsymbol{\Theta}_n) = \mathbb{E}_{k,\phi}\Big\{r_m(k,\boldsymbol{\Theta}_m) r_n^*(k,\boldsymbol{\Theta}_n)\Big\} - \mathbb{E}_{k,\phi}\Big\{r_m(k,\boldsymbol{\Theta}_m)\Big\}\mathbb{E}\Big\{r_n^*(k,\boldsymbol{\Theta}_n)\Big\}, \quad (5.8)$$

where

$$\mathbb{E}_{k,\phi}\Big\{r_m(k,\boldsymbol{\Theta}_m) r_n^*(k,\boldsymbol{\Theta}_n)\Big\} = \mathbb{E}_{k,\phi}\Big\{|x(k,\phi)|^2 \sqrt{g_m(\phi,\boldsymbol{\Theta}_m)}\sqrt{g_n(\phi,\boldsymbol{\Theta}_n)} e^{jk_0(m-n)d_r \sin(\phi)}\Big\}, \quad (5.9)$$

and

$$\mathbb{E}_{k,\phi}\Big\{r_i(k,\boldsymbol{\Theta}_i)\Big\} = \mathbb{E}_{k,\phi}\Big\{x(k,\phi)\sqrt{g_i(\phi,\boldsymbol{\Theta}_i)} e^{jk_0 d_r (i-1)\sin(\phi)}\Big\},\ i \in \{m,n\}. \quad (5.10)$$

Since $x(k,\phi)$ is zero mean in any azimuth ϕ and independent of antenna characteristics, e.g., beamwidth, gain and pointing angle, $\mathbb{E}_{k,\phi}\Big\{r_i(k,\boldsymbol{\Theta}_i)\Big\}$, for $i \in \{m,n\}$, becomes zero and subsequently, (5.8) can be rewritten as

$$[\mathbf{R}_r]_{m,n}(\boldsymbol{\Theta}_m,\boldsymbol{\Theta}_n) = \mathbb{E}_{k,\phi}\Big\{r_m(k,\boldsymbol{\Theta}_m)r_n^*(k,\boldsymbol{\Theta}_n)\Big\}$$
$$= \mathbb{E}_{\phi}\Big\{\mathbb{E}_{k|\phi}\big[|x(k,\phi)|^2\big]\sqrt{g_m(\phi,\boldsymbol{\Theta}_m)}\sqrt{g_n(\phi,\boldsymbol{\Theta}_n)}e^{jk_0(m-n)d_r\sin(\phi)}\Big\}, \quad (5.11)$$
$$= \int \sqrt{g_m(\phi,\boldsymbol{\Theta}_m)}\sqrt{g_n(\phi,\boldsymbol{\Theta}_n)}e^{jk_0d_r(m-n)\sin(\phi)}p(\phi)\,d\phi. \quad (5.12)$$

By replacing (5.5) in the above equation, we can compute the covariance coefficient as follows:

$$[\mathbf{R}_r]_{m,n}(\boldsymbol{\Theta}_m,\boldsymbol{\Theta}_n) = \sum_{l=1}^{L}\frac{b_l}{\sqrt{2}\sigma_l}\int_{\phi_0^l-\triangle_l}^{\phi_0^l+\triangle_l}\sqrt{g_m(\phi,\boldsymbol{\Theta}_m)}\sqrt{g_n(\phi,\boldsymbol{\Theta}_n)}e^{jk_0d_r(m-n)\sin(\phi)}p_l(\phi)\,d\phi,$$
$$= \sum_{l=1}^{L}\frac{b_l}{\sqrt{2}\sigma_l}[\boldsymbol{\mathcal{R}}_r^l]_{m,n}(\boldsymbol{\Theta}_m,\boldsymbol{\Theta}_n). \quad (5.13)$$

Considering the following identity [80],

$$e^{jD_r\sin(\phi)} = J_0(D_r) + 2\sum_{k=1}^{\infty}J_{2k}(D_r)\cos(2k\phi) + 2j\sum_{k=0}^{\infty}J_{2k+1}(D_r)\sin[(2k+1)\phi]. \quad (5.14)$$

where $D_r = k_0d_r(m-n)$ and $J_m(\cdot)$ is the Bessel function of the first kind of order m, the expression in (5.13) can be rewritten as

$$[\boldsymbol{\mathcal{R}}_r^l]_{m,n}(\boldsymbol{\Theta}_m,\boldsymbol{\Theta}_n) = J_0(D_r)\Lambda_o^{l,k}(\boldsymbol{\Theta}_m,\boldsymbol{\Theta}_n)$$
$$+ 2\sum_{k=1}^{\infty}J_{2k}(D_r)\Lambda_c^{l,k}(\boldsymbol{\Theta}_m,\boldsymbol{\Theta}_n)$$
$$+ 2j\sum_{k=0}^{\infty}J_{2k+1}(D_r)\Lambda_s^{l,k}(\boldsymbol{\Theta}_m,\boldsymbol{\Theta}_n). \quad (5.15)$$

In this expression, $\Lambda_o^{l,k}(\boldsymbol{\Theta}_m,\boldsymbol{\Theta}_n)$ (the index k is arbitrary and only included to conform with the two other functions), $\Lambda_c^{l,k}(\boldsymbol{\Theta}_m,\boldsymbol{\Theta}_n)$ and $\Lambda_s^{l,k}(\boldsymbol{\Theta}_m,\boldsymbol{\Theta}_n)$ are defined as:

$$\Lambda_o^{l,k}(\boldsymbol{\Theta}_m,\boldsymbol{\Theta}_n) = \int_{\phi_0^l-\triangle_l}^{\phi_0^l+\triangle_l}\sqrt{g_m(\phi,\psi_m)}\sqrt{g_n(\phi,\psi_n)}p_l(\phi)d\phi, \quad (5.16)$$
$$\Lambda_c^{l,k}(\boldsymbol{\Theta}_m,\boldsymbol{\Theta}_n) = \int_{\phi_0^l-\triangle_l}^{\phi_0^l+\triangle_l}\cos[2k\phi]\sqrt{g_m(\phi,\psi_m)}\sqrt{g_n(\phi,\psi_n)}p_l(\phi)d\phi, \quad (5.17)$$
$$\Lambda_s^{l,k}(\boldsymbol{\Theta}_m,\boldsymbol{\Theta}_n) = \int_{\phi_0^l-\triangle_l}^{\phi_0^l+\triangle_l}\sin[(2k+1)\phi]\sqrt{g_m(\phi,\psi_m)}\sqrt{g_n(\phi,\psi_n)}p_l(\phi)d\phi. \quad (5.18)$$

The (m,m)-th element of $\mathbf{R}_r(\boldsymbol{\Theta})$ can be computed as

$$\begin{aligned}[\mathbf{R}_r]_{m,m}(\boldsymbol{\Theta}_m,\boldsymbol{\Theta}_m) &= \mathbb{E}\Big\{|x(k,\phi)|^2 g_m(\phi,\boldsymbol{\Theta}_m)\Big\} \\ &= \int g_m(\phi,\boldsymbol{\Theta}_m)p(\phi)\,d\phi \qquad (5.19)\\ &= \sum_{l=1}^{L}\frac{b_l}{\sqrt{2}\sigma_l}[\boldsymbol{\mathcal{R}}_r^l]_{m,m}(\boldsymbol{\Theta}_m,\boldsymbol{\Theta}_m), \qquad (5.20)\end{aligned}$$

where $[\boldsymbol{\mathcal{R}}_r^l]_{m,m}(\boldsymbol{\Theta}_m,\boldsymbol{\Theta}_m)$ is given by

$$\begin{aligned}[\boldsymbol{\mathcal{R}}_r^l]_{m,m}(\boldsymbol{\Theta}_m,\boldsymbol{\Theta}_m) &= \int_{\phi_0^l-\triangle_l}^{\phi_0^l+\triangle_l} g_m(\phi,\boldsymbol{\Theta}_m)p_l(\phi)\,d\phi \\ &= \Xi^l(\boldsymbol{\Theta}_m), \qquad (5.21)\end{aligned}$$

To arrive at analytical expressions for the covariance coefficients, $\Lambda_i^{l,k}(\boldsymbol{\Theta}_m,\boldsymbol{\Theta}_n)$, $i\in\{o,s,c\}$ and $\Xi^l(\boldsymbol{\Theta}_m)$ in (5.15) and (5.21), respectively, need to be analytically computed. As shown in Fig. 5.1, the PAS and the radiation patterns are discontinuous functions. To evaluate the functions $\Lambda_i^{l,k}(\boldsymbol{\Theta}_m,\boldsymbol{\Theta}_n)$ and $\Xi^l(\boldsymbol{\Theta}_m)$, we therefore need to separate the different cases depending on how the PAS and the radiation patterns overlap. We assume that the antennas are ordered such that $\psi_m<\psi_n$ and $g_{c_i}=\beta$ for all $i\in\{1,\cdots,N_r\}$. We also assume that the radiation patterns of both reconfigurable antennas overlap ($\psi_n-\phi_c<\psi_m+\phi_c$). The results that we present below could be readily extended to non-overlapping radiation patterns using the same strategy. Due to the parabolic decrease in the radiation pattern gain and the exponential PAS decrease, the tail-end effects on the covariance coefficients are neglected. This approximation is justified by the close agreement between the analytical and numerical evaluation results.

Remark 5.1: In this work, we compute the covariance matrix coefficients for the case where only the receiver side is equipped with reconfigurable antennas. However, since the method to compute the transmit and receive correlation matrix is the same [34], the results presented in this chapter can also be used to compute the transmit-side covariance matrix by replacing the arrival PAS with the departure PAS.

Let us first define $f_o(\phi)=1$, $f_s(\phi)=\sin[(2k+1)\phi]$, $f_c(\phi)=\cos(2k\phi)$, and the following functions for $i\in\{o,s,c\}$:

$$f_i g_{c_m} g_{c_n} p_L(A,B) = \int_A^B f_i(\phi)\beta e^{-\frac{\sqrt{2}(\phi_0^l-\phi)}{\sigma_l}}d\phi \qquad (5.22)$$

$$f_i g_{c_m} g_{c_n} p_R(A,B) = \int_A^B f_i(\phi)\beta e^{-\frac{\sqrt{2}(\phi-\phi_0^l)}{\sigma_l}} d\phi \tag{5.23}$$

$$f_i g_{p_m} g_{c_n} p_L(A,B) = \int_A^B f_i(\phi)\sqrt{\beta}\sqrt{G_m e^{-\alpha_m(\phi-\psi_m)^2}} \times e^{-\frac{\sqrt{2}(\phi_0^l-\phi)}{\sigma_l}} d\phi \tag{5.24}$$

$$f_i g_{p_m} g_{c_n} p_R(A,B) = \int_A^B f_i(\phi)\sqrt{\beta}\sqrt{G_m e^{-\alpha_m(\phi-\psi_m)^2}} \times e^{-\frac{\sqrt{2}(\phi-\phi_0^l)}{\sigma_l}} d\phi \tag{5.25}$$

$$f_i g_{p_m} g_{p_n} p_L(A,B) = \int_A^B f_i(\phi)\sqrt{G_m e^{-\alpha_m(\phi-\psi_m)^2}} \times \sqrt{G_n e^{-\alpha_n(\phi-\psi_n)^2}} e^{-\frac{\sqrt{2}(\phi_0^l-\phi)}{\sigma_l}} d\phi \tag{5.26}$$

$$f_i g_{p_m} g_{p_n} p_R(A,B) = \int_A^B f_i(\phi)\sqrt{G_m e^{-\alpha_m(\phi-\psi_m)^2}} \times \sqrt{G_n e^{-\alpha_n(\phi-\psi_n)^2}} e^{-\frac{\sqrt{2}(\phi-\phi_0^l)}{\sigma_l}} d\phi \tag{5.27}$$

$$f_i g_{c_m} g_{p_n} p_L(A,B) = \int_A^B f_i(\phi)\sqrt{\beta}\sqrt{G_n e^{-\alpha_n(\phi-\psi_n)^2}} \times e^{-\frac{\sqrt{2}(\phi_0^l-\phi)}{\sigma_l}} d\phi \tag{5.28}$$

$$f_i g_{c_m} g_{p_n} p_R(A,B) = \int_A^B f_i(\phi)\sqrt{\beta}\sqrt{G_n e^{-\alpha_n(\phi-\psi_n)^2}} \times e^{-\frac{\sqrt{2}(\phi-\phi_0^l)}{\sigma_l}} d\phi. \tag{5.29}$$

In Appendix C, we evaluate the above integrals for computing $\Lambda_i^{l,k}(\boldsymbol{\Theta}_m, \boldsymbol{\Theta}_n)$.

Depending on the angle of incidence, ϕ, and the pointing angle of each reconfigurable antenna element, ψ_i, for $i \in \{m, n\}$, different integration areas emerge. Below, we evaluate $\Lambda_i^{l,k}(\boldsymbol{\Theta}_m, \boldsymbol{\Theta}_n)$ for all possible cases.

1) $\phi_0^l + \triangle_l < \psi_m - \phi_c$

As illustrated in Fig. 5.1, in this case, the PAS is in the far left and completely out of the scope of the parabolic part of the m-th reconfigurable antenna radiation pattern. We then have:

$$\Lambda_i^{l,k}(\boldsymbol{\Theta}_m, \boldsymbol{\Theta}_n) = f_i g_{c_m} g_{c_n} p_L(\phi_0^l - \triangle_l, \phi_0^l) + f_i g_{c_m} g_{c_n} p_R(\phi_0^l, \phi_0^l + \triangle_l). \tag{5.30}$$

2) $\phi_0^l < \psi_m - \phi_c < \phi_0^l + \triangle_l$

In this case, only half of the PAS is within the parabolic part of the radiation pattern of the reconfigurable antenna m. The PAS may be covered with the radiation pattern of antenna

n. We then have:

$$\begin{aligned}\Lambda_i^{l,k}(\boldsymbol{\Theta}_m,\boldsymbol{\Theta}_n) = {} & f_i g_{c_m} g_{c_n} p_L\Big(\phi_0^l - \triangle_l, \phi_0^l\Big) \\ & + f_i g_{c_m} g_{c_n} p_R\Big(\phi_0^l, \psi_m - \phi_c\Big) \\ & + f_i g_{p_m} g_{c_n} p_R\Big(\psi_m - \phi_c, \min(\phi_0^l + \triangle_l, \psi_n - \phi_c)\Big) \\ & + f_i g_{p_m} g_{p_n} p_R\Big(\min(\phi_0^l + \triangle_l, \psi_n - \phi_c), \min(\phi_0^l + \triangle_l, \psi_m + \phi_c)\Big) \\ & + f_i g_{c_m} g_{p_n} p_R\Big(\min(\phi_0^l + \triangle_l, \psi_m + \phi_c), \min(\phi_0^l + \triangle_l, \psi_n + \phi_c)\Big) \\ & + f_i g_{c_m} g_{c_n} p_R\Big(\min(\phi_0^l + \triangle_l, \psi_n + \phi_c), \phi_0^l + \triangle_l\Big). \end{aligned} \tag{5.31}$$

3) $\psi_m - \phi_c < \phi_0^l < \psi_n - \phi_c$

In this case, both halves of the PAS are within the parabolic part of the radiation pattern of the antenna m. Obviously, the PAS is also within the coverage of antenna n. We then have:

$$\begin{aligned}\Lambda_i^{l,k}(\boldsymbol{\Theta}_m,\boldsymbol{\Theta}_n) = {} & f_i g_{c_m} g_{c_n} p_L\Big(\phi_0^l - \triangle_l, \max(\phi_0^l - \triangle_l, \psi_m - \phi_c)\Big) \\ & + f_i g_{p_m} g_{c_n} p_L\Big(\max(\phi_0^l - \triangle_l, \psi_m - \phi_c), \phi_0^l\Big) \\ & + f_i g_{p_m} g_{c_n} p_R\Big(\phi_0^l, \min(\phi_0^l + \triangle_l, \psi_n - \phi_c)\Big) \\ & + f_i g_{p_m} g_{p_n} p_R\Big(\min(\phi_0^l + \triangle_l, \psi_n - \phi_c), \min\big(\phi_0^l + \triangle_l, \min(\phi_0^l + \triangle_l, \psi_m + \phi_c)\big)\Big) \\ & + f_i g_{c_m} g_{p_n} p_R\Big(\min(\phi_0^l + \triangle_l, \psi_m + \phi_c), \min(\phi_0^l + \triangle_l, \psi_n + \phi_c)\Big) \\ & + f_i g_{c_m} g_{c_n} p_R\Big(\min(\phi_0^l + \triangle_l, \psi_n + \phi_c), \phi_0^l + \triangle_l\Big), \end{aligned} \tag{5.32}$$

4) $\psi_n - \phi_c < \phi_0^l < \psi_m + \phi_c$

In this case, both halves of the PAS are within the parabolic part of the radiation pattern of both antennas. We then have:

$$\begin{aligned}\Lambda_i^{l,k}(\boldsymbol{\Theta}_m,\boldsymbol{\Theta}_n) = {} & f_i g_{c_m} g_{c_n} p_L\Big(\phi_0^l - \triangle_l, \max(\phi_0^l - \triangle_l, \psi_m - \phi_c)\Big) \\ & + f_i g_{p_m} g_{c_n} p_L\Big(\max(\phi_0^l - \triangle_l, \psi_m - \phi_c), \max(\phi_0^l - \triangle_l, \psi_n - \phi_c)\Big) \\ & + f_i g_{p_m} g_{p_n} p_L\Big(\max(\phi_0^l - \triangle_l, \psi_n - \phi_c), \phi_0^l\Big) \\ & + f_i g_{p_m} g_{p_n} p_R\Big(\phi_0^l, \min(\phi_0^l + \triangle_l, \psi_n + \phi_c)\Big) \\ & + f_i g_{c_m} g_{p_n} p_R\Big(\min(\phi_0^l + \triangle_l, \psi_m + \phi_c), \min(\phi_0^l + \triangle_l, \psi_n + \phi_c)\Big) \\ & + f_i g_{c_m} g_{c_n} p_R\Big(\min(\phi_0^l + \triangle_l, \psi_n + \phi_c), \phi_0^l + \triangle_l\Big), \end{aligned} \tag{5.33}$$

5) $\psi_m + \phi_c < \phi_0^l < \psi_n + \phi_c$

In this case, both halves of the PAS are within the parabolic part of the radiation pattern of the reconfigurable antenna n. The PAS may be covered with the radiation pattern of antenna m. We then have:

$$\begin{aligned}\Lambda_i^{l,k}(\boldsymbol{\Theta}_m, \boldsymbol{\Theta}_n) = {} & f_i g_{c_m} g_{c_n} p_L\Big(\phi_0^l - \triangle_l, \max(\phi_0^l - \triangle_l, \psi_m - \phi_c)\Big) \\ & + f_i g_{p_m} g_{c_n} p_L\Big(\max(\phi_0^l - \triangle_l, \psi_m - \phi_c), \max(\phi_0^l - \triangle_l, \psi_n - \phi_c)\Big) \\ & + f_i g_{p_m} g_{p_n} p_L\Big(\max(\phi_0^l - \triangle_l, \psi_n - \phi_c), \max(\phi_0^l - \triangle_l, \psi_m + \phi_c)\Big) \\ & + f_i g_{c_m} g_{p_n} p_L\Big(\max(\phi_0^l - \triangle_l, \psi_m + \phi_c), \phi_0^l\Big) \\ & + f_i g_{c_m} g_{p_n} p_R\Big(\phi_0^l, \min(\phi_0^l + \triangle_l, \psi_n + \phi_c)\Big) \\ & + f_i g_{c_m} g_{c_n} p_R\Big(\min(\phi_0^l + \triangle_l, \psi_n + \phi_c), \phi_0^l + \triangle_l\Big), \end{aligned} \tag{5.34}$$

6) $\phi_0^l - \triangle_l < \psi_n + \phi_c < \phi_0^l$

In this case, only half of the PAS is within the parabolic part of the radiation pattern of the reconfigurable antenna with larger pointing angle. We then have:

$$\begin{aligned}\Lambda_i^{l,k}(\boldsymbol{\Theta}_m, \boldsymbol{\Theta}_n) = {} & f_i g_{c_m} g_{c_n} p_L\Big(\phi_0^l - \triangle_l, \max(\phi_0^l - \triangle_l, \psi_m - \phi_c)\Big) \\ & + f_i g_{p_m} g_{c_n} p_L\Big(\max(\phi_0^l - \triangle_l, \psi_m - \phi_c), \max(\phi_0^l - \triangle_l, \psi_n - \phi_c)\Big) \\ & + f_i g_{p_m} g_{p_n} p_L\Big(\max(\phi_0^l - \triangle_l, \psi_n - \phi_c), \max(\phi_0^l - \triangle_l, \psi_m + \phi_c)\Big) \\ & + f_i g_{c_m} g_{p_n} p_L\Big(\max(\phi_0^l - \triangle_l, \psi_m + \phi_c), \psi_n + \phi_c\Big) \\ & + f_i g_{c_m} g_{c_n} p_L\Big(\psi_n + \phi_c, \phi_0^l\Big) \\ & + f_i g_{c_m} g_{c_n} p_R\Big(\phi_0^l, \phi_0^l + \triangle_l\Big), \end{aligned} \tag{5.35}$$

7) $\phi_0^l - \triangle_l > \psi_n + \phi_c$

In this case, the PAS is completely out of the scope of the parabolic part of the reconfigurable antenna radiation pattern with larger pointing angle. We then have:

$$\Lambda_i^{l,k}(\boldsymbol{\Theta}_m, \boldsymbol{\Theta}_n) = f_i g_{c_m} g_{c_n} p_L(\phi_0^l - \triangle_l, \phi_0^l) + f_i g_{c_m} g_{c_n} p_R(\phi_0^l, \phi_0^l + \triangle_l). \tag{5.36}$$

As explained previously, the computation of $\Xi^l(\boldsymbol{\Theta}_m)$ involves evaluating integrals that correspond to PAS areas which are impacted with only one of the antenna radiation patterns.

Let us first define the following functions:

$$g_{c_m} g_{c_m} p_L(A, B) = \int_A^B \beta e^{-\frac{\sqrt{2}(\phi_0^l - \phi)}{\sigma_l}} d\phi, \tag{5.37}$$

$$g_{c_m} g_{c_m} p_R(A, B) = \int_A^B \beta e^{-\frac{\sqrt{2}(\phi - \phi_0^l)}{\sigma_l}} d\phi, \tag{5.38}$$

$$g_{p_m} g_{p_m} p_L(A, B) = \int_A^B G_m e^{-\alpha_m(\phi - \psi_m)^2} e^{-\frac{\sqrt{2}(\phi_0^l - \phi)}{\sigma_l}} d\phi, \tag{5.39}$$

$$g_{p_m} g_{p_m} p_R(A, B) = \int_A^B G_m e^{-\alpha_m(\phi - \psi_m)^2} e^{-\frac{\sqrt{2}(\phi - \phi_0^l)}{\sigma_l}} d\phi. \tag{5.40}$$

The analytical evaluation of these functions are given in Appendix D. Below, we evaluate $\Xi^l(\mathbf{\Theta}_m)$ for all possible cases depending on DoA and pointing angle of each reconfigurable antenna element.

1) $\phi_0^l + \triangle_l < \psi_m - \phi_c$

In this case, the PAS is on the far left and completely out of the scope of the parabolic part of the radiation pattern. We then have:

$$\Xi^l(\mathbf{\Theta}_m) = g_{c_m} g_{c_m} p_L(\phi_0^l - \triangle_l, \phi_0^l) + g_{c_m} g_{c_m} p_R(\phi_0^l, \phi_0^l + \triangle_l). \tag{5.41}$$

2) $\phi_0^l < \psi_m - \phi_c < \phi_0^l + \triangle_l$

In this case, only half of the PAS is within the parabolic part of the radiation pattern of the reconfigurable antenna on the right-hand side. We then have:

$$\begin{aligned}\Xi^l(\mathbf{\Theta}_m) = {} & g_{c_m} g_{c_m} p_L\Big(\phi_0^l - \triangle_l, \phi_0^l\Big) \\ & + g_{c_m} g_{c_m} p_R\Big(\phi_0^l, \psi_m - \phi_c\Big) \\ & + g_{p_m} g_{p_m} p_R\Big(\psi_m - \phi_c, \min(\phi_0^l + \triangle_l, \psi_m + \phi_c)\Big) \\ & + g_{c_m} g_{c_m} p_R\Big(\min(\phi_0^l + \triangle_l, \psi_m + \phi_c), \phi_0^l + \triangle_l\Big).\end{aligned} \tag{5.42}$$

3) $\psi_m - \phi_c < \phi_0^l < \psi_m + \phi_c$

In this case, both halves of the PAS are within the parabolic part of the radiation pattern of

the reconfigurable antenna. We then have:

$$\begin{aligned}\Xi^l(\boldsymbol{\Theta}_m) = {} & g_{c_m} g_{c_m} p_L\Big(\phi_0^l - \triangle_l, \max(\phi_0^l - \triangle_l, \psi_m - \phi_c)\Big) \\ & + g_{p_m} g_{p_m} p_L\Big(\max(\phi_0^l - \triangle_l, \psi_m - \phi_c), \phi_0^l\Big) \\ & + g_{p_m} g_{p_m} p_R\Big(\phi_0^l, \min(\phi_0^l + \triangle_l, \psi_m + \phi_c)\Big) \\ & + g_{c_m} g_{c_m} p_R\Big(\min(\phi_0^l + \triangle_l, \psi_m + \phi_c), \phi_0^l + \triangle_l\Big). \end{aligned} \tag{5.43}$$

4) $\phi_0^l - \triangle_l < \psi_m + \phi_c < \phi_0^l$

In this case, only half of the PAS is within the parabolic part of the radiation pattern of the reconfigurable antenna on the right-hand side. We then have:

$$\begin{aligned}\Xi^l(\boldsymbol{\Theta}_m) = {} & g_{c_m} g_{c_m} p_L\Big(\phi_0^l - \triangle_l, \max(\phi_0^l - \triangle_l, \psi_m - \phi_c)\Big) \\ & + g_{p_m} g_{p_m} p_L\Big(\max(\phi_0^l - \triangle_l, \psi_m - \phi_c), \psi_m + \phi_c\Big) \\ & + g_{c_m} g_{c_m} p_L\Big(\psi_m + \phi_c, \phi_0^l\Big) \\ & + g_{c_m} g_{c_m} p_R\Big(\phi_0^l, \phi_0^l + \triangle_l\Big). \end{aligned} \tag{5.44}$$

5) $\phi_0^l - \triangle_l > \psi_m + \phi_c$

In this case, the PAS is completely out of the scope of the parabolic part of the radiation pattern on the right-hand side. We then have:

$$\begin{aligned}&\Xi^l(\boldsymbol{\Theta}_m) \\ &\quad = g_{c_m} g_{c_m} p_L(\phi_0^l - \triangle_l, \phi_0^l) + g_{c_m} g_{c_m} p_R(\phi_0^l, \phi_0^l + \triangle_l). \end{aligned} \tag{5.45}$$

Remark 5.2: In this work, we only considered steering the antennas in azimuth plane. However, (5.1) can be extended to consider both vertical and horizontal steering of the radiation pattern. For this purpose, the channel model has to be extended to include the elevation power angular spectrum. In the cases where a two-dimensional Laplacian or a general double exponential functions can model the incoming signal distribution [81], a similar methodology as the one presented in this section can then be followed to obtain series expressions for the covariance matrix coefficients. However, the number of cases to be considered will increase as there is an extra variable to consider.

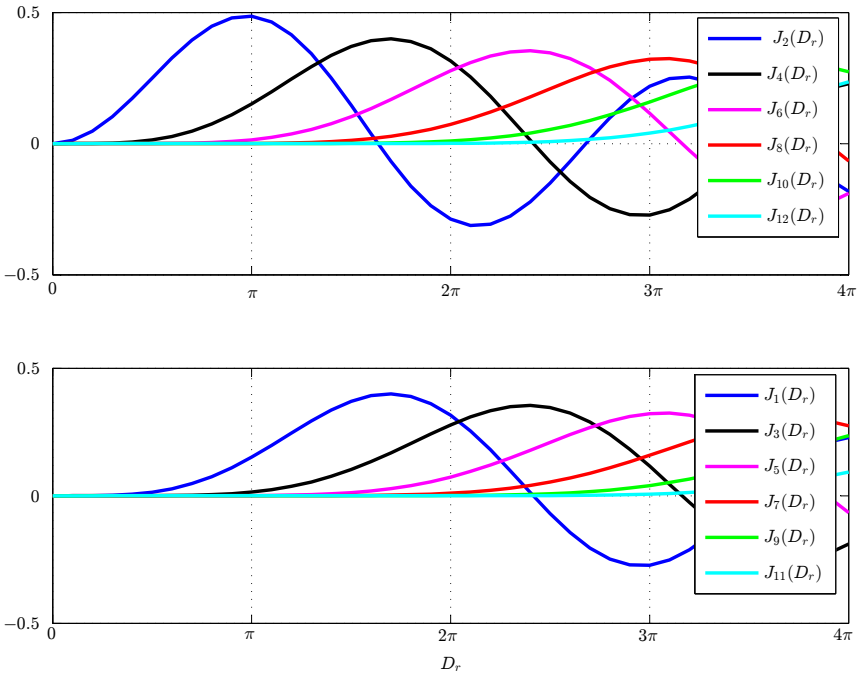

Figure 5.2 Plot of Bessel function of the first kind, $J_{2k}(D_r)$ at the top for integer orders k = 1, 2, 3, 4, 5, 6 and J_{2k+1} at the bottom for integer orders k = 0, 1, 2, 3, 4, 5.

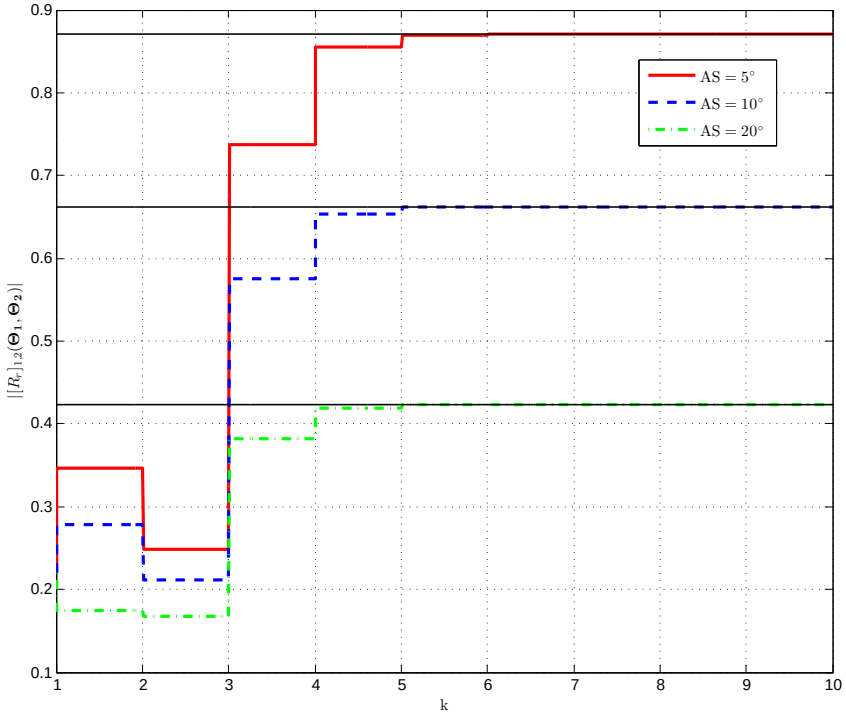

Figure 5.3 Convergence of correlation coefficient as a function of number of terms in summation

5.2.1 Computer Experiments

In this section, we evaluate the derived analytical expression for covariance matrix coefficient between two reconfigurable antenna elements. This expression is a function of the antenna spacing, both antennas pointing angle, angular spread, and angle of arrival. The analytical results obtained from the derived expression are validated by comparing with the results computed from the numerical integration of (5.12) and (5.19). In Fig. 5.4, Fig. 5.6, and Fig. 5.7, the unmarked lines correspond to the analytical results, while the marks correspond to the numerical integration. Unless indicated otherwise, we assumed in this section and Section 5.3 that $d_r = \lambda$ and that the radiation pattern of both antennas have similar characteristics with gain $G_1 = G_2 = 1$ and a sidelobe level of $g_{c_1}[\text{dB}] = g_{c_2}[\text{dB}] = -20$ dB. Moreover, the truncation angle $\triangle_l$ is set to be π.

Although the covariance matrix coefficient in (5.15) is defined as an infinite series, only a limited number of terms k in the sum are required to adequately converge. This is due to the fact that the Bessel function of order k for typical values of antenna spacing quickly converges to zero as k increases. To show that the series converge for a finite number of terms, we have plotted the Bessel function of the first kind versus D_r for different integer orders, k, in Fig. 5.2. Note that the Bessel function $J_i(D_r)$, for $i \in \{2k, 2k+1\}$, is a function of antenna spacing, d_r, since:

$$D_r = k_0(m-n)d_r \tag{5.46}$$

In practice, the distance between antenna elements is chosen to satisfy:

$$\frac{\lambda}{4} \leq d_r \leq 4\lambda, \tag{5.47}$$

and therefore

$$\frac{1}{2}(m-n)\pi \leq D_r \leq 8(m-n)\pi. \tag{5.48}$$

For antenna spacing $d_r = \frac{\lambda}{2}$, and two adjacent antenna elements, we obtain $D_r = \pi$. In this scenario, as illustrated in Fig. 5.2, $J_{2k}(D_r)$ becomes negligible for $k \geq 4$ and $J_{2k+1}(D_r)$ becomes negligible for $k \geq 2$. Therefore, only three and two terms of the sum are needed for computing $J_{2k}(D_r)$ and $J_{2k+1}(D_r)$, respectively. The worse case scenario is when D_r takes its largest value which corresponds to the distance between the first and the last antenna elements in the array.

To illustrate the analytical expressions convergence properties, we plotted in Fig. 5.3, for different angular spreads, the absolute value of the covariance coefficient versus the number of terms used in the summation. The solid black line shows the computed values using

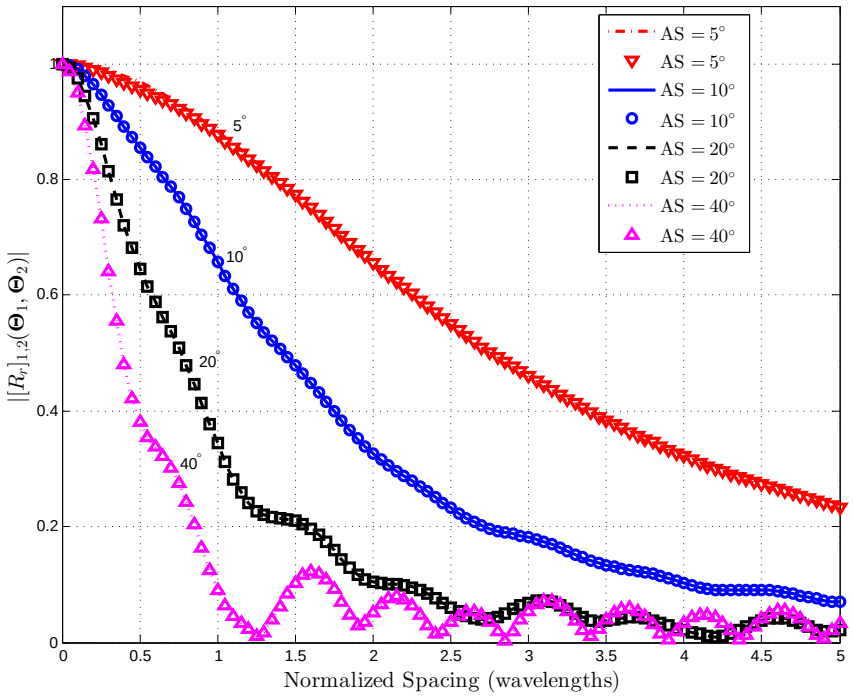

Figure 5.4 Covariance coefficient with $\phi_0^1 = 20°$ and $\psi_1 = \psi_2 = \phi_0^1$ as a function of antenna spacing.

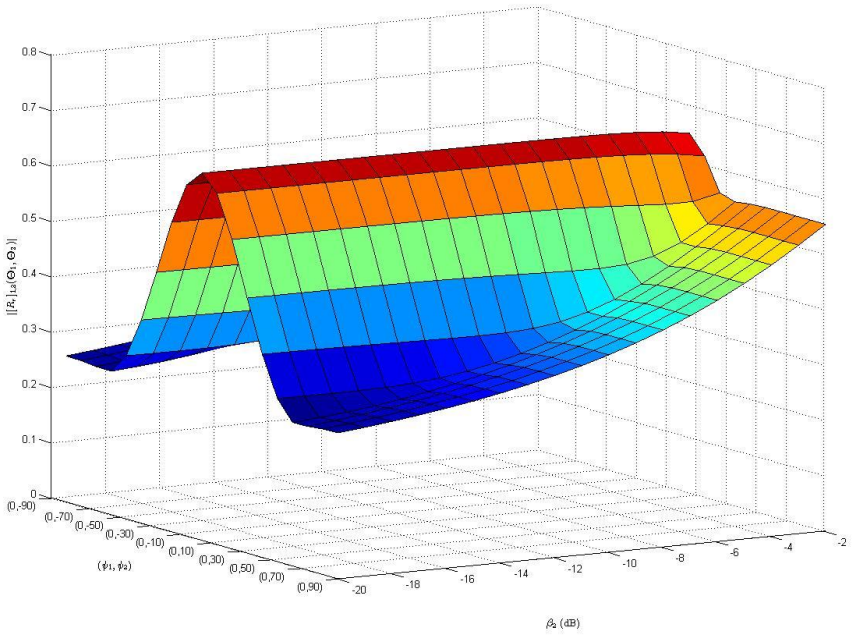

Figure 5.5 Covariance coefficient with AS $= 10°$ and $\psi_1 = \phi_0^1 = 0°$ as a function of ψ_2 and β_2.

numerical integration. As can be observed, the number of summation terms required to accurately compute the covariance is limited and decreases as the angular spread increases.

Fig. 5.4 shows the absolute value of the covariance coefficient versus the normalized spacing between two antenna elements for different angular spreads. In this case, both reconfigurable antennas steer their radiation patterns toward the mean DoA $\phi_0^1 = 20°$, and the beamwidth for both antennas is set to $B_1 = B_2 = 70°$. As shown in this figure, the results obtained from the analytical expression match with that of the numerical integration, thus validating our derivation. It can be observed that the spatial covariance decreases as angular spread or antenna spacing increases due to reduced covariance between the received signals at different antenna elements.

Fig. 5.5 depicts the 3D plot of the absolute value of the covariance coefficient as a function of the second antenna radiation pattern pointing angle, ψ_2, and side lobe level, β_2, (the analytical results have also been validated with simulation results, but the later have not been included in the figure for clarity). The first antenna steers its radiation pattern toward the mean DoA of the cluster ($\psi_1 = \phi_0^1 = 0°$) and its side lobe level is fixed to β_1 = -20 dB. It can be observed that, as expected, the spatial covariance is maximized when the two antennas steer their patterns in the same direction. Furthermore, the covariance between the antenna elements increases as the side lobe increases.

Fig. 5.6 shows the absolute value of the covariance when both pointing angles vary in opposite directions with a mean DoA $\phi_0^1 = 0°$ and for $B_1 = B_2 = 45°$. At the left end of the figure, both reconfigurable antenna elements steer toward the angle of incidence and then we let the pointing angle steer away from the mean DoA in opposite directions such that the overlap between the two radiation patterns decreases. The results validate our analysis for the case where both antennas steer at different angles relative to the DoA.

In Fig. 5.7, the absolute value of the covariance is plotted versus the radiation pattern pointing angles (ψ_1, ψ_2) for a bi-modal truncated Laplacian PAS with DoAs of $\phi_0^1 = 0°$ and $\phi_0^2 = 45°$ for $B_1 = B_2 = 70°$. One of the reconfigurable antenna elements steers its radiation pattern toward the first cluster mode ($\psi_1 = \phi_0^1$) and the other one changes its radiation pattern direction (ψ_2) from $-60°$ to $60°$. As expected, the covariance value is at its lowest when the second antenna is pointing toward the second cluster at $45°$.

5.3 Reconfigurable MIMO Channel Capacity

In this section, we show how the derived analytical expressions of the covariance matrix coefficients can be used to study the capacity of a RE-MIMO wireless communication system equipped with reconfigurable antennas at the receiver. This case study also demonstrates

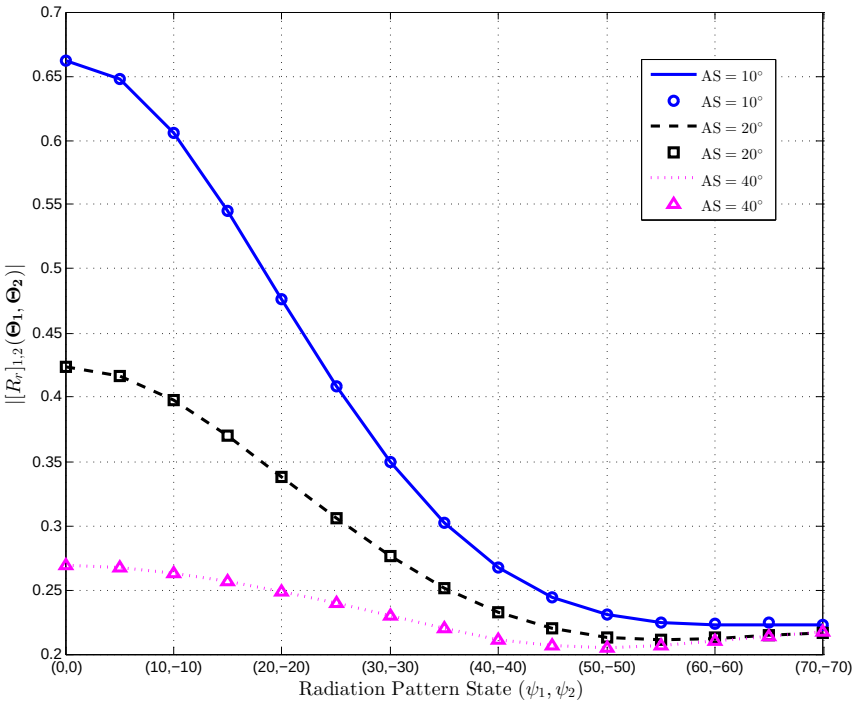

Figure 5.6 Covariance coefficient with $\phi_0^1 = 0°$ as a function of ψ_1 and ψ_2.

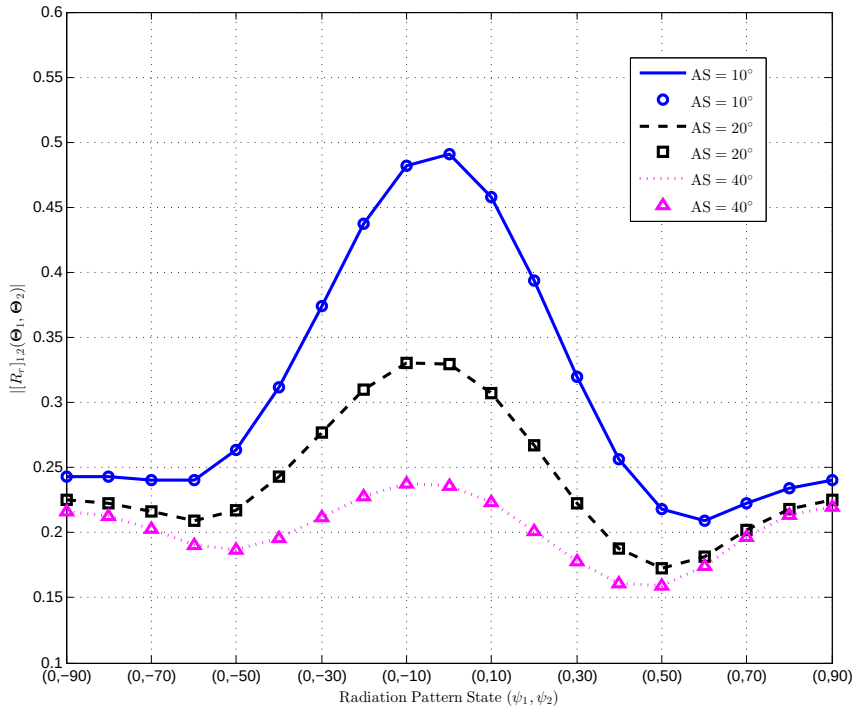

Figure 5.7 Covariance coefficient with $\psi_1 = \phi_0^1 = 0°$ and $\phi_0^2 = 45°$ as a function of ψ_2.

how, based on a PAS estimation obtained for example using the RPS-MUSIC DoA estimation algorithm presented in Chapter 3, the receiver can optimize the antenna configuration to maximize the link throughput. For the numerical results, we assume that the transmitter is surrounded by uniformly distributed scatterers, meaning that the radiating signals from the transmitter side are uncorrelated.

The ergodic channel capacity for the RE-MIMO system with no channel state information at the transmitter is given by [82]

$$C = \mathbb{E}\left\{ \log_2 \left[\det \left(\mathbf{I}_{N_r} + \frac{\gamma}{N_t} \mathbf{H}(\mathbf{\Theta}) \mathbf{H}(\mathbf{\Theta})^H \right) \right] \right\}, \tag{5.49}$$

where γ is the average signal-to-noise-ratio (SNR), and $\mathbf{H}(\mathbf{\Theta})$ is the channel matrix when the array of receive antennas is configured according to $\mathbf{\Theta} = [\mathbf{\Theta}_1 \dots \mathbf{\Theta}_{N_r}]$.

Let us define $\mathbf{v}$ as the vector of eigenvalues of the covariance matrix. Then, the closed-form ergodic capacity can be expressed as [83],

$$C = N_r! H_{Nr,Nt}(\mathbf{v}) \sum_{k=1}^{N_r} \det \left[\frac{(N_t - j)!}{v_i^{-(N_t - j + 1)}} \left[\frac{e^{N_t/(v_i \gamma)}}{\ln 2} \sum_{p=0}^{N_t - j} \frac{1}{p!} \sum_{l=0}^{p} \binom{p}{l} \left(- \frac{N_t}{v_i \gamma} \right)^{p-l} \Gamma\left(l, \frac{N_t}{v_i \gamma}\right) \right]^{\sigma_{kj}} \right]_{N_r \times N_r} \tag{5.50}$$

where N_t is the number of antenna elements at the transmitter, $\Gamma(s, x)$ is the incomplete gamma function, σ_{kj} denotes the Kronecker delta function, and $H_{Nr,Nt}(\mathbf{v})$ is

$$H_{Nr,Nt}(\mathbf{v}) = \frac{\left(\det \left[(-1)^{N_r - j} v_i^{N_t - N_r + j} \right] \right)^{-1}}{n! \pi^{n(1-n)} \tilde{\Gamma}_n(N_t) \tilde{\Gamma}_n(N_r)} \left[\prod_{p=N_r - n}^{N_r - 1} p! \right]. \tag{5.51}$$

In (5.51), $\tilde{\Gamma}_m(a)$ is the complex multivariate gamma function given by

$$\tilde{\Gamma}_m(a) = \pi^{\frac{1}{2} m(m-1)} \prod_{i=1}^{m} \Gamma(a - i + 1). \tag{5.52}$$

where $\Gamma(.)$ is the gamma function.

5.3.1 Computer Experiments

In order to calculate the system capacity, the correlation coefficients are computed using both analytical expressions (5.13) and (5.15) and numerical integration (5.12). In the results presented in this section, the unmarked lines correspond to the analytical results, while the

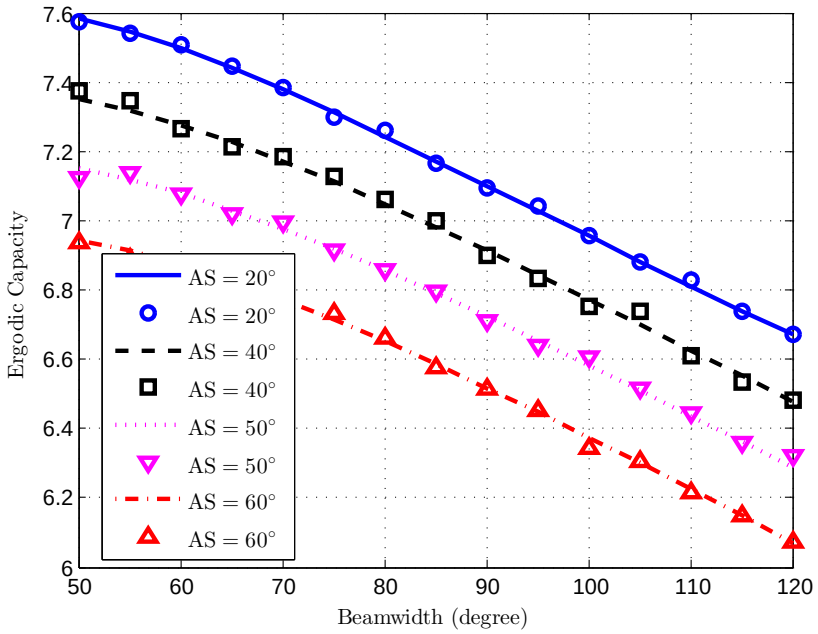

Figure 5.8 Ergodic channel capacity of a 2×2 RE-MIMO system versus antenna beamwidth for different angular spread values.

marks correspond to the results obtained by numerical integration.

Fig. 5.8 shows the ergodic capacity of a RE-MIMO system versus antenna beamwidth for different angular spreads and mean DoA $\phi_0^1 = 10°$. For this scenario, we consider that the antenna gain is inversely proportional to the beamwidth (i.e., $G_i = 1/B_i$) and that both antennas point to the mean DoA ($\psi_1 = \psi_2 = \phi_0^1$). It can be observed that the RE-MIMO capacity increases when the angular spread decreases. Although the covariance coefficient increases as the angular spread decreases (see Fig 5.4), with a lower angular spread more multipath energy gets focused in the angle where the antenna has a higher gain. The latter phenomenon compensates the MIMO capacity decrease due to the covariance increase, which leads to the observed increase in capacity. Similarly, as the beamwidth decreases, the covariance increases but the antenna gain also increases which leads to an improved average SNR and thus a capacity increase.

Figs. 5.9 and 5.10 show the ergodic capacity in low and high SNR ($\gamma = 5$ and 20 dB), respectively, for a bi-modal PAS scenario. We consider $\phi_0^1 = -40°$, $\phi_0^2 = 40°$, $P_1 = -1.7$, and $P_2 = -5$ dB. It can be observed that at low SNR, the system achieves the highest capacity when both reconfigurable antennas are approximatively pointing to the strongest path. A second local optimum is observed when the second antenna points to the second path. On the other hand, at high SNR, the maximum capacity is achieved when each antenna points to a different path. This is due to the fact that at low SNR, the system is power limited and

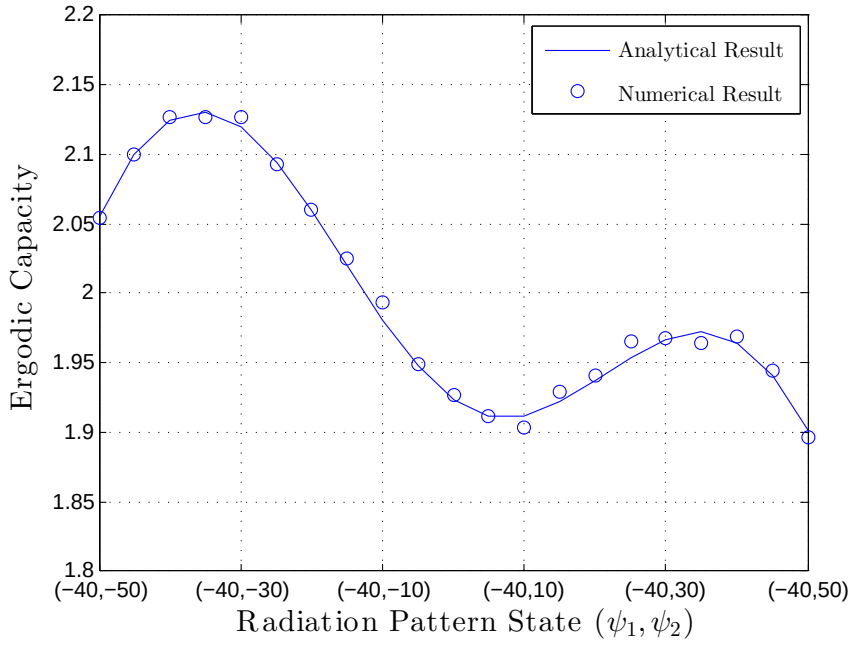

Figure 5.9 Ergodic channel capacity of a 2×2 RE-MIMO system at low SNR for a bi-modal truncated Laplacian PAS with $\phi_0^1 = -40°$, $\phi_0^2 = 40°$, $P_1 = -1.7$ dB, and $P_1 = -5$ dB.

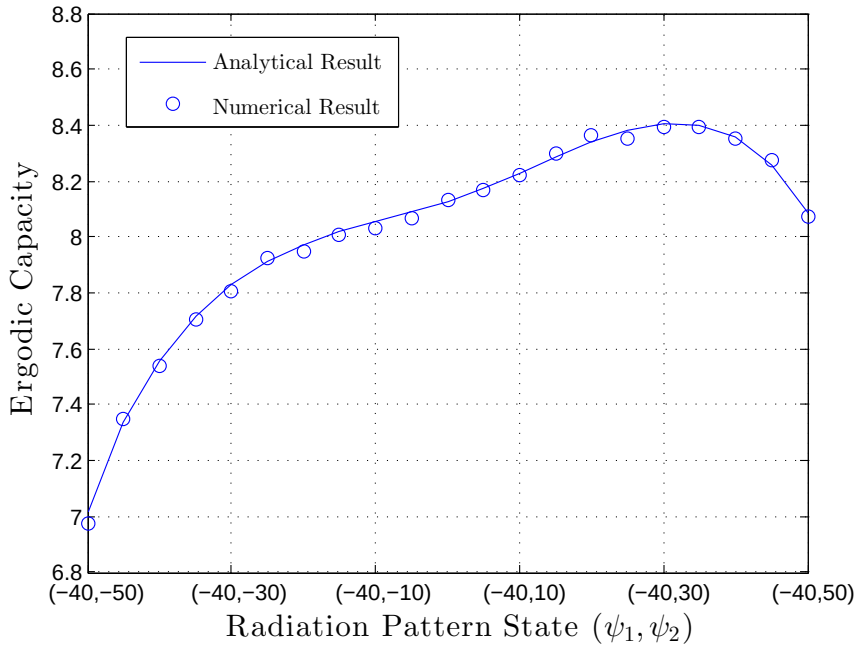

Figure 5.10 Ergodic channel capacity of a 2×2 RE-MIMO system at high SNR for a bi-modal truncated Laplacian PAS with $\phi_0^1 = -40°$, $\phi_0^2 = 40°$, $P_1 = -1.7$ dB, and $P_1 = -5$ dB.

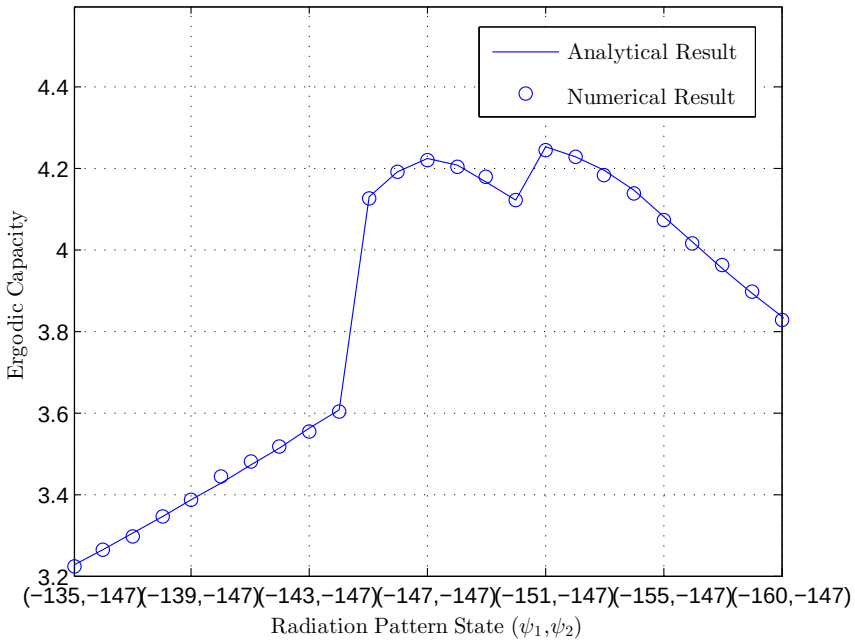

Figure 5.11 Ergodic channel capacity of a 2×2 RE-MIMO system with 2° beamwidth antennas at SNR= 20dB for a channel model with $\phi_0^1 = -152°$, $\phi_0^2 = -147°$, $AS_1 = 33°$, $AS_2 = 37°$, $P_1 = -1.7$ dB, and $P_2 = -5$ dB.

therefore pointing both antennas at the strongest path provides the required power increase. By contrast, at high SNR, it is better to improve the usage of the degrees of freedom which is achieved by decreasing the covariance by pointing at the different paths (see Fig. 5.7). Note that the highest capacity is not exactly achieved when the antenna points directly at the DoA due to the compromise that exists between power increase and covariance decrease. Those results clearly illustrate how the analytical results presented in this chapter can be used to optimally configure in real-time the antenna parameters of a MIMO system as a function of the estimated channel parameters.

In Fig. 5.11, we consider the capacity of a 2×2 RE-MIMO system for a channel model with overlapping clusters with close DoA. This channel model is derived from the 60 GHz channel models considered for 802.11ad test scenarios [84]. It is observed that a very narrow beamwidth of about 2° is required to achieve some decorrelation between the two clusters separated by 5°.

5.4 Conclusion

In this chapter, we derived analytical expressions for computing the covariance matrix coefficients of the received signals impinging on a reconfigurable antenna array. The derived

expressions were validated using a numerical integration method. We investigated the impact of radiation pattern characteristics and array configurations on the covariance coefficients. We also studied the capacity of a reconfigurable MIMO system using the derived analytical expressions. We showed how the results presented in this chapter can be used to quickly choose the optimal configuration for each reconfigurable antenna element in the array.

CHAPTER 6

Full-Diversity Full-Rate Space-Frequency-State Block Codes for Reconfigurable MIMO Systems [1]

An additional type of diversity known as multipath or frequency diversity is offered in frequency-selective fading channels. To achieve spatial and frequency diversity, a space-frequency code has been designed for a MIMO-OFDM system in [39]. In particular, SF codes use the two dimensions of space (antenna) and frequency tones (subcarriers) to enhance the system performance. It has been proved that a MIMO-OFDM system can achieve a maximum diversity gain equal to the product of the number of its transmit antennas, the number of its receive antennas and the number of multipaths present in the frequency selective channel considering a full rank channel correlation matrix. The design criteria to achieve such diversity gains are presented in [39, 40, 85]. Space-time coded OFDM was first introduced in [37] by using space-time trellis codes over frequency tones. In [86], the authors introduced a space-frequency-time coding method over MIMO-OFDM channels. They used trellis coding to code over space and frequency and space-time block codes to code over OFDM blocks. The authors used the Alamouti block code structure [50] for the case of two transmit antennas and proposed to use Orthogonal Space-Time Block Code (OSTBC) structures introduced in [56] for larger numbers of transmit antennas. It is worthwhile to mention that in the case of more than two transmit antennas, OSTBC can provide at most a rate of 3/4 and we are thus not able to have rate-one transmission with OSTBC. In [44], the authors point out the analogy between antennas and frequency tones and based on capacity calculation, propose a grouping method that reduces the complexity of code design for MIMO-OFDM systems. The idea of subcarrier grouping is further pursued in [85] and [87] with precoding and in [88] with bit interleaving. In [45], a repetition mapping technique has been proposed that obtains full-diversity in frequency-selective fading channels. Although their proposed technique achieves full-diversity order, it does not guarantee full coding rate. Subsequently, a block coding technique that offers full-diversity and full coding rate was derived [46, 47].

1. Part of the work presented in this chapter was published in:
   - V. Vakilian, J.-F. Frigon, and S. Roy, "Space-Frequency Block Code for MIMO-OFDM Communication Systems with Reconfigurable Antennas", *Proc. IEEE Global Commun. Conf. (GLOBECOM)*, Atlanta, GA, USA, Dec. 2013.
   - V. Vakilian, J.-F. Frigon, and S. Roy, "Full-Diversity Full-Rate Space-Frequency-State Block Codes for MIMO-OFDM Communication Systems with Reconfigurable Antennas", *Submitted for publication in IEEE Trans. Wireless Commun.*

However, the SF codes proposed in the above studies and other similar works on the topic are not able to exploit the radiation pattern state diversity available in reconfigurable multiple antenna systems.

In this chapter, we propose a coding scheme for reconfigurable MIMO-OFDM systems that achieves multiple diversity gains, including, space, frequency, and radiation pattern state. Basically, the proposed scheme consists of a code that is sent over transmit antennas, OFDM tones, and radiation states. In order to obtain radiation state diversity, we configure each transmit antenna element to independently switch its radiation pattern to a direction that can be selected according to different optimization criteria, e.g., to minimize the correlation among different radiation states or increase the received power. We construct our proposed code based on the fundamental concept of rotated quasi-orthogonal space-time block codes [58, 60, 89]. By using the rotated QOSTBC, the proposed coding structure provides rate-one transmission (i.e., one symbol per frequency subcarrier per radiation state) and leads to a simpler ML decoder. As the simulation results indicate, our proposed code outperforms the existing space-frequency codes substantially.

6.1 System Model for Reconfigurable MIMO-OFDM Systems

Consider a MIMO-OFDM system with M_t reconfigurable elements at the transmitter where each of these elements is capable of electronically changing its radiation pattern and creating P different radiation states as shown in Fig. 6.1. In this system, we assume the receiver antenna array consist of M_r omni-directional elements with fixed radiation patterns. Moreover, we consider an N_c-tone OFDM modulation and frequency-selective fading channels with L propagation paths between each pair of transmit and receiver antenna in each radiation state. The channel gains are quasi-static over one OFDM symbol interval. The channel impulse response between transmit antenna i and receive antenna j in the p-th radiation state can be modelled as

$$h_p^{i,j}(\tau) = \sum_{l=0}^{L-1} \alpha_p^{i,j}(l)\delta(\tau - \tau_{l,p}), \tag{6.1}$$

where $\tau_{l,p}$ is the l-th path delay in the p-th radiation state, and $\alpha_p^{i,j}(l)$ is the complex amplitude of the l-th path between the i-th reconfigurable transmit antenna and the j-th receive antenna in the p-th radiation state. The average total received power is normalized to one.

The frequency response of the channel at the n-th subcarrier between transmit antenna i

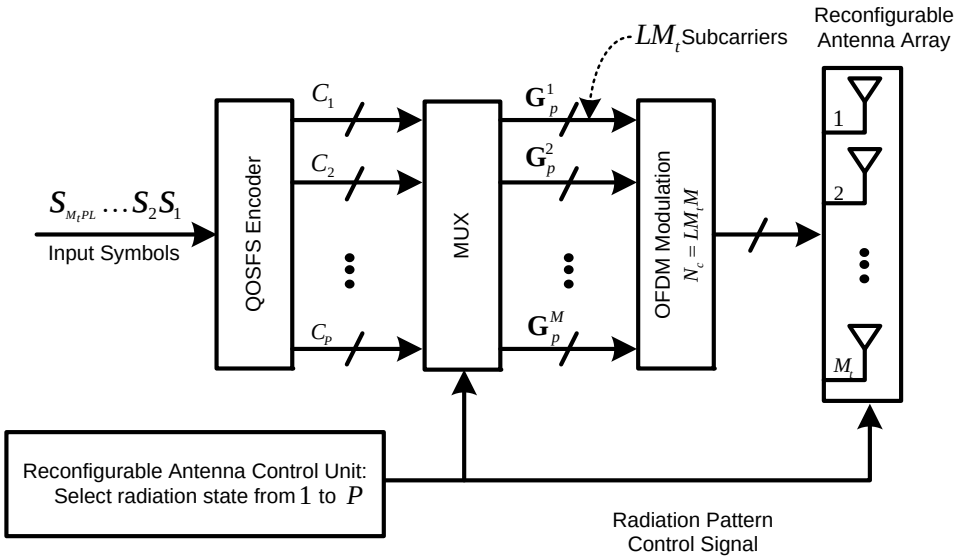

Figure 6.1 Block diagram of a Reconfigurable MIMO-OFDM system employing reconfigurable antennas at the transmitter.

and receive antenna j in the p-th radiation state is given by

$$H_p^{i,j}(n) = \sum_{l=0}^{L-1} \alpha_p^{i,j}(l) e^{-j2\pi n \Delta f \tau_{l,p}}, \tag{6.2}$$

where $\Delta f = 1/T_s$ is the subcarrier frequency spacing and T_s is the OFDM symbol duration. The space-frequency codeword transmitted during the p-th radiation state, $\mathbf{C}_p \in \mathcal{C}^{M_t \times N_c}$, can be expressed as

$$\mathbf{C}_p = \begin{bmatrix} c_p^1(0) & c_p^1(1) & \cdots & c_p^1(N_c-1) \\ c_p^2(0) & c_p^2(1) & \cdots & c_p^2(N_c-1) \\ \vdots & \vdots & \ddots & \vdots \\ c_p^{M_t}(0) & c_p^{M_t}(1) & \cdots & c_p^{M_t}(N_c-1) \end{bmatrix}, \tag{6.3}$$

where $c_p^i(n)$ denotes the data symbol transmitted by transmit antenna i on the n-th subcarrier during the p-th radiation state.

At the receiver, after cyclic prefix removal and FFT, the received frequency domain signal of the n-th subcarrier and p-th radiation state at the j-th receive antenna can be written as

$$r_p^j(n) = \sqrt{\frac{E_s}{M_t}}\mathbf{H}_p^j(n)\mathbf{c}_p(n) + z_p^j(n), \tag{6.4}$$

where

$$\mathbf{H}_p^j(n) = \left[H_p^{1,j}(n), H_p^{2,j}(n), \cdots, H_p^{M_t,j}(n)\right], \tag{6.5}$$

and $\mathbf{c}_p(n)$ is the n-th column of $\mathbf{C}_p$ matrix defined in (6.3), $z_p^j(n)$ is the additive complex Gaussian noise with zero mean and unit variance at the n-th subcarrier, and E_s is the energy normalization factor.

The received signal during the p-th radiation state $\mathbf{r}_p = [\mathbf{r}_p^T(0)\ \mathbf{r}_p^T(1)\ \cdots\ \mathbf{r}_p^T(N_c-1)]^T$ with $\mathbf{r}_p(n) = [r_p^1(n)\ r_p^2(n)\ \cdots\ r_p^{M_r}(n)]^T$, can be written as

$$\mathbf{r}_p = \sqrt{\frac{E_s}{M_t}}\mathbf{H}_p\mathbf{c}_p + \mathbf{z}_p, \tag{6.6}$$

where

$$\mathbf{H}_p = \left[\mathbf{H}_p^{1^T}, \mathbf{H}_p^{2^T}, \cdots, \mathbf{H}_p^{M_r^T}\right]^T, \tag{6.7}$$

$$\mathbf{H}_p^j = \mathrm{diag}\{\mathbf{H}_p^j(0),\ \mathbf{H}_p^j(1),\ \cdots,\ \mathbf{H}_p^j(N_c-1)\} \tag{6.8}$$

is the channel matrix, $\mathbf{c}_p = \mathrm{vec}(\mathbf{C}_p)$ is the transmitted codeword, and $\mathbf{z}_p \in \mathcal{C}^{N_cM_r\times 1}$ is the noise vector during the p-th radiation state.

6.2 Quasi-Orthogonal Space-Frequency Block Codes

In [39], the authors showed that there is no guarantee to achieve the multipath diversity gain of a frequency selective fading channel by applying the existing orthogonal space-time block codes to frequency domain. In this section, we introduce a space-frequency block coding technique based on quasi-orthogonal designs which is able to exploit any desired level of multipath diversity.

Each QOSF codeword, $\mathbf{C}_{SF} \in \mathcal{C}^{M_t\times N_c}$, is a concatenation of some matrices $\mathbf{G}^m$ that can be expressed as

$$\mathbf{C}_{SF} = [\mathbf{G}^{1^T}\mathbf{G}^{2^T}\cdots\mathbf{G}^{M^T}\mathbf{0}_{N_c-MLM_t}^T], \tag{6.9}$$

where $M = \lfloor\frac{N_c}{LM_t}\rfloor$ and $\mathbf{0}_N$ is the all-zeros $N\times N$ matrix. In this expression, $\mathbf{0}_N$ will disappear if N_c is an integer multiple of LM_t. In this work, for simplicity, we assume $N_c = LM_tq$, for

some integer q. Each $\mathbf{G}^m$ matrix, $m \in \{1, 2, \cdots, M\}$, takes the following form:

$$\mathbf{G}^m = \text{col}\{\mathbf{X}_1,\ \mathbf{X}_2,\ \cdots,\ \mathbf{X}_L\} \in \mathcal{C}^{LM_t \times M_t}, \tag{6.10}$$

where $\mathbf{X}_l$ is the $M_t \times M_t$ block coding matrix which is equivalent to an Alamouti code structure for $M_t = 2$. To maintain simplicity in our presentation, we design the code for $M_t = 2$ transmit antennas, however, extension to $M_t > 2$ is possible by following the similar procedure with a QOSTBC. In the case of having two transmit antennas, $\mathbf{X}_l = \mathbf{A}\big(x_1, x_2\big)$, where

$$\mathbf{A}\big(x_1, x_2\big) = \begin{bmatrix} x_1 & x_2 \\ -x_2^* & x_1^* \end{bmatrix}, \tag{6.11}$$

is the Alamoutti OSTBC and therefore $\mathbf{G}^m$ can be expressed as

$$\mathbf{G}^m = \begin{bmatrix} \mathbf{A}(\mathcal{S}_1^m, \mathcal{S}_2^m) \\ \mathbf{A}(\mathcal{S}_3^m, \mathcal{S}_4^m) \\ \vdots \\ \mathbf{A}(\mathcal{S}_{2L-1}^m, \mathcal{S}_{2L}^m) \end{bmatrix}. \tag{6.12}$$

where $\mathcal{S}_i^m$ is a set of combined symbols, defined as follows

$$\begin{aligned} \begin{bmatrix} \mathcal{S}_1^m\ \mathcal{S}_3^m\ \cdots\ \mathcal{S}_{2L-1}^m \end{bmatrix}^T &= \Theta \begin{bmatrix} s_1^m\ s_3^m\ \cdots\ s_{2L-1}^m \end{bmatrix}^T, \\ \begin{bmatrix} \mathcal{S}_2^m\ \mathcal{S}_4^m\ \cdots\ \mathcal{S}_{2L}^m \end{bmatrix}^T &= \Theta \begin{bmatrix} s_2^m\ s_4^m\ \cdots\ s_{2L}^m \end{bmatrix}^T, \end{aligned} \tag{6.13}$$

where $\{s_1^m, \cdots, s_{2L}^m\}$ is a block of symbols belonging to a constellation $\mathcal{A}$,

$$\Theta = \mathbf{U} \times \text{diag}\{1, e^{j\theta_1}, \ldots, e^{j\theta_{L-1}}\},$$

and $\mathbf{U}$ is a $L \times L$ Hadamard matrix. The θ_i's are the rotation angles.

6.3 Quasi-Orthogonal Space-Frequency-State Block Codes

In this section, we present our proposed quasi-orthogonal space-frequency-state (QOSFS) coding scheme illustrated in Fig. 6.1 for a reconfigurable antenna system, where each antenna elements can independently change its radiation pattern direction. In particular, we construct the code based on the principle of a quasi-orthogonal coding structure for an arbitrary number of transmit antennas and radiation pattern states.

6.3.1 Code Structure

The QOSFS codeword over all P radiation states can be represented as

$$\mathbf{C} = \text{diag}\big\{\mathbf{C}_1,\ \mathbf{C}_2,\ \cdots,\ \mathbf{C}_P\big\}, \tag{6.14}$$

where $\mathbf{C}_p$ is given in (6.3). The received signals over all radiation states is defined by $\mathbf{r} = [\mathbf{r}_1^T\ \mathbf{r}_2^T\ \cdots\ \mathbf{r}_P^T]^T \in \mathcal{C}^{PN_cM_r\times 1}$ and can be represented by

$$\mathbf{r} = \sqrt{\frac{E_s}{M_t}}\mathbf{H}\mathbf{c} + \mathbf{z}, \tag{6.15}$$

where $\mathbf{H} = \text{diag}\{\mathbf{H}_1,\ \mathbf{H}_2,\ \cdots,\ \mathbf{H}_P\} \in \mathcal{C}^{PN_cM_r\times PN_cM_t}$ is the overall channel matrix, $\mathbf{c} = \text{dvec}(\mathbf{C}) \in \mathcal{C}^{PN_cM_t\times 1}$, and $\mathbf{z} = [\mathbf{z}_1^T\ \mathbf{z}_2^T\ \cdots\ \mathbf{z}_P^T]^T \in \mathcal{C}^{PN_cM_r\times 1}$ is the noise vector.[2] In each radiation state, we consider a coding strategy where the $M_t \times N_c$ QOSFS codeword $\mathbf{C}_p$ given in (6.3) is a concatenation of $M = \lfloor Nc/LM_t \rfloor$ $\mathbf{G}_p^m \in \mathcal{C}^{LM_t\times M_t}$ codewords as follows:

$$\mathbf{C}_p = [\mathbf{G}_p^{1^T}\mathbf{G}_p^{2^T}\cdots\mathbf{G}_p^{M^T}\mathbf{0}_{M_t\times N_c - MLM_t}], \tag{6.16}$$

In the following, for simplicity and without loss of generality, we assume $N_c = LM_tq$, for some integer q. Each $\mathbf{G}_p^m$ matrix, $m \in \{1, 2, \cdots, M\}$, is a space-frequency codeword which takes the following form:

$$\mathbf{G}_p^m = \text{col}\{\boldsymbol{\mathcal{G}}_{(p-1)L+1}^m,\ \boldsymbol{\mathcal{G}}_{(p-1)L+2}^m,\ \cdots,\ \boldsymbol{\mathcal{G}}_{(p-1)L+L}^m\}, \tag{6.17}$$

where $\boldsymbol{\mathcal{G}}_i^m$ is an $M_t \times M_t$ space block coding matrix which is equivalent to an Alamouti code structure for $M_t = 2$. To maintain simplicity in our presentation, we design the code for $M_t = 2$ transmit antennas, however, extension to $M_t > 2$ is possible by following a similar procedure using rotated QOSTBC [58,60,89]. For the case of $M_t = 2$, we have $\boldsymbol{\mathcal{G}}_i^m = \mathbf{A}(x_1, x_2)$ is the Alamouti block code

$$\mathbf{A}(x_1, x_2) = \begin{bmatrix} x_1 & x_2 \\ -x_2^* & x_1^* \end{bmatrix}. \tag{6.18}$$

and therefore $\mathbf{G}_p^m$ can be expressed as

2. Suppose that $\mathbf{A} = \text{diag}\big\{\mathbf{A}_1, \mathbf{A}_2, \cdots, \mathbf{A}_p\big\}$ is a block diagonal matrix of size $pm \times pn$. Then, $\text{dvec}(\mathbf{A}) = \big[\big(\text{vec}(\mathbf{A}_1)\big)^T, \big(\text{vec}(\mathbf{A}_2)\big)^T, \cdots, \big(\text{vec}(\mathbf{A}_N)\big)^T\big]^T$ with size of $pmn \times 1$.

$$\mathbf{G}_p^m = \begin{bmatrix} \mathbf{A}(\mathcal{S}_{2(p-1)L+1}^m, \mathcal{S}_{2(p-1)L+2}^m) \\ \mathbf{A}(\mathcal{S}_{2(p-1)L+3}^m, \mathcal{S}_{2(p-1)L+4}^m) \\ \vdots \\ \mathbf{A}(\mathcal{S}_{2pL-1}^m, \mathcal{S}_{2pL}^m) \end{bmatrix}. \tag{6.19}$$

In (6.19), $\mathcal{S}_i^m$ is a set of combined symbols, computed as

$$\begin{aligned} \begin{bmatrix} \mathcal{S}_1^m & \mathcal{S}_3^m & \cdots & \mathcal{S}_{2PL-1}^m \end{bmatrix}^T &= \Theta \begin{bmatrix} s_1^m & s_3^m & \cdots & s_{2PL-1}^m \end{bmatrix}^T, \\ \begin{bmatrix} \mathcal{S}_2^m & \mathcal{S}_4^m & \cdots & \mathcal{S}_{2PL}^m \end{bmatrix}^T &= \Theta \begin{bmatrix} s_2^m & s_4^m & \cdots & s_{2PL}^m \end{bmatrix}^T, \end{aligned} \tag{6.20}$$

where $\{s_1^m, \cdots, s_{2PL}^m\}$ is a block of symbols belonging to a constellation $\mathcal{A}$, $\Theta = \mathbf{U} \times \text{diag}\{1, e^{j\theta_1}, \ldots, e^{j\theta_{PL-1}}\}$ and $\mathbf{U}$ is a $PL \times PL$ Hadamard matrix. The θ_i's are the rotation angles. Different optimization strategies can be used to find the optimal values of rotation angles θ_i's, such that they maximize the coding and diversity gains. The objective function in this optimization is defined as the minimum Euclidean distance between constellation points.

6.4 Example of a Space-Frequency-State Block Code

As an example, consider a reconfigurable MIMO-OFDM system with $M_t = 2$ transmit antennas, $P = 2$ radiation states, and $L = 2$ multipaths. In this scenario, the transmitted codewords $\mathbf{C}_1$ and $\mathbf{C}_2$ are constructed according to (6.16) and given as:

$$\mathbf{C}_1 = \frac{1}{4} \begin{bmatrix} \mathcal{S}_1^1 & -\mathcal{S}_2^{1^*} & \mathcal{S}_3^1 & -\mathcal{S}_4^{1^*} & \cdots & \mathcal{S}_1^M & -\mathcal{S}_2^{M^*} & \mathcal{S}_3^M & -\mathcal{S}_4^{M^*} \\ \mathcal{S}_2^1 & \mathcal{S}_1^{1*} & \mathcal{S}_4^1 & \mathcal{S}_3^{1*} & \cdots & \mathcal{S}_2^M & \mathcal{S}_1^{M*} & \mathcal{S}_4^M & \mathcal{S}_3^{M*} \end{bmatrix} \tag{6.21}$$

$$\mathbf{C}_2 = \frac{1}{4} \begin{bmatrix} \mathcal{S}_5^1 & -\mathcal{S}_6^{1^*} & \mathcal{S}_7^1 & -\mathcal{S}_8^{1^*} & \cdots & \mathcal{S}_5^M & -\mathcal{S}_6^{M^*} & \mathcal{S}_7^M & -\mathcal{S}_8^{M^*} \\ \mathcal{S}_6^1 & \mathcal{S}_5^{1*} & \mathcal{S}_8^1 & \mathcal{S}_7^{1*} & \cdots & \mathcal{S}_6^M & \mathcal{S}_5^{M*} & \mathcal{S}_8^M & \mathcal{S}_7^{M*} \end{bmatrix} \tag{6.22}$$

The entries of $\mathbf{C}_p$ are computed using (6.20). As a result, we obtain $\mathbf{C}_1^T$ as

$$\begin{bmatrix} s_1^1+\tilde{s}_3^1+\hat{s}_5^1+\check{s}_7^1 & s_2^1+\tilde{s}_4^1+\hat{s}_6^1+\check{s}_8^1 \\ -s_2^{1^*}-\tilde{s}_4^{1^*}-\hat{s}_6^{1^*}-\check{s}_8^{1^*} & s_1^{1^*}+\tilde{s}_3^{1^*}+\hat{s}_5^{1^*}+\check{s}_7^{1^*} \\ s_1^1-\tilde{s}_3^1+\hat{s}_5^1-\check{s}_7^1 & s_2^1-\tilde{s}_4^1+\hat{s}_6^1-\check{s}_8^1 \\ -s_2^{1^*}+\tilde{s}_4^{1^*}-\hat{s}_6^{1^*}+\check{s}_8^{1^*} & s_1^{1^*}-\tilde{s}_3^{1^*}+\hat{s}_5^{1^*}-\check{s}_7^{1^*} \\ \vdots & \vdots \\ s_1^M+\tilde{s}_3^M+\hat{s}_5^M+\check{s}_7^M & s_2^M+\tilde{s}_4^M+\hat{s}_6^M+\check{s}_8^M \\ -s_2^{M^*}-\tilde{s}_4^{M^*}-\hat{s}_6^{M^*}-\check{s}_8^{M^*} & s_1^{M^*}+\tilde{s}_3^{M^*}+\hat{s}_5^{M^*}+\check{s}_7^{M^*} \\ s_1^M-\tilde{s}_3^M+\hat{s}_5^M-\check{s}_7^M & s_2^M-\tilde{s}_4^M+\hat{s}_6^M-\check{s}_8^M \\ -s_2^{M^*}+\tilde{s}_4^{M^*}-\hat{s}_6^{M^*}+\check{s}_8^{M^*} & s_1^{M^*}-\tilde{s}_3^{M^*}+\hat{s}_5^{M^*}-\check{s}_7^{M^*} \end{bmatrix}, \tag{6.23}$$

and $\mathbf{C}_2^T$ as

$$\begin{bmatrix} s_1^1+\tilde{s}_3^1-\hat{s}_5^1-\check{s}_7^1 & s_2^1+\tilde{s}_4^1-\hat{s}_6^1-\check{s}_8^1 \\ -s_2^{1^*}-\tilde{s}_4^{1^*}+\hat{s}_6^{1^*}+\check{s}_8^{1^*} & s_1^{1^*}+\tilde{s}_3^{1^*}-\hat{s}_5^{1^*}-\check{s}_7^{1^*} \\ s_1^1-\tilde{s}_3^1-\hat{s}_5^1+\check{s}_7^1 & s_2^1-\tilde{s}_4^1-\hat{s}_6^1+\check{s}_8^1 \\ -s_2^{1^*}+\tilde{s}_4^{1^*}+\hat{s}_6^{1^*}-\check{s}_8^{1^*} & s_1^{1^*}-\tilde{s}_3^{1^*}-\hat{s}_5^{1^*}+\check{s}_7^{1^*} \\ \vdots & \vdots \\ s_1^M+\tilde{s}_3^M-\hat{s}_5^M-\check{s}_7^M & s_2^M+\tilde{s}_4^M-\hat{s}_6^M-\check{s}_8^M \\ -s_2^{M^*}-\tilde{s}_4^{M^*}+\hat{s}_6^{M^*}+\check{s}_8^{M^*} & s_1^{M^*}+\tilde{s}_3^{M^*}-\hat{s}_5^{M^*}-\check{s}_7^{M^*} \\ s_1^M-\tilde{s}_3^M-\hat{s}_5^M+\check{s}_7^M & s_2^M-\tilde{s}_4^M-\hat{s}_6^M+\check{s}_8^M \\ -s_2^{M^*}+\tilde{s}_4^{M^*}+\hat{s}_6^{M^*}-\check{s}_8^{M^*} & s_1^{M^*}-\tilde{s}_3^{M^*}-\hat{s}_5^{M^*}+\check{s}_7^{M^*} \end{bmatrix}, \tag{6.24}$$

where $\tilde{s}_i = e^{j\theta_1}s_i$, $\hat{s}_i = e^{j\theta_2}s_i$, and $\check{s}_i = e^{j\theta_3}s_i$. Note that the above codeword provides rate-one transmission (i.e., one symbol per OFDM tone per radiation state).

6.5 Error Rate Performance for Space-Frequency-State Block Codes

Consider two distinct SFS codewords $\mathbf{C}$ and $\tilde{\mathbf{C}}$. The pairwise error probability (PEP) for QOSFS codes can then be written as

$$P(\mathbf{C} \to \tilde{\mathbf{C}}|\mathbf{H}) = Q\Big(\sqrt{\frac{\gamma}{2M_t}||\mathbf{H}\ \mathrm{dvec}(\mathbf{C}-\tilde{\mathbf{C}})||^2}\Big). \tag{6.25}$$

By defining $\mathbf{Y} = \mathbf{H}\,\mathrm{dvec}(\mathbf{C} - \tilde{\mathbf{C}})$ and using the Chernoff bound $Q(x) \leq e^{-x^2/2}$, (6.25) can be rewritten as

$$P(\mathbf{C} \to \tilde{\mathbf{C}}|\mathbf{H}) \leq e^{-\frac{\gamma}{4M_t}||\mathbf{Y}||^2}. \tag{6.26}$$

By averaging (6.26) over all channel realizations, we then obtain [90]

$$P(\mathbf{C} \to \tilde{\mathbf{C}}) \leq \binom{2r-1}{r} \left(\prod_{i=1}^{r} \lambda_i(\mathbf{C_Y})^{-1} \right) \left(\frac{\gamma}{M_t} \right)^{-r}, \tag{6.27}$$

where r and $\lambda_i(\mathbf{C_Y})$ are, respectively, the rank and the i-th eigenvalue of the covariance matrix of $\mathbf{Y}$ defined as $\mathbf{C_Y} = \mathbb{E}\{\mathbf{Y}\mathbf{Y}^H\}$. The covariance matrix $\mathbf{C_Y}$ is a $PN_cM_r \times PN_cM_r$ matrix that is given, as derived in Appendix E, by

$$\mathbf{C_Y} = \sum_{l=0}^{L-1} \mathrm{diag}\Big\{\mathbf{X}_1, \cdots, \mathbf{X}_p\Big\} \mathbf{R_h}(l) \mathrm{diag}\Big\{\mathbf{X}_1^*, \cdots, \mathbf{X}_p^*\Big\} \tag{6.28}$$

where

$$\begin{aligned}
\mathbf{X}_i &= \Big[I_{M_r} \otimes \mathbf{\Omega}^{\tau_{l,i}} (\mathbf{C}_i - \tilde{\mathbf{C}}_i)^T \Big], \\
\mathbf{\Omega} &= \mathrm{diag}\big\{\omega^k\big\}_{k=0}^{N_c-1} \text{with } \omega = e^{-\jmath(2\pi/N_c)} \\
\mathbf{R_h}(l) &= \mathbb{E}\big\{\mathbf{h}(l)\mathbf{h}^H(l)\big\} \in PM_tM_r \times PM_tM_r, \\
\mathbf{h}(l) &= \big[\mathbf{h}_1(l), \mathbf{h}_2(l), \cdots, \mathbf{h}_P(l)\big]^T, \\
\mathbf{h}_p(l) &= \big[\mathbf{h}_p^1(l), \mathbf{h}_p^2(l), \cdots, \mathbf{h}_p^{M_r}(l)\big], \\
\mathbf{h}_p^j(l) &= \big[\alpha_p^{1,j}(l), \alpha_p^{2,j}(l), \cdots, \alpha_p^{M_t,j}(l)\big].
\end{aligned} \tag{6.29}$$

6.6 QOSFS Code Design Criteria

In this section, we find the maximum achievable diversity order and coding gain of the space-frequency-state coding technique proposed in section 6.3.

6.6.1 Maximum Diversity Order

Theorem 6.1 Having a full rank correlation matrix, the maximum diversity order achievable by the QOSFS block code is LPM_tM_r.

Proof. As can be seen from the PEP expression (6.27), the maximum achievable diversity order of the QOSFS block coding is determined by the minimum rank of the covariance matrix $\mathbf{C_Y}$ over all codeword pairs $\{\mathbf{C}, \tilde{\mathbf{C}}\}$. To compute the rank of the covariance matrix

defined in (6.28) for a codeword pairs $\{\mathbf{C}, \tilde{\mathbf{C}}\}$, we rewrite it as [91]

$$\mathbf{C}_{\mathbf{Y}} = \mathbf{F}(\mathbf{C}, \tilde{\mathbf{C}})\mathbf{R}_{\mathbf{h}}\mathbf{F}^H(\mathbf{C}, \tilde{\mathbf{C}}), \tag{6.30}$$

where the $PN_cM_r \times LPM_tM_r$ $\mathbf{F}(\mathbf{C}, \tilde{\mathbf{C}})$ matrix and the $LPM_tM_r \times LPM_tM_r$ $\mathbf{R}_{\mathbf{h}}$ matrix, are given by

$$\begin{aligned}\mathbf{F}(\mathbf{C}, \tilde{\mathbf{C}}) = \Big[&(\mathbf{C} - \tilde{\mathbf{C}})^T, \Big((I_P \otimes \mathbf{\Omega})(\mathbf{C} - \tilde{\mathbf{C}})^T\Big), \\ &\cdots, I_{M_r} \otimes \Big((I_P \otimes \mathbf{\Omega}^{L-1})(\mathbf{C} - \tilde{\mathbf{C}})^T\Big)\Big],\end{aligned} \tag{6.31}$$

$$\mathbf{R}_{\mathbf{h}} = \text{diag}\Big\{\mathbf{R}_{\mathbf{h}}(0), \mathbf{R}_{\mathbf{h}}(1), \cdots, \mathbf{R}_{\mathbf{h}}(L-1)\Big\}. \tag{6.32}$$

In (6.31), $\mathbf{I}(\mathbf{C}, \tilde{\mathbf{C}}) \in \mathcal{C}^{PN_c \times LPM_t}$ is

$$\mathbf{I}(\mathbf{C}, \tilde{\mathbf{C}}) = \text{diag}\big\{\mathbf{I}(\mathbf{C}_1, \tilde{\mathbf{C}}_1), \mathbf{I}(\mathbf{C}_2, \tilde{\mathbf{C}}_2), \cdots, \mathbf{I}(\mathbf{C}_P, \tilde{\mathbf{C}}_P)\big\}, \tag{6.33}$$

where

$$\mathbf{I}(\mathbf{C}_p, \tilde{\mathbf{C}}_p) = \Big[(\mathbf{C}_p - \tilde{\mathbf{C}}_p)^T,\ \mathbf{\Omega}(\mathbf{C}_p - \tilde{\mathbf{C}}_p)^T, \cdots\ \mathbf{\Omega}^{L-1}(\mathbf{C}_p - \tilde{\mathbf{C}}_p)^T\Big], \tag{6.34}$$

with $\mathbf{\Omega}$ defined in (6.29). As it is defined in (6.14), $\mathbf{C}$ and $\tilde{\mathbf{C}}$ are block diagonal matrices with diagonal blocks $\mathbf{C}_p$ and $\tilde{\mathbf{C}}_p$, respectively. And $\mathbf{C}_p$ and $\tilde{\mathbf{C}}_p$ are constructed using (6.16) from matrices $\mathbf{G}_p^m$ and $\tilde{\mathbf{G}}_p^m$, respectively. For two distinct codewords $\mathbf{C}$ and $\tilde{\mathbf{C}}$, there exists at least one index m_0 ($1 \leq m_0 \leq M$) such that $\mathbf{G}_p^{m_0} \neq \tilde{\mathbf{G}}_p^{m_0}$ for all p, for a properly chosen rotation matrix Θ. Without loss of generality, we assume that $\mathbf{G}_p^m = \tilde{\mathbf{G}}_p^m$ for any $m \neq m_0$ since the rank of $\mathbf{F}(\mathbf{C}, \tilde{\mathbf{C}})$ does not decreases if $\mathbf{G}_p^m = \tilde{\mathbf{G}}_p^m$ for some $m \neq m_0$. Now, let us define $\mathbf{F}(\mathbf{G}^{m_0}, \tilde{\mathbf{G}}^{m_0}) \in \mathcal{C}^{LPM_tM_r \times LPM_tM_r}$ as follows:

$$\mathbf{F}(\mathbf{G}^{m_0}, \tilde{\mathbf{G}}^{m_0}) = I_{M_r} \otimes \mathbf{I}(\mathbf{G}^{m_0}, \tilde{\mathbf{G}}^{m_0}), \tag{6.35}$$

where

$$\mathbf{I}(\mathbf{G}^{m_0}, \tilde{\mathbf{G}}^{m_0}) = \text{diag}\big\{\mathbf{I}(\mathbf{G}_1^{m_0}, \tilde{\mathbf{G}}_1^{m_0}),\ \mathbf{I}(\mathbf{G}_2^{m_0}, \tilde{\mathbf{G}}_2^{m_0}), \cdots\ \mathbf{I}(\mathbf{G}_P^{m_0}, \tilde{\mathbf{G}}_P^{m_0})\big\}, \tag{6.36}$$

and

$$\mathbf{I}(\mathbf{G}_p^{m_0}, \tilde{\mathbf{G}}_p^{m_0}) = \Big[(\mathbf{G}_p^{m_0} - \tilde{\mathbf{G}}_p^{m_0}),\ \mathbf{\Omega}(\mathbf{G}_p^{m_0} - \tilde{\mathbf{G}}_p^{m_0}), \cdots\ \mathbf{\Omega}^{L-1}(\mathbf{G}_p^{m_0} - \tilde{\mathbf{G}}_p^{m_0})\Big]. \tag{6.37}$$

We also define

$$\lambda_i\big(\mathbf{F}(\mathbf{G}^{m_0},\tilde{\mathbf{G}}^{m_0})\mathbf{F}^H(\mathbf{G}^{m_0},\tilde{\mathbf{G}}^{m_0})\big),$$

as the i-th eigenvalue of $\big(\mathbf{F}(\mathbf{G}^{m_0},\tilde{\mathbf{G}}^{m_0})\mathbf{F}^H(\mathbf{G}^{m_0},\tilde{\mathbf{G}}^{m_0})\big)$ and $\lambda_i\big(\mathbf{R_h}\big)$ as the i-th eigenvalue of $\mathbf{R_h}$, which are the eigenvalues arranged in increasing order. Applying Ostrowski's Theorem [3] [92, p. 283], we then have that

$$\lambda_i\Big(\mathbf{F}(\mathbf{G}^{m_0},\tilde{\mathbf{G}}^{m_0})\mathbf{R_h}\mathbf{F}^H(\mathbf{G}^{m_0},\tilde{\mathbf{G}}^{m_0})\Big)=\zeta_i\lambda_i(\mathbf{R_h}), \tag{6.38}$$

where ζ_i is a nonnegative real number such that

$$\lambda_{\min}\Big(\mathbf{F}(\mathbf{G}^{m_0},\tilde{\mathbf{G}}^{m_0})\mathbf{F}^H(\mathbf{G}^{m_0},\tilde{\mathbf{G}}^{m_0})\Big)\le\zeta_i\le\lambda_{\max}\Big(\mathbf{F}(\mathbf{G}^{m_0},\tilde{\mathbf{G}}^{m_0})\mathbf{F}^H(\mathbf{G}^{m_0},\tilde{\mathbf{G}}^{m_0})\Big). \tag{6.39}$$

Thus, the eigenvalues of $\mathbf{C_Y}$ have a relation with the eigenvalues of $\big(\mathbf{F}(\mathbf{G}^{m_0},\tilde{\mathbf{G}}^{m_0})\mathbf{F}^H(\mathbf{G}^{m_0},\tilde{\mathbf{G}}^{m_0})\big)$, which is a submatrix of $\mathbf{C_Y}$ obtained by deleting an equal number of its rows and columns. We therefore have that [93]

$$\lambda_i(\mathbf{C_Y})\ge\lambda_i\Big(\mathbf{F}(\mathbf{G}^{m_0},\tilde{\mathbf{G}}^{m_0})\mathbf{R_h}\mathbf{F}^H(\mathbf{G}^{m_0},\tilde{\mathbf{G}}^{m_0})\Big). \tag{6.40}$$

Replacing $\lambda_i\big(\mathbf{F}(\mathbf{G}^{m_0},\tilde{\mathbf{G}}^{m_0})\mathbf{R_h}\mathbf{F}^H(\mathbf{G}^{m_0},\tilde{\mathbf{G}}^{m_0})\big)$ by (6.38), we get for any codeword pair

$$\lambda_i(\mathbf{C_Y})\ge\zeta_i\lambda_i\big(\mathbf{R_h}\big). \tag{6.41}$$

Therefore, the rank of the covariance matrix for any codeword pairs is given by

$$r(\mathbf{C_Y})=r\big(\mathbf{R_h}\big), \tag{6.42}$$

and the diversity order offered by the SFS code is

$$d=r\big(\mathbf{R_h}\big). \tag{6.43}$$

The PEP computed in (6.27) can be rewritten as

$$P(\mathbf{C}\to\tilde{\mathbf{C}})\le\Big(\frac{\gamma}{4M_t}\Big)^{-r(\mathbf{R_h})}\prod_{i=1}^{r(\mathbf{R_h})}\lambda_i^{-1}\big(\mathbf{R_h}\big). \tag{6.44}$$

Therefore, the maximum diversity gain offered by the proposed QOSFS block code in the

3. Suppose that $\mathbf{A}$ and $\mathbf{S}$ be $n\times n$ matrices with $\mathbf{A}$ Hermitian and $\mathbf{S}$ nonsingular. Let the eigenvalues of $\mathbf{A}$ and $\mathbf{SS}^H$ be arranged in increasing order. For each $i=1,2,\cdots n$ there exists a nonnegative real number θ_i such that $0<\lambda_1(\mathbf{SS}^H)\le\theta_i\le\lambda_i(\mathbf{SS}^H)$ and $\lambda_i(\mathbf{SAS}^H)=\theta_i\lambda_i(\mathbf{A})$.

case of having a full rank equivalent channel matrix $\mathbf{R_h}$ is given by

$$\begin{aligned} \max \quad d &= r\big(\mathbf{F}(\mathbf{G}^{m_0}, \tilde{\mathbf{G}}^{m_0})\mathbf{R_h}\mathbf{F}^H(\mathbf{G}^{m_0}, \tilde{\mathbf{G}}^{m_0})\big) \\ &= r(\mathbf{R_h}) = LPM_tM_r. \end{aligned} \tag{6.45}$$

□

6.6.2 Coding Gain

The minimum coding gain can be defined as the product of the non-zero eigenvalues of the matrix $\mathbf{C_Y}$ over all pairs of codewords, which can be written as

$$\begin{aligned} G_c &= \prod_{i=1}^{r(\mathbf{R_h})} \lambda_i(\mathbf{F}(\mathbf{G}^{m_0}, \tilde{\mathbf{G}}^{m_0})\mathbf{R_h}\mathbf{F}^H(\mathbf{G}^{m_0}, \tilde{\mathbf{G}}^{m_0})) \\ &= \prod_{i=1}^{r(\mathbf{R_h})} \zeta_i\lambda_i\big(\mathbf{R_h}\big). \end{aligned} \tag{6.46}$$

6.7 Optimal Rotation Angles

In this section, we find the optimal rotation angles θ_i's such that full-diversity and maximum coding gain can be achieved for the proposed QOSFS coding scheme. For simplicity, in this section, we consider $M_t = 2$ for the development and provide the extension of the final results for $M_t > 2$ at the end. Consider two QOSFS distinct codewords as follows,

$$\begin{aligned} \mathbf{C} &= \text{diag}\{\mathbf{C}_1, \mathbf{C}_2, \cdots, \mathbf{C}_P\} \in \mathcal{C}^{PM_t \times PN_c}, \\ \tilde{\mathbf{C}} &= \text{diag}\{\tilde{\mathbf{C}}_1, \tilde{\mathbf{C}}_2, \cdots, \tilde{\mathbf{C}}_P\} \in \mathcal{C}^{PM_t \times PN_c}, \end{aligned} \tag{6.47}$$

where $\mathbf{C}_p$ and $\tilde{\mathbf{C}}_p$ are constructed using (6.16) from matrices $\mathbf{G}_p^m$ and $\tilde{\mathbf{G}}_p^m$, respectively. As defined in (6.19), $\mathbf{G}_p^m$ and $\tilde{\mathbf{G}}_p^m$ are constructed from sets of combined symbols,

$$\{\mathcal{S}^m_{2(p-1)L+1}, \cdots, \mathcal{S}^m_{2pL}\}, \tag{6.48}$$

$$\{\mathcal{V}^m_{2(p-1)L+1}, \cdots, \mathcal{V}^m_{2pL}\}, \tag{6.49}$$

corresponding to two sets of distinct symbols respectively denoted by

$$\{s_1^m, s_2^m, \cdots, s_{2PL}^m\}, \tag{6.50}$$

$$\{v_1^m, v_2^m, \cdots, v_{2PL}^m\}. \tag{6.51}$$

As we discussed in Section 6.6.1, the diversity order of the QOSFS block code for these two distinct codewords is determined by the minimum rank of covariance matrix $\mathbf{C_Y} \in \mathcal{C}^{PN_cM_r \times PN_cM_r}$, defined in (6.30). With $\mathbf{R_h} = \mathbf{I}$, the minimum rank of $\mathbf{C_Y}$ is equal to the minimum rank of $\mathbf{F}(\mathbf{C}, \tilde{\mathbf{C}})\mathbf{F}^H(\mathbf{C}, \tilde{\mathbf{C}})$, where its minimum rank can be determined by using the minimum rank of $\mathbf{I}(\mathbf{C}, \tilde{\mathbf{C}})$. To achieve the minimum rank of $\mathbf{I}(\mathbf{C}, \tilde{\mathbf{C}})$, we assume that there exists at least one index $m_0 (1 \leq m_0 \leq M)$ such that $\mathbf{G}_p^{m_0} \neq \tilde{\mathbf{G}}_p^{m_0}$, $\forall p \in \{1, 2, \cdots, P\}$. Without loss of generality, we assume that $\mathbf{G}_p^m = \tilde{\mathbf{G}}_p^m$ for any $m \neq m_0$ since the rank of $\mathbf{I}(\mathbf{C}, \tilde{\mathbf{C}})$ does not decreases if $\mathbf{G}_p^m = \tilde{\mathbf{G}}_p^m$ for some $m \neq m_0$. Now, let us define for this case the full-rank part of $\mathbf{I}(\mathbf{C}, \tilde{\mathbf{C}})$ by $\mathbf{I}(\mathbf{G}^{m_0}, \tilde{\mathbf{G}}^{m_0}) \in \mathcal{C}^{2PL \times 2PL}$ given as,

$$\mathbf{I}(\mathbf{G}^{m_0}, \tilde{\mathbf{G}}^{m_0}) = \text{diag}\big\{\mathbf{I}(\mathbf{G}_1^{m_0}, \tilde{\mathbf{G}}_1^{m_0}),\ \mathbf{I}(\mathbf{G}_2^{m_0}, \tilde{\mathbf{G}}_2^{m_0}), \cdots\ \mathbf{I}(\mathbf{G}_P^{m_0}, \tilde{\mathbf{G}}_P^{m_0})\big\}, \tag{6.52}$$

where

$$\mathbf{I}(\mathbf{G}_p^{m_0}, \tilde{\mathbf{G}}_p^{m_0}) = \Big[(\mathbf{G}_p^{m_0} - \tilde{\mathbf{G}}_p^{m_0}),\ \mathbf{\Omega}(\mathbf{G}_p^{m_0} - \tilde{\mathbf{G}}_p^{m_0}), \cdots\ \mathbf{\Omega}^{L-1}(\mathbf{G}_p^{m_0} - \tilde{\mathbf{G}}_p^{m_0})\Big]. \tag{6.53}$$

$\mathbf{I}(\mathbf{G}_p^{m_0}, \tilde{\mathbf{G}}_p^{m_0}) \in \mathcal{C}^{2L \times 2L}$ can be written as,

$$\begin{bmatrix}
D_{2(p-1)L+1}^{m_0} & D_{2(p-1)L+2}^{m_0} & \cdots & D_{2(p-1)L+1}^{m_0} & D_{2(p-1)L+2}^{m_0} \\
-D_{2(p-1)L+2}^{m_0 *} & D_{2(p-1)L+1}^{m_0 *} & \cdots & -\omega^{L-1} D_{2(p-1)L+2}^{m_0 *} & \omega^{L-1} D_{2(p-1)L+1}^{m_0 *} \\
D_{2(p-1)L+3}^{m_0} & D_{2(p-1)L+4}^{m_0} & \cdots & \omega^{2(L-1)} D_{2(p-1)L+3}^{m_0} & \omega^{2(L-1)} D_{2(p-1)L+4}^{m_0} \\
\vdots & \vdots & \ddots & \vdots & \vdots \\
D_{2pL-1}^{m_0} & D_{2pL}^{m_0} & \cdots & \omega^{2(L-1)(L-1)} D_{2pL-1}^{m_0} & \omega^{2(L-1)(L-1)} D_{2pL}^{m_0} \\
-D_{2pL}^{m_0 *} & D_{2pL-1}^{m_0 *} & \cdots & -\omega^{(L-1)(2L-1)} D_{2pL}^{m_0 *} & \omega^{(L-1)(2L-1)} D_{2pL-1}^{m_0 *}
\end{bmatrix} \tag{6.54}$$

where $D_i^{m_0} = \mathcal{S}_i^{m_0} - \mathcal{V}_i^{m_0}$ which for $i \in \{1, 3, \cdots, 2PL-1\}$ is given by,

$$D_i^{m_0} = u_{i+1/2,1} d_1^{m_0} + u_{i+1/2,2} e^{j\theta_1} d_3^{m_0} + \cdots + u_{i+1/2,PL} e^{j\theta_{PL-1}} d_{2PL-1}^{m_0}, \tag{6.55}$$

and for $i \in \{2, 4, \cdots, 2PL\}$ is given by,

$$D_i^{m_0} = u_{i/2,1} d_2^{m_0} + u_{i/2,2} e^{j\theta_1} d_4^{m_0} + \cdots + u_{i/2,PL} e^{j\theta_{PL-1}} d_{2PL}^{m_0}, \tag{6.56}$$

where $u_{k,l}$ is the entry of Hadamard matrix $\mathbf{U}$ in the k-th row and l-th column and $d_i^{m_0} = s_i^{m_0} - v_i^{m_0}$. For the QOSFS code, the coding gain can be computed as follows,

$$\begin{aligned}
&\det\big\{(\mathbf{G}^{m_0}-\tilde{\mathbf{G}}^{m_0})^H(\mathbf{G}^{m_0}-\tilde{\mathbf{G}}^{m_0})\big\} \\
&\qquad = \prod_{p=1}^{P} \det\big\{(\mathbf{G}_p^{m_0}-\tilde{\mathbf{G}}_p^{m_0})^H(\mathbf{G}_p^{m_0}-\tilde{\mathbf{G}}_p^{m_0})\big\} \\
&\qquad = \prod_{p=1}^{P}\sum_{l=1}^{2L} |\mathcal{S}_{2(p-1)L+l}^{m_0} - \mathcal{V}_{2(p-1)L+l}^{m_0}|^2 \\
&\qquad = \prod_{p=1}^{P}\sum_{l=1}^{2L} |D_{2(p-1)L+l}^{m_0}|^2, \qquad (6.57)
\end{aligned}$$

Note that the minimum non-zero coding gain is achieved when one of the sets below is zero:

$$\{D_1^{m_0}, D_3^{m_0}, \cdots, D_{2PL-1}^{m_0}\},$$

$$\{D_2^{m_0}, D_4^{m_0}, \cdots, D_{2PL}^{m_0}\}.$$

As an example, for the QOSFS codewords shown in (6.23) and (6.24), we get

$$\begin{aligned}
&\det\big\{(\mathbf{G}^{m_0}-\tilde{\mathbf{G}}^{m_0})^H(\mathbf{G}^{m_0}-\tilde{\mathbf{G}}^{m_0})\big\} \\
&\qquad = \big(|D_1^{m_0}|^2 + |D_2^{m_0}|^2 + |D_3^{m_0}|^2 + |D_4^{m_0}|^2\big)^2 \\
&\qquad \times \big(|D_5^{m_0}|^2 + |D_6^{m_0}|^2 + |D_7^{m_0}|^2 + |D_8^{m_0}|^2\big)^2.
\end{aligned}$$

For this QOSFS code, the minimum coding gain is achieved when one of the $D_i^{m_0}$ for $i \in \{1,2,3,4\}$ and one of the $D_j^{m_0}$ for $j \in \{5,6,7,8\}$ are non-zeros. As it can be observed from (6.55), if $D_1^{m_0} = 0$ then $D_i^{m_0} = 0$ for $i \in \{3,5,7\}$. Also as it is given in (6.56), if $D_2^{m_0} = 0$ then $D_i^{m_0} = 0$ for $i \in \{2,4,6\}$. Moreover, if $D_1^{m_0} \neq 0$ then $D_i^{m_0} \neq 0$ for $i \in \{3,5,7\}$ and if $D_2^{m_0} \neq 0$ then $D_i^{m_0} \neq 0$ for $i \in \{2,4,6\}$. Therefore, the minimum coding gain is achieved when one of the sets $\{D_1^{m_0}, D_3^{m_0}, D_5^{m_0}, D_7^{m_0}\}$ or $\{D_2^{m_0}, D_4^{m_0}, D_6^{m_0}, D_8^{m_0}\}$ is zero. Without loss of generality, we assume $\{D_2^{m_0}, D_4^{m_0}, \cdots, D_{2PL}^{m_0}\} = 0$. Then, (6.54) can be rewritten as $\bar{\mathbf{I}}(\mathbf{G}_p^{m_0}, \tilde{\mathbf{G}}_p^{m_0})$ defined

as follows:

$$\begin{bmatrix} D^{m_0}_{2(p-1)L+1} & 0 & \cdots & D^{m_0}_{2(p-1)L+1} & 0 \\ 0 & D^{m_0*}_{2(p-1)L+1} & \cdots & 0 & \omega^{L-1} D^{m_0*}_{2(p-1)L+1} \\ D^{m_0}_{2(p-1)L+3} & 0 & \cdots & \omega^{2(L-1)} D^{m_0}_{2(p-1)L+3} & 0 \\ \vdots & \vdots & \ddots & \vdots & \vdots \\ D^{m_0}_{2pL-1} & 0 & \cdots & \omega^{2(L-1)(L-1)} D^{m_0}_{2pL-1} & 0 \\ 0 & D^{m_0*}_{2pL-1} & \cdots & 0 & \omega^{(L-1)(2L-1)} D^{m_0*}_{2pL-1} \end{bmatrix}. \tag{6.58}$$

As it can be observed from (6.58), any even and odd columns of $\bar{\mathbf{I}}(\mathbf{G}^{m_0}_p, \tilde{\mathbf{G}}^{m_0}_p)$ are independent. This relation also holds for $\bar{\mathbf{I}}(\mathbf{G}^{m_0}, \tilde{\mathbf{G}}^{m_0})$, which is given by,

$$\bar{\mathbf{I}}(\mathbf{G}^{m_0}, \tilde{\mathbf{G}}^{m_0}) = \text{diag}\big\{\bar{\mathbf{I}}(\mathbf{G}^{m_0}_1, \tilde{\mathbf{G}}^{m_0}_1),\ \bar{\mathbf{I}}(\mathbf{G}^{m_0}_2, \tilde{\mathbf{G}}^{m_0}_2), \cdots\ \bar{\mathbf{I}}(\mathbf{G}^{m_0}_P, \tilde{\mathbf{G}}^{m_0}_P)\big\}. \tag{6.59}$$

Therefore, we define two new matrices: one is constructed from the odd rows and odd columns of $\bar{\mathbf{I}}(\mathbf{G}^{m_0}, \tilde{\mathbf{G}}^{m_0})$, denoted $\bar{\mathbf{I}}_O(\mathbf{G}^{m_0}, \tilde{\mathbf{G}}^{m_0}) \in \mathcal{C}^{PL\times PL}$, and the second one is constructed from the even rows and even columns of $\bar{\mathbf{I}}(\mathbf{G}^{m_0}, \tilde{\mathbf{G}}^{m_0})$, denoted $\bar{\mathbf{I}}_E(\mathbf{G}^{m_0}, \tilde{\mathbf{G}}^{m_0}) \in \mathcal{C}^{PL\times PL}$. These matrices are given below,

$$\bar{\mathbf{I}}_O(\mathbf{G}^{m_0}, \tilde{\mathbf{G}}^{m_0}) = \text{diag}\{D^{m_0}_1, D^{m_0}_3, \cdots, D^{m_0}_{2PL-1}\}(I_p \otimes \mathbf{W}), \tag{6.60}$$

$$\bar{\mathbf{I}}_E(\mathbf{G}^{m_0}, \tilde{\mathbf{G}}^{m_0}) = \text{diag}\{D^{m_0*}_1, D^{m_0*}_3, \cdots, D^{m_0*}_{2PL-1}\}(I_p \otimes \mathbf{W}). \tag{6.61}$$

In (6.60) and (6.61), $\mathbf{W}$ is

$$\begin{bmatrix} 1 & 1 & 1 & \cdots & 1 \\ 1 & \omega^2 & \omega^4 & \cdots & \omega^{2(L-1)} \\ 1 & \omega^4 & \omega^8 & \cdots & \omega^{4(L-1)} \\ \vdots & \vdots & \vdots & \ddots & \vdots \\ 1 & \omega^2(L-1) & \omega^4(L-1) & \cdots & \omega^{2(L-1)(L-1)} \end{bmatrix}. \tag{6.62}$$

The determinant of $\bar{\mathbf{I}}(\mathbf{G}^{m_0}, \tilde{\mathbf{G}}^{m_0}) \in \mathcal{C}^{2PL\times 2PL}$ can be computed as,

$$\det\Big(\bar{\mathbf{I}}(\mathbf{G}^{m_0}, \tilde{\mathbf{G}}^{m_0})\Big) = \det\Big(\bar{\mathbf{I}}_O(\mathbf{G}^{m_0}, \tilde{\mathbf{G}}^{m_0})\Big) \det\Big(\bar{\mathbf{I}}_E(\mathbf{G}^{m_0}, \tilde{\mathbf{G}}^{m_0})\Big) \tag{6.63}$$

where

$$\det\left(\bar{\mathbf{I}}_O(\mathbf{G}^{m_0},\tilde{\mathbf{G}}^{m_0})\right) = D_1^{m_0} D_3^{m_0} \cdots D_{2PL-1}^{m_0} \det^P(\mathbf{W}) \tag{6.64}$$

$$\det\left(\bar{\mathbf{I}}_E(\mathbf{G}^{m_0},\tilde{\mathbf{G}}^{m_0})\right) = D_1^{m_0 *} D_3^{m_0 *} \cdots D_{2PL-1}^{m_0 *} \det^P(\mathbf{W}). \tag{6.65}$$

Now, the optimal rotation angles has to be chosen such that the code provides full-diversity and maximal coding gain. As it can be observed from (6.63), to achieve full-diversity of $2PL$, both $\bar{\mathbf{I}}_O(\mathbf{G}^{m_0},\tilde{\mathbf{G}}^{m_0})$ and $\bar{\mathbf{I}}_E(\mathbf{G}^{m_0},\tilde{\mathbf{G}}^{m_0})$ matrices have to be full-rank. To meet this requirement, the first and second terms in (6.64) and (6.65) need to be non-zero. The second term in both equations is non-zero because of assuming $N > 2L$. In order to have a non-zero first term, the rotation angles have to be chosen to satisfy the following condition:

$$|D_i^{m_0}| = |u_{i+1/2,1} d_1^{m_0} + u_{i+1/2,2} e^{j\theta_1} d_3^{m_0} + \cdots + u_{i+1/2,PL} e^{j\theta_{PL-1}} d_{2PL-1}^{m_0}| \neq 0, \quad i = 1, 3, \cdots, 2PL-1. \tag{6.66}$$

Also, to maximize the coding gain, the following optimization problem needs to be solved,

$$\max_{\theta_1,\cdots,\theta_{PL-1}} \min_{d_1,d_3,\cdots,d_{2PL-1}} |D_1 D_3 \cdots D_{2PL-1}|. \tag{6.67}$$

The constraint in (6.66) and the optimization problem in (6.67) for choosing optimal rotation angles can be generalized for $M_t > 2$ as,

$$|D_i^{m_0}| = |u_{i+1/2,1} d_1^{m_0} + u_{i+1/2,2} e^{j\theta_1} d_{M_t+1}^{m_0} + \cdots + u_{i+1/2,PL} e^{j\theta_{PL-1}} d_{M_t PL-(M_t-1)}^{m_0}| \neq 0, \quad i = 1, M_t+1, \cdots, M_t PL-(M_t-1). \tag{6.68}$$

$$\max_{\theta_1,\cdots,\theta_{PL-1}} \min_{d_1,d_{M_t+1}\cdots,d_{M_t PL-(M_t-1)}} |D_1 D_{M_t+1} \cdots D_{M_t PL-(M_t-1)}|. \tag{6.69}$$

Figs. 6.2-6.4 show the values for the minimum determinant versus the rotation angles for P = 1 radiation state and for BPSK, QPSK, and 8PSK constellations. For example, for 8PSK constellation, the optimal rotation angle for the proposed SFS-BC is $\pi/8$.

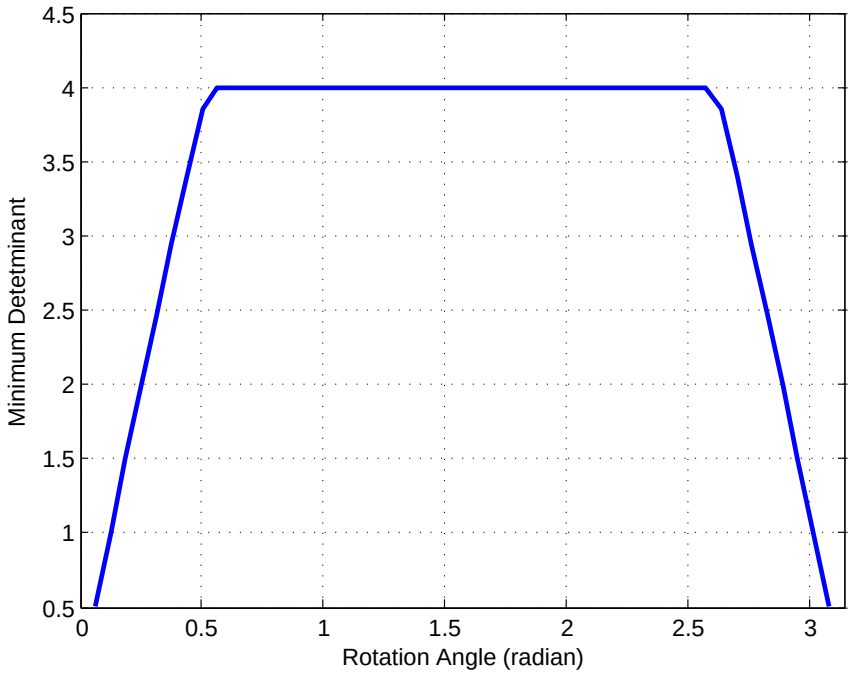

Figure 6.2 Optimal rotation angle for BPSK constellation

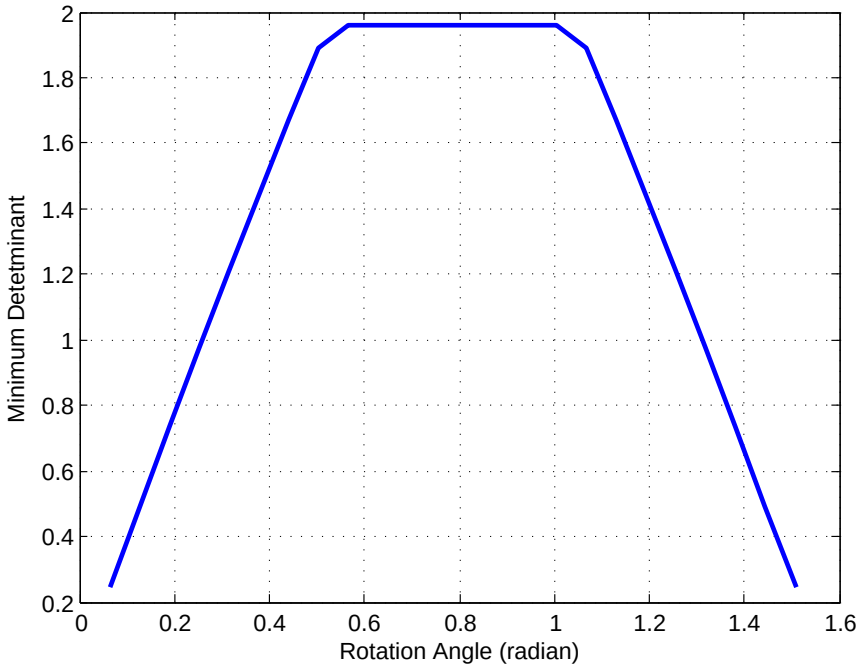

Figure 6.3 Optimal rotation angle for QPSK constellation

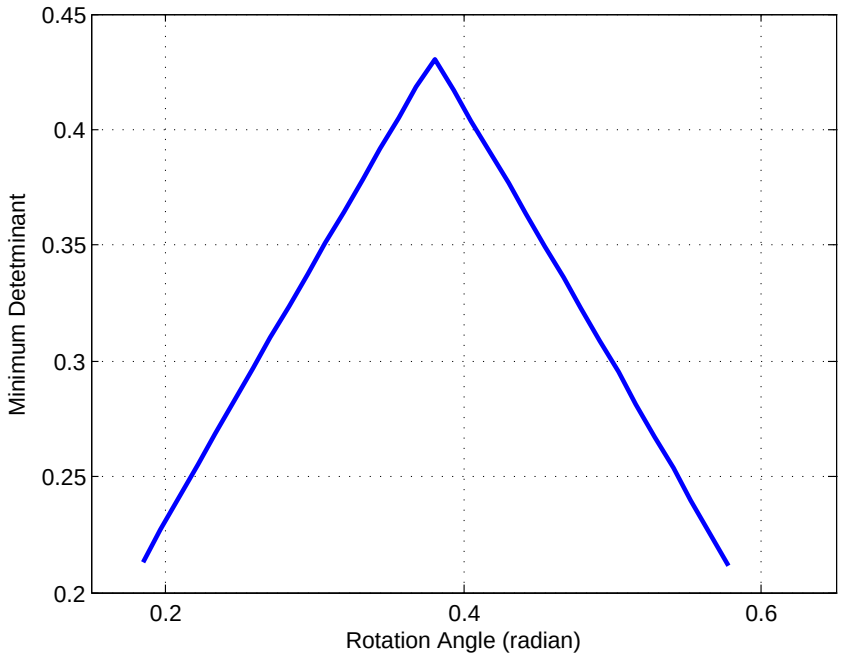

Figure 6.4 Optimal rotation angle for 8PSK constellation

6.8 Simulation Results

In this section, we provide simulation results for both conventional and reconfigurable MIMO-OFDM systems in two different channel models: 2-ray equal power channel model and clustered channel model. In the reconfigurable MIMO-OFDM system, we assume that at the transmitter the antenna elements in the array are capable of dynamically changing their radiation pattern directions. In contrast, the conventional MIMO-OFDM system uses omni-directional antenna elements with fixed radiation pattern at both transmitter and receiver ends. For both systems, we consider $M_t = 2$ antennas at the transmitter and $M_r = 1$ antenna at the receiver and an OFDM modulation technique with $N_c = 128$ subcarriers as well as a cyclic prefix equal to or longer than the maximum channel delay spread. In our simulations, we consider that the receiver has perfect channel state information. We also assume that the symbols are chosen from a BPSK constellation, leading to a spectral efficiency of 1 bit/sec/Hz if the cyclic prefix overhead is ignored. The average symbol power per transmit antenna is set to be $E_s = 1/M_t$ and the noise variance is $\sigma_n^2 = 1/\gamma$. Furthermore, for a reconfigurable antenna system, we assume the same delay spread for both radiation states (i.e., $\tau_{l,1} = \tau_{l,2}$). The powers of all paths in each radiation state are normalized such that $\sum_{l=0}^{L-1} \sigma_{l,p}^2 = 1$. For our proposed QOSFS scheme, the rotation angles are chosen as $\theta_i = i\pi/PL$ for BPSK constellation.

6.8.1 2-Ray Channel Model

In this part, we present simulation results for a 2-ray equal power channel model. The channel coefficients $\alpha_p^{i,j}(l)$ are zero-mean identically-distributed Gaussian random variables with a variance of $\sigma_{l,p}^2$. We assumed that they are independent for each multipath, transmit antenna and radiation state.

Fig. 6.5 shows BER performance of the proposed code for a delay spread of $\tau = 5\mu s$. As shown in this figure, the proposed code outperforms those of [46] and [47]. In particular, at a bit error rate of 10^{-5}, the performance improvement compared to [46] and [47] is nearly 7 and 6 dB, respectively. This performance improvement demonstrates the superiority of our proposed scheme which is due to the extra radiation pattern diversity gain offered by the use of reconfigurable antenna elements. Fig. 6.6 depicts the BER performance of the proposed code for a delay spread of $\tau = 20\mu s$. As shown in this figure, at a BER of 10^{-5}, our proposed coding scheme outperforms the codes presented in [46] and [47] by about 6 and 4 dB, respectively. It can be observed from the figure that the proposed scheme provides a diversity gain of $LPM_tM_r = 8$ while QOSF code proposed in [47] is capable of achieving a diversity of $LM_tM_r = 4$. Compared to the results in Fig. 6.5, it can be seen that as delay spread increases, the BER performance improves. This is due to benefiting from lower correlation between subcarriers, and therefore higher frequency diversity in multipath propagation channels. *Remark 6.1:* In large delay spread, the frequency response of the channel may vary rapidly and therefore adjacent subcarriers experience different fading with high probability, whereas in small delay spread cases, the frequency response of the channel varies slowly and adjacent subcarriers may experience similar fading. Therefore, a distributed subcarrier approach [94] will improve the system diversity when the delay spread in the system is small. It follows that employing such approach will improve the BER value illustrated in Fig. 6.5, such that the performance difference between Figs. 6.5 and 6.6 will be significantly reduced.

Fig. 6.7 shows the performance of the QOSFS block code for various number of radiation states (P = 1, 2, 3 or 4). From this figure, we observe that higher diversity and coding gains can be extracted as the number of radiation states increases. However, note that the decoding complexity also increases with the number of radiation states.

In Fig. 6.8, the BER performance of the QOSFS block code has been plotted versus the number of radiation pattern states for SNR = 9 dB and two different delay spread values. By increasing the number of radiation pattern states, we are able to extract higher levels of diversity and achieve higher coding gains. However, the decoding complexity increases correspondingly. Therefore, we conclude that considering the complexity of the system, it may not be worthwhile to increase the total number of radiation states beyond 5 states in a rich scattering environment.

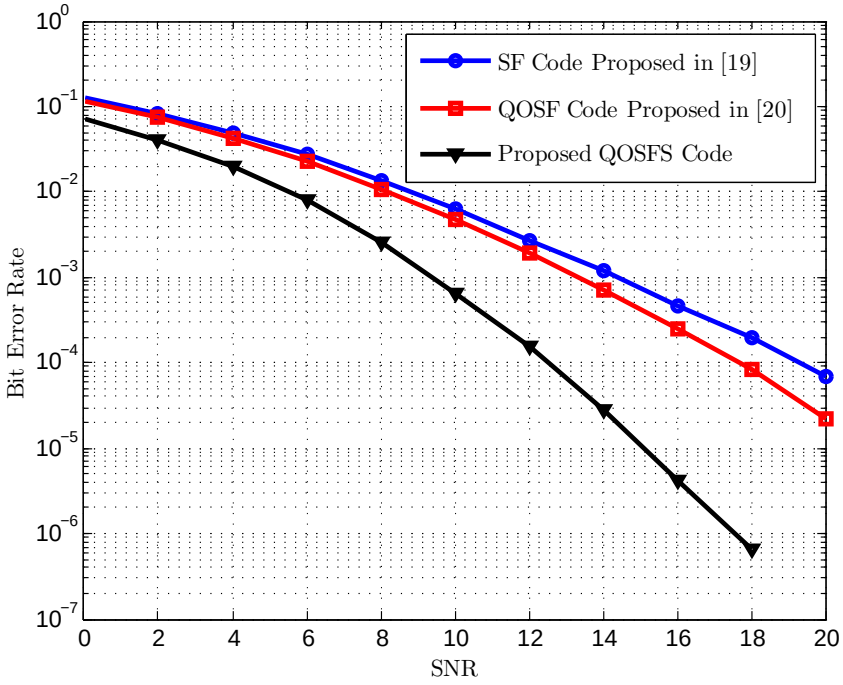

Figure 6.5 BER vs. SNR for a reconfigurable multi-antenna system with $M_t = 2$, $P = 2$, $M_r = 1$ in a 2-ray channel with a delay spread of $5\mu s$

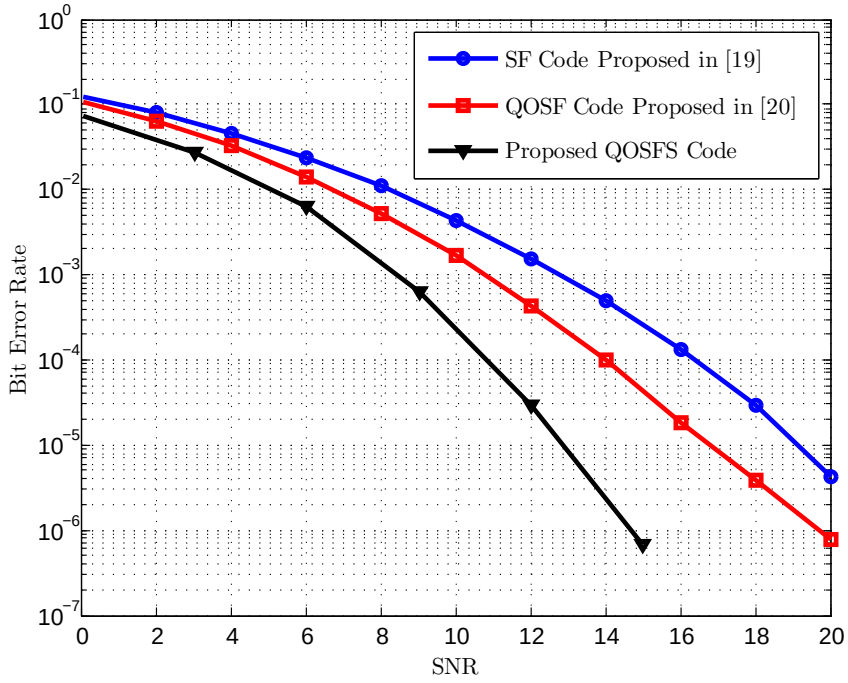

Figure 6.6 BER vs. SNR for a reconfigurable multi-antenna system with $M_t = 2$, $P = 2$, $M_r = 1$ in a 2-ray channel with a delay spread of $20\mu s$

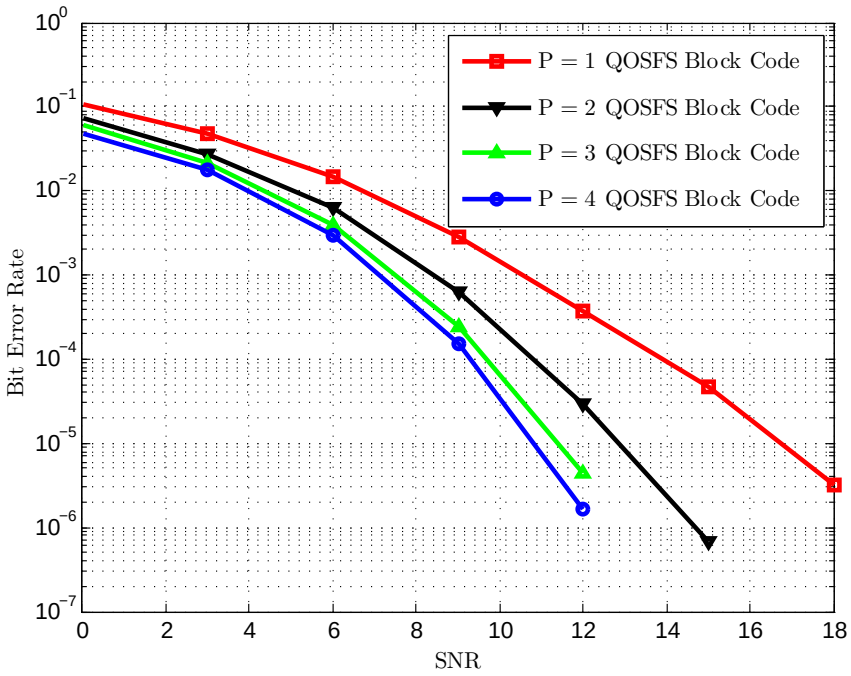

Figure 6.7 BER vs. SNR for a reconfigurable multi-antenna system in a 2-ray channel with delay spread of $20\mu s$ for different number of radiation states

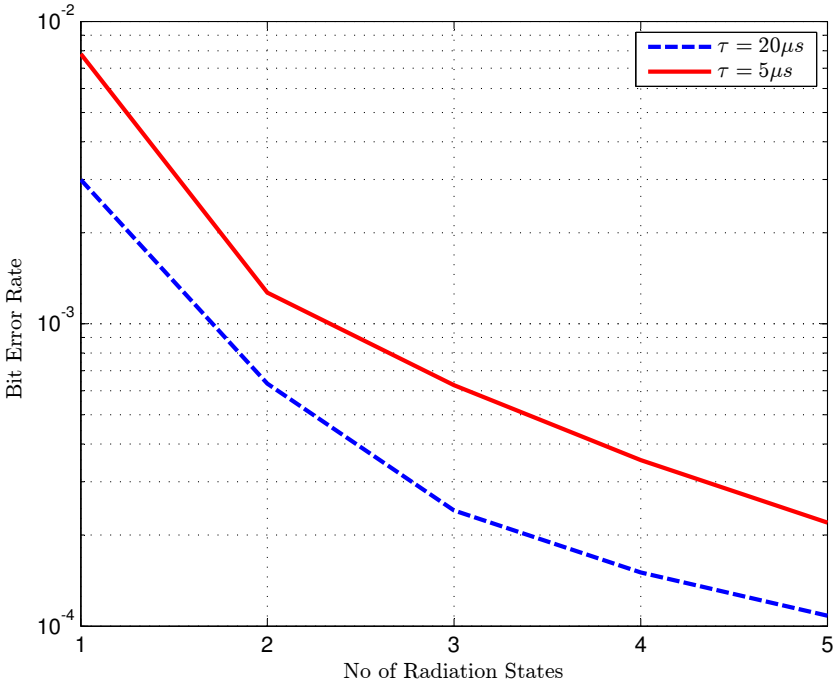

Figure 6.8 BER vs. number of radiaion states, P, for a reconfigurable multi-antenna system with $M_t = 2$, $M_r = 1$ and SNR= 9dB in a 2-ray channel with delay spreads of $5\mu s$ and $20\mu s$

6.8.2 Clustered Channel Model

In this part, we first recall the spatial channel model which is a statistical-based model proposed for evaluating MIMO system performance in urban micro-cell, urban macro-cell and suburban macro-cell fading environments [74]. Then, we evaluate the performance of the QOSFS block code for this channel model.

The channel coefficient between transmitter antenna i and receiver antenna j for the l-th cluster during the p-th radiation state, $l \in \{0, 1, \cdots, L-1\}$, is given by

$$\begin{aligned} \alpha_p^{i,j}(l) &= \sqrt{\frac{P_l}{M}} \sum_{m=1}^{M} \beta_m^l \\ &\times \sqrt{g_i^t(\phi_m^l, \mathbf{\Theta}_{i,t}^p)} e^{\jmath k_0 d_t (i-1) \sin(\phi_m^l)} \\ &\times \sqrt{g_j^r(\theta_m^l, \mathbf{\Theta}_{j,t}^p)} e^{\jmath k_0 d_r (j-1) \sin(\theta_m^l)}, \end{aligned} \tag{6.70}$$

where P_l is the power of the l-th cluster which is normalized so that the total average power for all clusters is equal to one, M is the number of unresolvable multipaths per cluster that have similar characteristics, β_m^l is the complex gain of the m-th multipath for the l-th path (the β_m^l are zero-mean unit-variance i.i.d complex random variables), $g_i^t(\phi, \mathbf{\Theta})$ is the gain of the i-th reconfigurable transmit antenna element with configuration parameters $\mathbf{\Theta}$ at the AoD ϕ, and $g_j^r(\theta, \mathbf{\Theta})$ is the gain of the j-th reconfigurable receive antenna element with configuration parameters $\mathbf{\Theta}$ at the AoA θ, $\mathbf{\Theta}_{i,t}^p = [\psi_i^p, G_i, B_i]$ is a vector of reconfiguration parameters related to the antenna radiation pattern, ψ_i^p denotes the pointing angle of the antenna at the p-th radiation state (i.e., the azimuth angle with maximum gain), G_i is the antenna gain, B_i is the 3-dB antenna beamwidth, $k_0 = 2\pi/\lambda$ is the free space wavenumber, where λ is the free-space wavelength, d_t and d_r are the antenna spacing between two elements at the transmitter and receiver side, respectively. ϕ_m^l and θ_m^l are the AoD and AoA for the m-th multipath of the l-th cluster, respectively, and can be given by

$$\phi_m^l = \phi_{l,AoD} + \vartheta_{m,AoD}^l, \tag{6.71}$$

$$\theta_m^l = \theta_{l,AoA} + \vartheta_{m,AoA}^l, \tag{6.72}$$

where $\phi_{l,AoD}$ and $\theta_{l,AoA}$ are the mean AoD and the mean AoA of the l^{th} cluster, respectively. The $\vartheta_{m,AoD}^l$ and $\vartheta_{m,AoA}^l$ are the deviation of the paths from mean AoD and AoA, respectively. The $\vartheta_{l,AoD}^m$ and $\vartheta_{l,AoA}^m$ are modeled as i.i.d. Gaussian random variables, with zero mean and variance σ_{AoD}^2 and σ_{AoA}^2, respectively.

In this work, we consider non-reconfigurable omnidirectional antenna elements at the

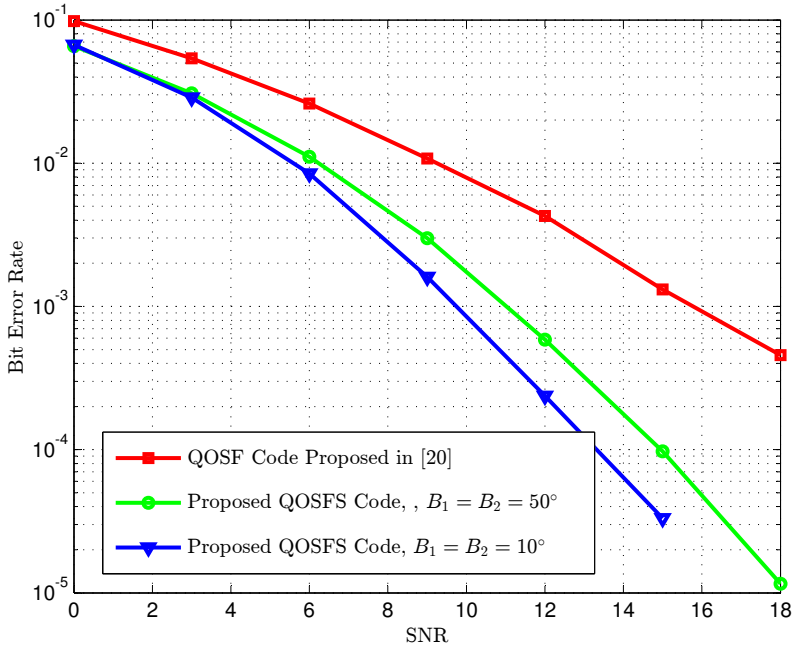

Figure 6.9 BER vs. SNR for a reconfigurable multi-antenna system with $M_t = 2$, $P = 2$, $M_r = 1$ in a clustered channel with a delay spread of $5\mu s$.

receiver side with $g_j^r(\theta, \Theta) = 1$ and reconfigurable antenna elements at the transmitter with $g_i^t(\phi_l^m, \mathbf{\Theta}_{i,t}^p)$ that can be approximated by a parabolic function as [74]:

$$g_i^t(\phi, \mathbf{\Theta}_{i,t}^p) = \max\left[G_i e^{-\alpha_i(\phi-\psi_i)^2}, g_{c_i}\right], \tag{6.73}$$

where $\phi \in [\psi_m - \pi, \psi_m + \pi)$ represents the azimuth angle, $\alpha_i = (\eta \ln 10)/(10B_i^2)$ with $\eta = 12$, and g_{c_i} is the constant gain of the antenna sidelobe.

Fig. 6.9 provides the BER performance of the proposed QOSFS code in a clustered channel model with $L = 2$ clusters and a delay spread of $\tau = 5\mu s$. Note that for the QOSFS code, the channel is considered to be independent from one state to another. For the reconfigurable MIMO-OFDM system, we consider $\phi_{1,AoD} = 10°$, $\phi_{2,AoD} = -10°$, $\theta_{1,AoA} = 30°$, $\theta_{2,AoA} = -30°$ for the first state, and $\phi_{1,AoD} = 30°$, $\phi_{2,AoD} = -30°$, $\theta_{1,AoA} = 20°$, $\theta_{2,AoA} = -20°$ for the second state. Moreover, the angular spread is set to 10 degrees at the transmitter and 5 degrees at the receiver. For these simulations, the radiation pattern of both antennas are assumed to have similar characteristics with gain $G_i = 360/B_i$ ($i \in \{1, 2\}$), beamwidth $B_1 = B_2 = \{50°, 10°\}$, and a sidelobe level of $g_{c_1}[\text{dB}] = g_{c_2}[\text{dB}] = -20$ dB. The antennas' pointing angles are $\psi_1^1 = 10°$, $\psi_2^1 = -10°$, $\psi_1^2 = 30°$ and $\psi_2^2 = -30°$. As demonstrated in this figure, the proposed QOSFS coding scheme achieves higher diversity and coding gains in a

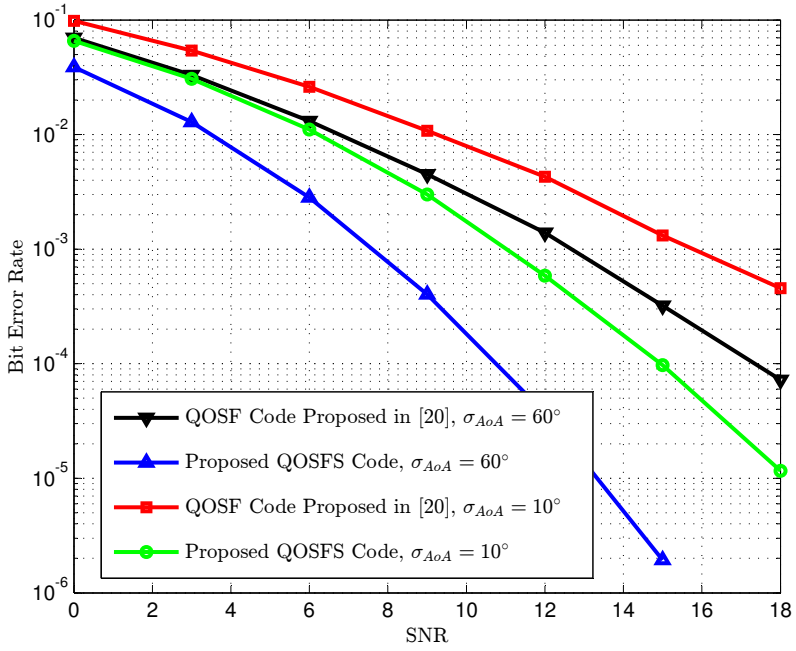

Figure 6.10 BER vs. SNR for a reconfigurable multi-antenna system with $M_t = 2$, $P = 2$, $M_r = 1$ in a clustered channel with a delay spread of $5\mu s$.

clustered environment as compared to the QOSF code presented in [47]. It can be seen that the QOSF and QOSFS codes provide lower diversity gain compared to the results in Fig. 6.5. This is due to the correlation between the signals arriving at the receiver introduced by the clusters. In Fig. 6.9, we also study the impact of antenna beamwidth on the average bit error rate performance of the proposed QOSFS code. As seen in the figure, as the antenna beamwidth gets narrower the antenna gain increases and therefore yields to a lower BER results. Furthermore, the narrower beamwidth decreases the decorrelation which slightly improves the diversity gain.

Fig. 6.10 shows the BER performance of the QOSFS and QOSF codes in a clustered channel for two different angular spread values at the transmitter. The proposed QOSFS code demonstrates a superior performance over the QOSF code, especially for larger angular spreads. It also can be observed from this figure that the QOSFS and QOSF codes exploit higher diversity and coding gains as the angular spread increases. The reason is that larger angular spread leads to lower correlation between the channel realizations.

Fig. 6.11 provides the BER performance of the proposed code in a clustered channel model with $L = 2$ clusters for a delay spread of $\tau = 5\mu s$. For the QOSFS code, we consider that the cluster parameters such as, AoD, AoA and the complex gain of all unresolvable multipaths are

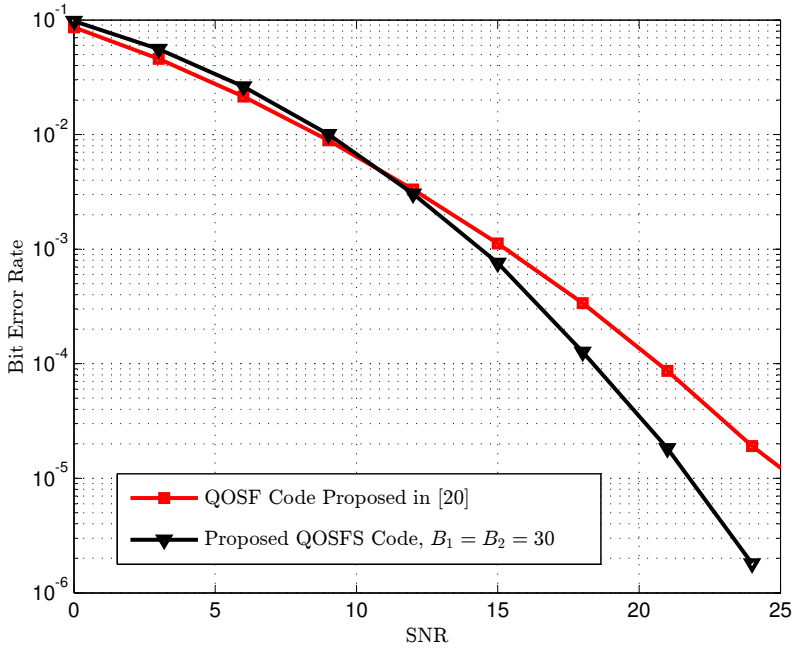

Figure 6.11 BER vs. SNR for a reconfigurable multi-antenna system with $M_t = 2$, $P = 2$, $M_r = 1$ in a clustered channel with a delay spread of $5\mu s$.

maintained at the same values for both radiation state (i.e., we have a block fading channel over the different radiation pattern states). In fact, only the antenna pointing angles, ψ_i^p, are changed form one state to another. For these simulations, we consider $\phi_{1,AoD} = 20°$, $\phi_{2,AoD} = -20°$, $\theta_{1,AoA} = 20°$, $\theta_{2,AoA} = -20°$ for both radiation states. The angular spread is set to be 10 degrees at the transmitter and 5 degrees at the receiver. Moreover, we assume that the radiation pattern of both antennas have similar characteristics with gain $G_i = 360/B_i$ ($i \in \{1, 2\}$), beamwidth $B_1 = B_2 = 30°$, and a sidelobe level of $g_{c_1}[\text{dB}] = g_{c_2}[\text{dB}] = -20$ dB. $\psi_1^1 = 10°$, $\psi_2^1 = -30°, \psi_1^2 = 30°$ and $\psi_2^2 = -10°$. It is interesting to note that at low SNR values, the QOSFS gets less coding gain compared to QOSF code due to the fact that each antenna only captures one cluster, but as the SNR increases the QOSFS achieves higher diversity gain and therefore provides a better BER performance.

6.9 Conclusion

We proposed a quasi-orthogonal space-frequency-state coding technique for MIMO-OFDM systems using antennas with reconfigurable radiation patterns. The proposed code is constructed based on the principle of quasi-orthogonal space-frequency coding scheme and consists of a block of transmitted symbols expanding over space, frequency, and radiation pat-

tern state dimensions. We evaluated the diversity and coding gains of the proposed code, and provide the criteria to select the code rotation angles to optimize the code performance and achieve maximum diversity. We provided simulation results to demonstrate the performance of the proposed coding scheme and make comparisons with that of previous SF coding schemes. In these experiments, it has been shown that the proposed code provides additional diversity and coding gains compared to the previously designed SF codes in MIMO-OFDM systems.

CHAPTER 7

Conclusion

We here summarize the work in this dissertation and discuss some of the foreseeable future research directions that this research may lead to.

7.1 Summary

In this dissertation, we first introduced a DoA estimation algorithm for a single-element reconfigurable antenna system. We then evaluated the performance of this algorithm in an anechoic chamber using an actual reconfigurable antenna called CRLH-LWA. We examined the effect of number of scanning steps on the accuracy of the estimated DoA. From the results, we observed that the DoA can be estimated accurately if the two chosen scanning steps are sufficiently far apart. In the case of having two scanning steps where they are very close and there is a large overlap in their radiation patterns, the algorithm fails to estimate the DoA properly and creates large fluctuations in the power spectrum. Moreover, we examined the impact of the DoA estimation error on the BER of the reconfigurable SISO system. Simulation results showed that the BER of the RE-SISO system with fixed antenna beamwidth and angular spread increases due to error in DoA estimation. Furthermore, it was shown that with small DoA estimation error, the system with smaller angular spread has a better performance than that with larger angular spread. However, for large DoA estimation error, this relationship is reversed. We also examined the BER performance of the system for different values of antenna beamwidth. While the BER of the system with narrower beamwidth has a better performance in small DoA estimation error, it is observed that in large DoA estimation error the system with wider beamwidth outperforms the system with narrower bandwidth.

In the following part of the dissertation, we proposed a low-complexity MIMO system employing reconfigurable antennas with electronically controllable radiation patterns over the frequency-selective channels to mitigate multipath effects and therefore remove inter symbol interference without using OFDM modulation technique. We studied the impact of angular spread and antenna beamwidth on its performance and make comparison with that of MIMO-OFDM system. We observed that as the angular spread decreases, the proposed RE-MIMO outperforms the MIMO-OFDM system. We also showed that the performance of the RE-MIMO system improves as the antenna beamwidth decreases.

In the next part of this dissertation, we derived analytical expressions for computing covariance matrix coefficients of the received signals impinging on a reconfigurable antenna array. The derived expressions were validated using a numerical integration method. We investigated the impact of radiation pattern characteristics and array configurations on the covariance coefficients. We also studied the capacity of a reconfigurable MIMO system using the derived analytical expressions. We showed how the presented results can be used to quickly choose the optimal configuration for each reconfigurable antenna element in the array.

In the last part of this dissertation, we proposed a space-frequency coding technique for MIMO-OFDM systems using antennas with reconfigurable radiation patterns. The proposed code is constructed based on the principle of quasi-orthogonal coding scheme and consists of a block of transmitted symbols expanding over space, frequency, and radiation state dimensions. We provided simulation results to demonstrate the performance of the proposed coding scheme and make comparisons with that of the previous SF coding schemes. In these experiments, it has been shown that the proposed code provides additional diversity and coding gains compared to the previously designed SF codes in MIMO-OFDM systems.

The developed algorithms and schemes in this dissertation can be used in 5th generation (5G) of wireless communication systems. As an example, our proposed block coding technique in Chapter 6 can be deployed in millimeter-wave wireless gigabit networks, where directional beamforming with real-time radiation pattern configuration and OFDM modulation are considered as key technologies to improve the BER performance of the system in an open-loop mode. The analytical expressions derived in Chapter 5 can be adopted in 5G to find the optimal radiation configuration at the receiver to enhance the system capacity. The correlation coefficients information obtained using the derived expressions can also be shared with the transmitter in a closed-loop system to find a superior transmission state, which can be utilized for the proposed space-frequency-state block code in Chapter 6.

In summary, in this dissertation, we achieve our stated general objectives by evaluating the performance of reconfigurable antenna systems and proposing new methods and algorithms to improve the system performance.

7.2 Future Works

A number of possible extensions of the research presented in this dissertation are briefly described below:

– In this dissertation, we derived the closed-form expressions for computing covariance matrix coefficients of the received signals at a reconfigurable antenna array. Using these expressions, we studied the capacity of a reconfigurable MIMO system for different ra-

diation pattern states. The future research direction in this area can be defined as to develop an optimal selection algorithm to choose the optimal configuration for each reconfigurable antenna element in the array that maximizes the system capacity based on the computed correlation coefficients using derived close-form expressions.

– Throughout this dissertation, we considered in the theoretical analysis a parabolic function model for the radiation pattern of a reconfigurable antenna. In this model, the antenna only steers in azimuth plane. Another extension of this work is to include vertical cuts as well which is needed for millimeter wave communications standard as beam steering will be required for both vertical and horizontal cuts. In this respect, the channel model also needs to be extended to include elevation power angular spectrum. In cases where a two-dimensional Laplacian or a general double exponential functions can model the incoming signal distribution, a similar methodology as the one presented in this dissertation can then be followed to obtain series expressions for the covariance matrix coefficients. However, the number of cases to be considered will increase as there is an extra variable to consider.

– In this dissertation, we focused on designing three dimensional block codes. One extension of this work is to consider the generalization of three dimensional block codes to n dimensional block codes where n is greater than three. Assume $n = 4$ which adds another orthogonal resource to the three dimensional channel model introduced in this dissertation. A simple method of designing four dimensional block codes based on the three dimensional block codes presented in this dissertation, is to apply a repetition coding over the forth orthogonal dimension.

– Throughout this dissertation, we have incorporated coherent detection schemes which require the knowledge of channel information at the receiver. However, due to the presence of multiple propagation at both the transmitter and the receiver, the channel estimation problem is more complicated and costly compared to a non-reconfigurable MIMO system. Novel channel estimation methods and techniques are required to make efficient channel estimation for reconfigurable MIMO systems possible.

Bibliography

[1] B. Cetiner, H. Jafarkhani, J. Qian, H. Yoo, A. Grau, and F. De Flaviis, "Multifunctional reconfigurable MEMS integrated antennas for adaptive MIMO systems," *IEEE Communications Magazine*, vol. 42, pp. 62–70, Dec. 2004.

[2] B. Cetiner, J. Qian, G. Li, and F. De Flaviis, "A reconfigurable spiral antenna for adaptive MIMO systems," *EURASIP Journal on Wireless Communications and Networking*, vol. 2005, pp. 382–389, Mar. 2005.

[3] T. Roach, G. Huff, and J. Bernhard, "On the applications for a radiation reconfigurable antenna," in *Proc. Second NASA/ESA Conference on Adaptive Hardware and Systems, AHS*, Edinburgh, UK, Aug. 2007, pp. 7–13.

[4] B. Cetiner, E. Akay, E. Sengul, and E. Ayanoglu, "A MIMO system with multifunctional reconfigurable antennas," *IEEE Antennas and Wireless Propagation Letters*, vol. 5, pp. 463–466, Jan. 2006.

[5] D. Piazza, N. Kirsch, A. Forenza, R. Heath, and K. Dandekar, "Design and evaluation of a reconfigurable antenna array for MIMO systems," *IEEE Trans. Antennas and Propagat.*, vol. 56, pp. 869–881, Mar. 2008.

[6] A. Grau, H. Jafarkhani, and F. De Flaviis, "A reconfigurable multiple-input multiple-output communication system," *IEEE Trans. Wireless Commun.*, vol. 7, pp. 1719–1733, May 2008.

[7] J. Frigon, C. Caloz, and Y. Zhao, "Dynamic radiation pattern diversity (DRPD) MIMO using CRLH leaky-wave antennas," in *Proc. IEEE Radio and Wireless Symposium*, Jan. 2008, pp. 635–638.

[8] A. Yokoi, T. Mitsui, B.-T. Yoon, and Y.-E. Kim, "Improvement of channel capacity on MIMO antenna systems with antenna pattern selection," in *Proc. IEEE Int. Symp. on Antennas and Propagat.*, Honolulu, HI, Jun. 2007, pp. 3249–3252.

[9] J. D. Boerman and J. T. Bernhard, "Performance study of pattern reconfigurable antennas in MIMO communication systems," *IEEE Trans. Antennas and Propagat.*, vol. 56, pp. 231–236, Jan. 2008.

[10] H. Eslami, C. P. Sukumar, D. Rodrigo, S. Mopidevi, A. M. Eltawil, L. Jofre, and B. A. Cetiner, "Reduced overhead training for multi reconfigurable antennas with beam-tilting capability," *IEEE Trans. Wireless Commun.*, vol. 9, pp. 3810–3821, Dec. 2010.

[11] V. Vakilian, J.-F. Frigon, and S. Roy, "Performance evaluation of reconfigurable MIMO systems in spatially correlated frequency-selective fading channels," in *Proc. IEEE Veh. Technol. Conf.*, Sept. 2012, pp. 1–5.

[12] W. Weedon, W. Payne, and G. Rebeiz, "MEMS-switched reconfigurable antennas," in *Proc. IEEE Antennas and Propagation Society International Symposium*, Jul. 2001, pp. 654–657.

[13] C. Caloz and T. Itoh, *Electromagnetic Metamaterials: Transmission Line Theory and Microwave Applications*. Wiley-IEEE Press, 2005.

[14] C. won Jung, M.-j. Lee, G. Li, and F. De Flaviis, "Reconfigurable scan-beam single-arm spiral antenna integrated with RF-MEMS switches," *IEEE Trans. Antennas and Propagat.*, vol. 54, pp. 455–463, Feb. 2006.

[15] "IEEE standard for information technology–telecommunications and information exchange between systems–local and metropolitan area networks–specific requirements-part 11: Wireless LAN medium access control (MAC) and physical layer (PHY) specifications amendment 3: Enhancements for very high throughput in the 60 GHz band," *IEEE Std 802.11ad-2012*, pp. 1–628, Dec. 2012.

[16] V. Vakilian, J.-F. Frigon, and S. Roy, "Direction-of-arrival estimation in a clustered channel model," in *Proc. IEEE 10th Int. New Circuits and Systems Conf. (NEWCAS)*, June 2012, pp. 313–316.

[17] ——, "Effects of angle-of-arrival estimation errors, angular spread and antenna beamwidth on the performance of reconfigurable SISO systems," in *Proc. IEEE Pacific Rim Conf. on Commun., Computers and Signal Process. (PacRim)*, Aug. 2011, pp. 515–519.

[18] V. Vakilian, H. V. Nguyen, S. Abielmona, S. Roy, and J.-F. Frigon, "Experimental study of direction-of-arrival estimation using reconfigurable antennas," in *Proc. IEEE Canadian Conf. on Elect. and Comput. Eng. (CCECE)*.

[19] V. Vakilian, J.-F. Frigon, and S. Roy, "On the covariance matrix and capacity evaluation of reconfigurable antenna array systems," *IEEE Trans. Wireless Commun.*, vol. 13, pp. 3452–3463, June 2014.

[20] ——, "Space-frequency block code for MIMO-OFDM communication systems with reconfigurable antennas," in *Proc. IEEE Global Commun. Conf.*, Dec. 2013.

[21] R. Schmidt, "Multiple emitter location and signal parameter estimation," *IEEE Trans. Antennas and Propagat.*, vol. 34, pp. 276–280, Mar. 1986.

[22] A. Weiss and B. Friedlander, "Eigenstructure methods for direction finding with sensor gain and phase uncertainties," *Circuits, Systems, and Signal Processing*, vol. 9, pp. 271–300, Mar. 1990.

[23] C. Plapous, J. Cheng, E. Taillefer, A. Hirata, and T. Ohira, "Reactance domain MUSIC algorithm for electronically steerable parasitic array radiator," *IEEE Trans. Antennas and Propagat.*, vol. 52, p. 3257, Dec. 2004.

[24] H. Paaso, A. Mammela, D. Patron, and K. R. Dandekar, "Modified music algorithm for doa estimation using crlh leaky-wave antennas," in *Proc. International Conference on Cognitive Radio Oriented Wireless Networks (CROWNCOM)*, 2013, pp. 166–171.

[25] C. Caloz and T. Itoh, "Electromagnetic Metamaterial," *Willey Interscience*, 2006.

[26] X. Li and J. Frigon, "Capacity Analysis of MIMO Systems with Dynamic Radiation Pattern Diversity," in *Proc. IEEE Veh. Technol. Conf.*, Apr. 2009, pp. 1–5.

[27] W. Lee, "Effects on correlation between two mobile radio base-station antennas," *IEEE Trans. Commun.*, vol. 21, pp. 1214–1224, Nov. 1973.

[28] J. Salz and J. Winters, "Effect of fading correlation on adaptive arrays in digital mobile radio," *IEEE Trans. Veh. Technol.*, vol. 43, pp. 1049–1057, Apr. 1994.

[29] J. Tsai, R. Buehrer, and B. Woerner, "Spatial fading correlation function of circular antenna arrays with Laplacian energy distribution," *IEEE Commun. Lett.*, vol. 6, pp. 178–180, May 2002.

[30] P. Teal, T. Abhayapala, and R. Kennedy, "Spatial correlation for general distributions of scatterers," *IEEE Signal Process. Lett.*, vol. 9, pp. 305–308, Oct. 2002.

[31] W. Tsen and H. Li, "Correlations and channel capacities for multi-polarized MIMO systems," in *Proc. IEEE Int. Symp. on Pers. Indoor Mobile Radio Commun.*, Tokyo, Japan, Sept. 2009, pp. 1069–1073.

[32] B. Sieskul, C. Kupferschmidt, and T. Kaiser, "Spatial fading correlation for local scattering: A condition of angular distribution," *IEEE Trans. Veh. Technol.*, vol. 60, pp. 1271–1278, March 2011.

[33] L. Schumacher, K. I. Pedersen, and P. E. Mogensen, "From antenna spacings to theoretical capacities-guidelines for simulating MIMO systems," in *Proc. IEEE Int. Symp. on Pers. Indoor Mobile Radio Commun.*, vol. 2, Lisbon, Portugal, Sept. 2002, pp. 587–592.

[34] A. Forenza, D. J. Love, and R. W. Heath, "Simplified spatial correlation models for clustered MIMO channels with different array configurations," *IEEE Trans. Veh. Commun.*, vol. 56, pp. 1924–1934, Apr. 2007.

[35] L. Schumacher and B. Raghothaman, "Closed-form expressions for the correlation coefficient of directive antennas impinged by a multimodal truncated Laplacian PAS," *IEEE Trans. Wireless Commun.*, vol. 4, pp. 1351–1359, Apr. 2005.

[36] F. Fazel, A. Grau, H. Jafarkhani, and F. Flaviis, "Space-time-state block coded mimo communication systems using reconfigurable antennas," *IEEE Trans. Wireless Commun.*, vol. 8, pp. 6019–6029, Aug. 2009.

[37] D. Agrawal, V. Tarokh, A. Naguib, and N. Seshadri, "Space-time coded OFDM for high data-rate wireless communication over wideband channels," in *Proc. IEEE Veh. Technol. Conf.*, vol. 3, 1998, pp. 2232–2236.

[38] K. F. Lee and D. B. Williams, "A space-time coded transmitter diversity technique for frequency selective fading channels," in *Proc. IEEE Sensor Array and Multichannel Signal Processing Workshop*, Mar. 2000, pp. 149–152.

[39] H. Bolcskei and A. J. Paulraj, "Space-frequency coded broadband OFDM systems," in *in Proc. IEEE WCNC*, vol. 1, Sept. 2000, pp. 1–6.

[40] B. Lu and X. Wang, "Space-time code design in ofdm systems," in *Proc. IEEE Global Commun. Conf.*, vol. 2, 2000, pp. 1000–1004.

[41] R. S. Blum, Y. G. Li, J. H. Winters, and Q. Yan, "Improved space-time coding for MIMO-OFDM wireless communications," *IEEE Trans. Commun.*, vol. 49, pp. 1873–1878, Nov. 2001.

[42] Z. Hong and B. L. Hughes, "Robust space-time codes for broadband OFDM systems," in *Proc. IEEE Wireless Commun. Networking Conf.*, vol. 1, 2002, pp. 105–108.

[43] K. F. Lee and D. B. Williams, "A space-frequency transmitter diversity technique for OFDM systems," in *Proc. IEEE Global Commun. Conf.*, vol. 3, 2000, pp. 1473–1477.

[44] A. Molisch, M. Win, and J. Winters, "Space-time-frequency (STF) coding for MIMO-OFDM systems," *IEEE Commun. Lett.*, vol. 6, pp. 370–372, Sept. 2002.

[45] W. Su, Z. Safar, M. Olfat, and K. R. Liu, "Obtaining full-diversity space-frequency codes from space-time codes via mapping," *IEEE Trans. Signal Process.*, vol. 51, pp. 2905–2916, Nov. 2003.

[46] W. Su, Z. Safar, and K. R. Liu, "Full-rate full-diversity space-frequency codes with optimum coding advantage," *IEEE Trans. Inf. Theory*, vol. 51, pp. 229–249, Jan. 2005.

[47] F. Fazel and H. Jafarkhani, "Quasi-orthogonal space-frequency and space-time-frequency block codes for MIMO OFDM channels," *IEEE Trans. Wireless Commun.*, vol. 7, pp. 184–192, Jan. 2008.

[48] A. Papoulis and S. U. Pillai, *Probability, Random Variables, and Stochastic Processes*. Tata McGraw-Hill Education, 2002.

[49] T. S. Rappaport *et al.*, *Wireless Communications: Principles and Practice*. Prentice Hall PTR New Jersey, 1996, vol. 2.

[50] S. M. Alamouti, "A simple transmit diversity technique for wireless communications," *IEEE Journal on Selected Areas in Communications*, vol. 16, pp. 1451–1458, Aug.1998.

[51] V. Tarokh, N. Seshadri, and A. Calderbank, "Space-time codes for high data rate wireless communication: Performance criterion and code construction," *IEEE transactions on information theory*, vol. 44, pp. 744–765, Feb. 1998.

[52] J. H. Winters, "The diversity gain of transmit diversity in wireless systems with rayleigh fading," *IEEE Trans. Veh. Technol.*, vol. 47, pp. 119–123, Jan. 1998.

[53] L. Dong, H. Ling, and R. W. Heath, "Multiple-input multiple-output wireless communication systems using antenna pattern diversity," in *Proc. IEEE Global Telecommun. Conf.*, vol. 1, Nov. 2002, pp. 997–1001.

[54] P. Mattheijssen, M. H. Herben, G. Dolmans, and L. Leyten, "Antenna-pattern diversity versus space diversity for use at handhelds," *IEEE Trans. Veh. Technol.*, vol. 53, pp. 1035–1042, Apr. 2004.

[55] A. Forenza and R. Heath Jr, "Benefit of pattern diversity via two-element array of circular patch antennas in indoor clustered MIMO channels," *IEEE Trans. Commun.*, vol. 54, pp. 943–954, May 2006.

[56] V. Tarokh, H. Jafarkhani, and A. R. Calderbank, "Space-time block codes from orthogonal designs," *IEEE Transactions on Information Theory*, vol. 45, pp. 1456–1467, May 1999.

[57] H. Jafarkhani, "A quasi-orthogonal space-time block code," *IEEE Trans. Commun.*, vol. 49, pp. 1–4, Jan. 2001.

[58] O. Tirkkonen, "Optimizing space-time block codes by constellation rotations," in *Finnish Wireless Commun. Workshop (FWWC)*, Oct. 2001, pp. 59–60.

[59] W. Su and X.-G. Xia, "Quasi-orthogonal space-time block codes with full diversity," in *International Symposium on Optical Science and Technology*, 2002, pp. 283–294.

[60] N. Sharma and C. B. Papadias, "Improved quasi-orthogonal codes through constellation rotation," *IEEE Trans. Commun.*, vol. 51, pp. 332–335, March 2003.

[61] T. Ohira and K. Gyoda, "Electronically steerable passive array radiator antennas for low-cost analog adaptive beamforming," in *Proc. IEEE International Conference on Phased Array Systems and Technology*, 2002, pp. 101–104.

[62] A. Grau, M. Lee, J. Romeu, H. Jafarkhani, L. Jofre, and F. De Flaviis, "A multifunctional MEMS-reconfigurable pixel antenna for narrowband MIMO communications," in *Proc. IEEE Antennas and Propagation Society International Symposium*, Jun. 2007, pp. 489–492.

[63] A. Grau, J. Romeu, L. Jofre, and F. De Flaviis, "On the polarization diversity gain using the ORIOL antenna in fading indoor environments," in *Proc. IEEE Antennas and Propagation Society International Symposium*, Jul. 2005, pp. 14–17.

[64] G. Huff, J. Feng, S. Zhang, and J. Bernhard, "A novel radiation pattern and frequency reconfigurable single turn square spiral microstrip antenna," *IEEE Microwave Wireless Compon. Lett.*, vol. 13, pp. 57–59, Feb. 2003.

[65] C. Balanis and P. Ioannides, "Introduction to smart antennas," *Synthesis Lectures on Antennas*, vol. 2, pp. 1–175, Jan. 2007.

[66] E. Taillefer, C. Plapous, J. Cheng, K. Iigusa, and T. Ohira, "Reactance-domain MUSIC for ESPAR antennas (experiment)," Mar. 2003, pp. 98–102.

[67] C. Caloz and T. Itoh, "Array factor approach of leaky-wave antennas and application to 1-D/2-D composite right/left-handed (CRLH) structures," *IEEE Microwave and wireless components letters*, vol. 14, pp. 274–276, Jun. 2004.

[68] E. Taillefer, A. Hirata, and T. Ohira, "Direction-of-arrival estimation using radiation power pattern with an ESPAR antenna," *IEEE Trans. Antennas and Propagat.*, vol. 53, pp. 678–684, Feb. 2005.

[69] H. Li, Y.-D. Yao, and J. Yu, "Outage probabilities of wireless systems with imperfect beamforming," *IEEE Trans. Veh. Commun.*, vol. 55, pp. 1503–1515, May 2006.

[70] A. Saleh and R. Valenzuela, "A statistical model for indoor multipath propagation," *IEEE Journal on Selected Areas in Communications*, vol. 5, pp. 128–137, Feb. 1987.

[71] V. Erceg, "TGn channel models," *IEEE 802.11-03/940r4*, May 2004.

[72] "3GPP Technical Specification Group Spatial channel model SCM-134 text V6.0," *Spatial Channel Model AHG (Combined Ad-Hoc from 3GPP and 3GPP2)*, Apr. 2003.

[73] D. Tse, *Fundamentals of Wireless Communication.* Cambridge University Press, 2005.

[74] 3rd Generation Partnership Project (3GPP), "Spatial channel model for multiple input multiple output (MIMO) simulations(3GPP tr 25.996 version 6.1.0 release 6)," *ETSI, Tech. Rep*, 2003.

[75] Nutaq. [Online]. Available: http://www.nutaq.com/

[76] S. Lim, C. Caloz, and T. Itoh, "Metamaterial-based electronically controlled transmission-line structure as a novel leaky-wave antenna with tunable radiation angle and beamwidth," *IEEE Trans. Microw. Theory and Tech.*, vol. 52, pp. 2678–2690, Dec. 2004.

[77] T. Roach, G. Huff, and J. Bernhard, "Enabling high performance wireless communication systems using reconfigurable antennas," in *Proc. IEEE Military Communications Conference, MILCOM*, Washington, DC, Oct. 2006, pp. 1–6.

[78] B. Cetiner, Z. Li, D. Rodrigo, and L. Jofre, "A new class of antenna array with a reconfigurable element factor," *IEEE Trans. Antennas and Propagat.*, Apr. 2013.

[79] R. M. Buehrer, "The impact of angular energy distribution on spatial correlation," in *Proc. IEEE Veh. Technol. Conf.*, vol. 2, Vancouver, Canada, Sept. 2002, pp. 1173–1177.

[80] M. E. Abramowitz *et al.*, *Handbook of Mathematical Functions: with Formulas, Graphs, and Mathematical Tables*. Courier Dover Publications, 1964, vol. 55.

[81] K. Kalliola, K. Sulonen, H. Laitinen, O. Kivekas, J. Krogerus, and P. Vainikainen, "Angular power distribution and mean effective gain of mobile antenna in different propagation environments," *IEEE Trans. Veh. Technol.*, vol. 51, pp. 823–838, Sept. 2002.

[82] G. Foschini and M. Gans, "On limits of wireless communications in a fading environment when using multiple antennas," *Wireless personal communications*, vol. 6, pp. 311–335, Mar. 1998.

[83] P. Marques and S. Abrantes, "On the derivation of the exact, closed-form capacity formulas for receiver-sided correlated MIMO channels," *IEEE Trans. Inf. Theory*, vol. 54, pp. 1139–1161, March 2008.

[84] A. Maltsev *et al.*, "Channel models for 60 GHz WLAN systems," IEEE P802.11 Wireless LANs, Tech. Rep., Mar. 2010, IEEE doc. 802.11-09/0334r8.

[85] Z. Liu, Y. Xin, and G. B. Giannakis, "Space-time-frequency coded OFDM over frequency-selective fading channels," *IEEE Trans. Signal Process.*, vol. 50, pp. 2465–2476, Oct. 2002.

[86] Y. Gong and K. B. Letaief, "Space-frequency-time coded OFDM for broadband wireless communications," in *Proc. IEEE Global Commun. Conf.*, vol. 1, 2001, pp. 519–523.

[87] Y. Xin, Z. Wang, and G. B. Giannakis, "Space-time diversity systems based on linear constellation precoding," *IEEE Trans. Wireless Commun.*, vol. 2, pp. 294–309, Feb. 2003.

[88] L. Wei and W. Siqi, "Space-time-frequency block coding over Rayleigh fading channels for OFDM systems," in *Proc. International Conf. on Commun. Technol.*, vol. 2, Apr. 2003, pp. 1008–1012.

[89] W. Su and X.-G. Xia, "Signal constellations for quasi-orthogonal space-time block codes with full diversity," *IEEE Trans. Inf. Theory*, vol. 50, pp. 2331–2347, Oct. 2004.

[90] M. Fitz, J. Grimm, and S. Siwamogsatham, "A new view of performance analysis techniques in correlated rayleigh fading," in *in Proc. IEEE WCNC*, Sept. 1999, pp. 139–144.

[91] A. Sadek, W. Su, and K. Liu, "Maximum achievable diversity for MIMO-OFDM systems with arbitrary spatial correlation," in *Proc. IEEE Global Telecommun. Conf.*, vol. 4, 2004, pp. 2664–2668.

[92] R. A. Horn and C. R. Johnson, *Matrix Analysis*. Cambridge University Press, 2012.

[93] R. Horn and C. Johnson, *Topics in Matrix Analysis*. Cambridge University Press, 1994.

[94] S. Sesia, I. Toufik, and M. Baker, *LTE: The UMTS Long Term evolutionn: From Theory to Practice*. Wiley, Feb. 2009.

APPENDIX A

Computing Channel Variance

In this appendix, we compute the variance of h_m in (3.16). Let us rewrite (3.14) as

$$g_r(x) = \frac{2\pi}{B_{3dB}} 10^{-0.1\eta(\frac{x}{B_{3dB}})^2} \tag{A.1}$$

where $x \sim \mathcal{N}(0, \sigma^2_{DoA})$. Then,

$$g_r(y) = \frac{2\pi}{B_{3dB}} 10^{-y^2} \tag{A.2}$$

where $y \sim \mathcal{N}(0, \sigma^2)$ where $\sigma^2 = \frac{0.1\eta\sigma^2_{DoA}}{B^2_{3dB}}$. Thus, the expected value of $g_r(y)$ can be written as

$$\begin{aligned}
\mathbb{E}[g_r(y)] &= \int_{-\infty}^{\infty} g_r(y) p_Y(y) dy \\
&= \frac{1}{\sqrt{2\pi}\sigma} \int_{-\infty}^{\infty} \frac{2\pi}{B_{3dB}} 10^{-y^2} e^{-y^2/2\sigma^2} dy \\
&= \frac{\sqrt{2\pi}}{B_{3dB}\sigma} \int_{-\infty}^{\infty} e^{-y^2[(1/\log e) + \left(1/2\sigma^2\right)]} dy \\
&= \frac{2\pi}{B_{3dB}\sigma\sqrt{2/\log e + 1/\sigma^2}} \\
&= \frac{2\pi}{B_{3dB}\sqrt{2c\sigma^2 + 1}}
\end{aligned} \tag{A.3}$$

APPENDIX B

Computing Channel Variance with Imperfect DoA Estimation

In this appendix, we compute the variance of $\widetilde{h}_m$ in (3.23). Using (3.22), the antenna gain under imperfect DoA estimation can be written as

$$\widetilde{g_r}(x) = \frac{2\pi}{B_{3dB}} 10^{-0.1\eta(\frac{x-\theta_{Err}}{B_{3dB}})^2} \tag{B.1}$$

where $x \sim \mathcal{N}(0, \sigma^2_{DoA})$. Then,

$$\widetilde{g_r}(y) = \frac{2\pi}{B_{3dB}} 10^{-y^2} \tag{B.2}$$

where $y \sim \mathcal{N}(\mu, \sigma^2)$. Thus, the expected value of $\widetilde{g_r}(y)$ can be written as

$$\begin{aligned}
\mathbb{E}[\widetilde{g_r}(y)] &= \int_{-\infty}^{\infty} \widetilde{g_r}(y) p_Y(y) dy \\
&= \frac{1}{\sqrt{2\pi}\sigma} \int_{-\infty}^{\infty} \frac{2\pi}{B_{3dB}} 10^{-y^2} e^{-(y-\mu)^2/2\sigma^2} dy \\
&= \frac{\sqrt{2\pi}}{B_{3dB}\sigma} \int_{-\infty}^{\infty} e^{-Ay^2+By-C} dy
\end{aligned} \tag{B.3}$$

where $A = (1/\log e + 1/2\sigma^2)$, $B = \frac{\mu}{\sigma^2}$ and $C = \frac{\mu^2}{2\sigma^2}$. Then,

$$\begin{aligned}
\mathbb{E}[\widetilde{g_r}(y)] &= \frac{\sqrt{2\pi}}{B_{3dB}\sigma} \int_{-\infty}^{\infty} e^{A(y-\frac{B}{2A})^2+\frac{B^2}{4A}-C} dy \\
&= \frac{\sqrt{2\pi}}{B_{3dB}\sigma} e^{\frac{B^2}{4A}-C} \int_{-\infty}^{\infty} e^{-A(y-\frac{B}{2A})^2} dy \\
&= \frac{2\pi}{B_{3dB}\sigma\sqrt{2/\log e + 1/\sigma^2}} e^{\frac{B^2}{4A}-C} \\
&= \frac{2\pi}{B_{3dB}\sqrt{2c\sigma^2+1}} e^{\frac{(\frac{\mu}{\sigma^2})^2}{4(1/\log e+1/2\sigma^2)}-\frac{\mu^2}{2\sigma^2}}
\end{aligned} \tag{B.4}$$

where $c = \frac{1}{\log e}$ is a constant.

APPENDIX C

Derivation of Equations (5.22)-(5.29)

In this appendix, we derive the analytical expressions of (5.22)-(5.29) for computing $\Lambda_i^{l,k}(\mathbf{\Theta}_m, \mathbf{\Theta}_n)$.

$$f_o g_{c_m} g_{c_n} p_L(A,B) = \beta(\frac{\sigma_l}{\sqrt{2}}) e^{\frac{\sqrt{2}(\phi-\phi_0^l)}{\sigma_l}}\Big|_A^B \tag{C.1}$$

$$f_c g_{c_m} g_{c_n} p_L(A,B) = \beta \frac{(\frac{\sqrt{2}}{\sigma_l})\cos(2k\phi) + 2k\sin(2k\phi)}{(\frac{\sqrt{2}}{\sigma_l})^2 + 4k^2} e^{\frac{\sqrt{2}(\phi-\phi_0^l)}{\sigma_l}}\Big|_A^B \tag{C.2}$$

$$f_s g_{c_m} g_{c_n} p_L(A,B) = \beta \frac{(\frac{\sqrt{2}}{\sigma_l})\sin[(2k+1)\phi] - (2k+1)\cos[(2k+1)\phi]}{(\frac{\sqrt{2}}{\sigma_l})^2 + (2k+1)^2} e^{\frac{\sqrt{2}(\phi-\phi_0^l)}{\sigma_l}}\Big|_A^B \tag{C.3}$$

$$f_o g_{c_m} g_{c_n} p_R(A,B) = -\beta(\frac{\sigma_l}{\sqrt{2}}) e^{-\frac{\sqrt{2}(\phi-\phi_0^l)}{\sigma_l}}\Big|_A^B \tag{C.4}$$

$$f_c g_{c_m} g_{c_n} p_R(A,B) = \beta \frac{(\frac{-\sqrt{2}}{\sigma_l})\cos(2k\phi) + 2k\sin(2k\phi)}{(\frac{\sqrt{2}}{\sigma_l})^2 + 4k^2} e^{\frac{-\sqrt{2}(\phi-\phi_0^l)}{\sigma_l}}\Big|_A^B \tag{C.5}$$

$$f_s g_{c_m} g_{c_n} p_R(A,B) = \beta \frac{(\frac{-\sqrt{2}}{\sigma_l})\sin[(2k+1)\phi] - (2k+1)\cos[(2k+1)\phi]}{(\frac{\sqrt{2}}{\sigma_l})^2 + (2k+1)^2} e^{\frac{-\sqrt{2}(\phi-\phi_0^l)}{\sigma_l}}\Big|_A^B \tag{C.6}$$

$$f_o g_{p_m} g_{c_n} p_L(A,B) = \sqrt{\frac{G_m \beta \pi}{\alpha_m}} \left\{ \exp[X] \operatorname{erf}[Y] \right\} \Big|_A^B \tag{C.7}$$
$$\text{where } X = \frac{(\sqrt{2} + \alpha_m \psi_m \sigma_l)^2 - 2\sqrt{2}\alpha_m \sigma_l \phi_0^l - \alpha_m^2 \sigma_l^2 \psi_m^2}{2\alpha_m \sigma_l^2}$$
$$\text{and } Y = \frac{\alpha_m \sigma_l \phi - (\sqrt{2} + \alpha_m \psi_m \sigma_l)}{\sqrt{2\alpha_m \sigma_l^2}}$$

$$f_c g_{p_m} g_{c_n} p_L(A,B) = \sqrt{\frac{G_m \beta \pi}{\alpha_m}} \Re\{ \exp[X] \operatorname{erf}[Y] \} \Big|_A^B \tag{C.8}$$
$$\text{where } X = \frac{(\sqrt{2} + j2k\sigma_l + \alpha_m \psi_m \sigma_l)^2 - 2\sqrt{2}\alpha_m \sigma_l \phi_0^l - \alpha_m^2 \sigma_l^2 \psi_m^2}{2\alpha_m \sigma_l^2}$$
$$\text{and } Y = \frac{\alpha_m \sigma_l \phi - (\sqrt{2} + j2k\sigma_l + \alpha_m \psi_m \sigma_l)}{\sqrt{2\alpha_m \sigma_l^2}}$$

$$f_s g_{p_m} g_{c_n} p_L(A,B) = \sqrt{\frac{G_m \beta \pi}{\alpha_m}} \Im\{ \exp[X] \operatorname{erf}[Y] \} \Big|_A^B \tag{C.9}$$
$$\text{where } X = \frac{(\sqrt{2} + j(2k+1)\sigma_l + \alpha_m \psi_m \sigma_l)^2 - 2\sqrt{2}\alpha_m \sigma_l \phi_0^l - \alpha_m^2 \sigma_l^2 \psi_m^2}{2\alpha_m \sigma_l^2}$$
$$\text{and } Y = \frac{\alpha_m \sigma_l \phi - (\sqrt{2} + j(2k+1)\sigma_l + \alpha_m \psi_m \sigma_l)}{\sqrt{2\alpha_m \sigma_l^2}}$$

$$f_o g_{p_m} g_{c_n} p_R(A,B) = \sqrt{\frac{G_m \beta \pi}{\alpha_m}} \left\{ \exp[X] \operatorname{erf}[Y] \right\} \Big|_A^B \tag{C.10}$$
$$\text{where } X = \frac{(\sqrt{2} - \alpha_m \psi_m \sigma_l)^2 + 2\sqrt{2}\alpha_m \sigma_l \phi_0^l - \alpha_m^2 \sigma_l^2 \psi_m^2}{2\alpha_m \sigma_l^2}$$
$$\text{and } Y = \frac{\alpha_m \sigma_l \phi + (\sqrt{2} - \alpha_m \psi_m \sigma_l)}{\sqrt{2\alpha_m \sigma_l^2}}$$

$$f_c g_{p_m} g_{c_n} p_R(A,B) = \sqrt{\frac{G_m \beta \pi}{\alpha_m}} \Re\{ \exp[X] \operatorname{erf}[Y] \} \Big|_A^B \tag{C.11}$$
$$\text{where } X = \frac{(\sqrt{2} - j2k\sigma_l - \alpha_m \psi_m \sigma_l)^2 + 2\sqrt{2}\alpha_m \sigma_l \phi_0^l - \alpha_m^2 \sigma_l^2 \psi_m^2}{2\alpha_m \sigma_l^2}$$
$$\text{and } Y = \frac{\alpha_m \sigma_l \phi + (\sqrt{2} - j2k\sigma_l - \alpha_m \psi_m \sigma_l)}{\sqrt{2\alpha_m \sigma_l^2}}$$

$$f_s g_{p_m} g_{c_n} p_R(A,B) = \sqrt{\frac{G_m \beta \pi}{\alpha_m}}\, \Im\{\exp[X]\,\mathrm{erf}[Y]\}\Big|_A^B \tag{C.12}$$
$$\text{where } X = \frac{(\sqrt{2} - j(2k+1)\sigma_l - \alpha_m\psi_m\sigma_l)^2 + 2\sqrt{2}\alpha_m\sigma_l\phi_0^l - \alpha_m^2\sigma_l^2\psi_m^2}{2\alpha_m\sigma_l^2}$$
$$\text{and } Y = \frac{\alpha_m\sigma_l\phi + (\sqrt{2} - j(2k+1)\sigma_l - \alpha_m\psi_m\sigma_l)}{\sqrt{2\alpha_m\sigma_l^2}}$$

$$f_o g_{p_m} g_{p_n} p_L(A,B) = \sqrt{\frac{G_m G_n \pi}{2(\alpha_m+\alpha_n)}}\, \{\exp[X]\,\mathrm{erf}[Y]\}\Big|_A^B \tag{C.13}$$
$$\text{where } X = \frac{(\sqrt{2} + (\alpha_m\psi_m + \alpha_n\psi_n)\sigma_l)^2 - 2\sqrt{2}(\alpha_m+\alpha_n)\sigma_l\phi_0^l}{2(\alpha_m+\alpha_n)\sigma_l^2}$$
$$- \frac{(\alpha_m^2\psi_m^2 + \alpha_n^2\psi_n^2 + \alpha_m\alpha_n(\psi_m^2+\psi_n^2))\sigma_l^2}{2(\alpha_m+\alpha_n)\sigma_l^2}$$
$$\text{and } Y = \frac{(\alpha_m+\alpha_n)\sigma_l\phi - (\sqrt{2} + (\alpha_m\psi_m + \alpha_n\psi_n)\sigma_l)}{\sqrt{2(\alpha_m+\alpha_n)\sigma_l^2}}$$

$$f_c g_{p_m} g_{p_n} p_L(A,B) = \sqrt{\frac{G_m G_n \pi}{2(\alpha_m+\alpha_n)}}\, \Re\{\exp[X]\,\mathrm{erf}[Y]\}\Big|_A^B \tag{C.14}$$
$$\text{where } X = \frac{(\sqrt{2} + j2k\sigma_l + (\alpha_m\psi_m + \alpha_n\psi_n)\sigma_l)^2 - 2\sqrt{2}(\alpha_m+\alpha_n)\sigma_l\phi_0^l}{2(\alpha_m+\alpha_n)\sigma_l^2}$$
$$- \frac{(\alpha_m^2\psi_m^2 + \alpha_n^2\psi_n^2 + \alpha_m\alpha_n(\psi_m^2+\psi_n^2))\sigma_l^2}{2(\alpha_m+\alpha_n)\sigma_l^2}$$
$$\text{and } Y = \frac{(\alpha_m+\alpha_n)\sigma_l\phi - (\sqrt{2} + j2k\sigma_l + (\alpha_m\psi_m + \alpha_n\psi_n)\sigma_l)}{\sqrt{2(\alpha_m+\alpha_n)\sigma_l^2}}$$

$$f_s g_{p_m} g_{p_n} p_L(A,B) = \sqrt{\frac{G_m G_n \pi}{2(\alpha_m+\alpha_n)}}\, \Im\{\exp[X]\,\mathrm{erf}[Y]\}\Big|_A^B \tag{C.15}$$
$$\text{where } X = \frac{(\sqrt{2} + j(2k+1)\sigma_l + (\alpha_m\psi_m + \alpha_n\psi_n)\sigma_l)^2}{2(\alpha_m+\alpha_n)\sigma_l^2}$$
$$- \frac{2\sqrt{2}(\alpha_m+\alpha_n)\sigma_l\phi_0^l - (\alpha_m^2\psi_m^2 + \alpha_n^2\psi_n^2 + \alpha_m\alpha_n(\psi_m^2+\psi_n^2))\sigma_l^2}{2(\alpha_m+\alpha_n)\sigma_l^2}$$
$$\text{and } Y = \frac{(\alpha_m+\alpha_n)\sigma_l\phi - (\sqrt{2} + j(2k+1)\sigma_l + (\alpha_m\psi_m + \alpha_n\psi_n)\sigma_l)}{\sqrt{2(\alpha_m+\alpha_n)\sigma_l^2}}$$

$$f_o g_{p_m} g_{p_n} p_R(A,B) = \sqrt{\frac{G_m G_n \pi}{2(\alpha_m+\alpha_n)}}\ \{\exp[X]\ \mathrm{erf}[Y]\}\Big|_A^B \tag{C.16}$$
$$\text{where } X = \frac{(\sqrt{2}-(\alpha_m\psi_m+\alpha_n\psi_n)\sigma_l)^2}{2(\alpha_m+\alpha_n)\sigma_l^2} + \frac{2\sqrt{2}(\alpha_m+\alpha_n)\sigma_l\phi_0^l - (\alpha_m^2\psi_m^2+\alpha_n^2\psi_n^2+\alpha_m\alpha_n(\psi_m^2+\psi_n^2))\sigma_l^2}{2(\alpha_m+\alpha_n)\sigma_l^2}$$
$$\text{and } Y = \frac{(\alpha_m+\alpha_n)\sigma_l\phi + (\sqrt{2}-(\alpha_m\psi_m+\alpha_n\psi_n)\sigma_l)}{\sqrt{2(\alpha_m+\alpha_n)\sigma_l^2}}$$

$$f_c g_{p_m} g_{p_n} p_R(A,B) = \sqrt{\frac{G_m G_n \pi}{2(\alpha_m+\alpha_n)}}\ \Re\{\exp[X]\ \mathrm{erf}[Y]\}\Big|_A^B \tag{C.17}$$
$$\text{where } X = \frac{(\sqrt{2}-j2k\sigma_l-(\alpha_m\psi_m+\alpha_n\psi_n)\sigma_l)^2}{2(\alpha_m+\alpha_n)\sigma_l^2} + \frac{2\sqrt{2}(\alpha_m+\alpha_n)\sigma_l\phi_0^l - (\alpha_m^2\psi_m^2+\alpha_n^2\psi_n^2+\alpha_m\alpha_n(\psi_m^2+\psi_n^2))\sigma_l^2}{2(\alpha_m+\alpha_n)\sigma_l^2}$$
$$\text{and } Y = \frac{(\alpha_m+\alpha_n)\sigma_l\phi + (\sqrt{2}-j2k\sigma_l-(\alpha_m\psi_m+\alpha_n\psi_n)\sigma_l)}{\sqrt{2(\alpha_m+\alpha_n)\sigma_l^2}}$$

$$f_s g_{p_m} g_{p_n} p_R(A,B) = \sqrt{\frac{G_m G_n \pi}{2(\alpha_m+\alpha_n)}}\ \Im\{\exp[X]\ \mathrm{erf}[Y]\}\Big|_A^B \tag{C.18}$$
$$\text{where } X = \frac{(\sqrt{2}-j(2k+1)\sigma_l-(\alpha_m\psi_m+\alpha_n\psi_n)\sigma_l)^2}{2(\alpha_m+\alpha_n)\sigma_l^2} + \frac{2\sqrt{2}(\alpha_m+\alpha_n)\sigma_l\phi_0^l - (\alpha_m^2\psi_m^2+\alpha_n^2\psi_n^2+\alpha_m\alpha_n(\psi_m^2+\psi_n^2))\sigma_l^2}{2(\alpha_m+\alpha_n)\sigma_l^2}$$
$$\text{and } Y = \frac{(\alpha_m+\alpha_n)\sigma_l\phi + (\sqrt{2}-j(2k+1)\sigma_l-(\alpha_m\psi_m+\alpha_n\psi_n)\sigma_l)}{\sqrt{2(\alpha_m+\alpha_n)\sigma_l^2}}$$

$$f_o g_{c_m} g_{p_n} p_L(A,B) = \sqrt{\frac{G_n \beta \pi}{\alpha_n}}\ \{\exp[X]\ \mathrm{erf}[Y]\}\Big|_A^B \tag{C.19}$$
$$\text{where } X = \frac{(\sqrt{2}+\alpha_n\psi_n\sigma_l)^2 - 2\sqrt{2}\alpha_n\sigma_l\phi_0^l - \alpha_n^2\sigma_l^2\psi_n^2}{2\alpha_n\sigma_l^2}$$
$$\text{and } Y = \frac{\alpha_n\sigma_l\phi - (\sqrt{2}+\alpha_n\psi_n\sigma_l)}{\sqrt{2\alpha_n\sigma_l^2}}$$

$$f_c g_{c_m} g_{p_n} p_L(A,B) = \sqrt{\frac{G_n \beta \pi}{\alpha_n}}\, \Re\{\, \exp[X]\, \mathrm{erf}[Y]\,\}\Big|_A^B \tag{C.20}$$
$$\text{where } X = \frac{(\sqrt{2} + j2k\sigma_l + \alpha_n \psi_n \sigma_l)^2 - 2\sqrt{2}\alpha_n \sigma_l \phi_0^l - \alpha_n^2 \sigma_l^2 \psi_n^2}{2\alpha_n \sigma_l^2}$$
$$\text{and } Y = \frac{\alpha_n \sigma_l \phi - (\sqrt{2} + j2k\sigma_l + \alpha_n \psi_n \sigma_l)}{\sqrt{2\alpha_n \sigma_l^2}}$$

$$f_s g_{c_m} g_{p_n} p_L(A,B) = \sqrt{\frac{G_n \beta \pi}{\alpha_n}}\, \Im\{\, \exp[X]\, \mathrm{erf}[Y]\,\}\Big|_A^B \tag{C.21}$$
$$\text{where } X = \frac{(\sqrt{2} + j(2k+1)\sigma_l + \alpha_n \psi_n \sigma_l)^2 - 2\sqrt{2}\alpha_n \sigma_l \phi_0^l - \alpha_n^2 \sigma_l^2 \psi_n^2}{2\alpha_n \sigma_l^2}$$
$$\text{and } Y = \frac{\alpha_n \sigma_l \phi - (\sqrt{2} + j(2k+1)\sigma_l + \alpha_n \psi_n \sigma_l)}{\sqrt{2\alpha_n \sigma_l^2}}$$

$$f_o g_{c_m} g_{p_n} p_R(A,B) = \sqrt{\frac{G_n \beta \pi}{\alpha_n}}\, \{\, \exp[X]\, \mathrm{erf}[Y]\,\}\Big|_A^B \tag{C.22}$$
$$\text{where } X = \frac{(\sqrt{2} - \alpha_n \psi_n \sigma_l)^2 + 2\sqrt{2}\alpha_n \sigma_l \phi_0^l - \alpha_n^2 \sigma_l^2 \psi_n^2}{2\alpha_n \sigma_l^2}$$
$$\text{and } Y = \frac{\alpha_n \sigma_l \phi + (\sqrt{2} - \alpha_n \psi_n \sigma_l)}{\sqrt{2\alpha_n \sigma_l^2}}$$

$$f_c g_{c_m} g_{p_n} p_R(A,B) = \sqrt{\frac{G_n \beta \pi}{\alpha_n}}\, \Re\{\, \exp[X]\, \mathrm{erf}[Y]\,\}\Big|_A^B \tag{C.23}$$
$$\text{where } X = \frac{(\sqrt{2} - j2k\sigma_l - \alpha_n \psi_n \sigma_l)^2 + 2\sqrt{2}\alpha_n \sigma_l \phi_0^l - \alpha_n^2 \sigma_l^2 \psi_n^2}{2\alpha_n \sigma_l^2}$$
$$\text{and } Y = \frac{\alpha_n \sigma_l \phi + (\sqrt{2} - j2k\sigma_l - \alpha_n \psi_n \sigma_l)}{\sqrt{2\alpha_n \sigma_l^2}}$$
$$f_s g_{c_m} g_{p_n} p_R(A,B) = \sqrt{\frac{G_n \beta \pi}{\alpha_n}}\, \Im\{\, \exp[X]\, \mathrm{erf}[Y]\,\}\Big|_A^B \tag{C.24}$$
$$\text{where } X = \frac{(\sqrt{2} - j(2k+1)\sigma_l - \alpha_n \psi_n \sigma_l)^2 + 2\sqrt{2}\alpha_n \sigma_l \phi_0^l - \alpha_n^2 \sigma_l^2 \psi_n^2}{2\alpha_n \sigma_l^2}$$
$$\text{and } Y = \frac{\alpha_n \sigma_l \phi + (\sqrt{2} - j(2k+1)\sigma_l - \alpha_n \psi_n \sigma_l)}{\sqrt{2\alpha_n \sigma_l^2}}$$

APPENDIX D

Derivation of Equations (5.37)-(5.40)

In this appendix, we derive the analytical expressions of (5.37)-(5.40) for computing $\Xi^l(\mathbf{\Theta}_m)$.

$$g_{p_m} g_{p_m} p_L(A,B) = \sqrt{\frac{G_m^2 \pi}{2\alpha_m}} \left\{ \exp[X] \, \mathrm{erf}[Y] \right\} \Big|_A^B \tag{D.1}$$

$$\text{where } X = \frac{(\sqrt{2} + 2\alpha_m \psi_m \sigma_l)^2 - 4\sqrt{2}\alpha_m \sigma_l \phi_0^l - 4\alpha_m^2 \sigma_l^2 \psi_m^2}{4\alpha_m \sigma_l^2}$$

$$\text{and } Y = \frac{2\alpha_m \sigma_l \phi - (\sqrt{2} + 2\alpha_m \psi_m \sigma_l)}{\sqrt{4\alpha_m \sigma_l^2}}$$

$$g_{p_m} g_{p_m} p_R(A,B) = \sqrt{\frac{G_m^2 \pi}{2\alpha_m}} \left\{ \exp[X] \, \mathrm{erf}[Y] \right\} \Big|_A^B \tag{D.2}$$

$$\text{where } X = \frac{(\sqrt{2} - 2\alpha_m \psi_m \sigma_l)^2 + 4\sqrt{2}\alpha_m \sigma_l \phi_0^l - 4\alpha_m^2 \sigma_l^2 \psi_m^2}{4\alpha_m \sigma_l^2}$$

$$\text{and } Y = \frac{2\alpha_m \sigma_l \phi + (\sqrt{2} - 2\alpha_m \psi_m \sigma_l)}{\sqrt{4\alpha_m \sigma_l^2}}$$

$$g_{c_m} g_{c_m} p_L(A,B) = \beta(\frac{\sigma_l}{\sqrt{2}}) e^{\frac{\sqrt{2}(\phi - \phi_0^l)}{\sigma_l}} \Big|_A^B \tag{D.3}$$

$$g_{c_m} g_{c_m} p_R(A,B) = -\beta(\frac{\sigma_l}{\sqrt{2}}) e^{-\frac{\sqrt{2}(\phi - \phi_0^l)}{\sigma_l}} \Big|_A^B \tag{D.4}$$

APPENDIX E

Derivation of (6.28)

In this appendix, we compute the covariance matrix of the received signal given in 6.28. Since $\mathbf{Y} = \mathbf{H}\ \mathrm{dvec}(\mathbf{C} - \tilde{\mathbf{C}})$, the covariance matrix can be computed as:

$$\begin{aligned}\mathbf{C}_{\mathbf{Y}} &= \mathbb{E}\big\{\mathbf{H}\ \mathrm{dvec}(\mathbf{C} - \tilde{\mathbf{C}})\ \mathrm{dvec}^H(\mathbf{C} - \tilde{\mathbf{C}})\mathbf{H}^H\big\} \\ &= \mathbb{E}\left\{\begin{bmatrix} \boldsymbol{y}_1 \\ \vdots \\ \boldsymbol{y}_P \end{bmatrix}\begin{bmatrix} \boldsymbol{y}_1^H & \cdots & \boldsymbol{y}_P^H \end{bmatrix}\right\} \end{aligned} \tag{E.1}$$

where

$$\begin{aligned}\boldsymbol{y}_p &= \mathrm{col}\Big\{\boldsymbol{y}_p^1, \boldsymbol{y}_p^2, \cdots, \boldsymbol{y}_p^{M_r}\Big\} \\ \boldsymbol{y}_p^j &= \mathbf{H}_p^j\ \mathrm{vec}(\mathbf{C}_p - \tilde{\mathbf{C}}_p).\end{aligned} \tag{E.2}$$

In the above equation, we have that

$$\begin{aligned}\mathbb{E}\Big\{\boldsymbol{y}_i^m(\boldsymbol{y}_j^n)^H\Big\} &= \mathbb{E}\Big\{\mathbf{H}_i^m\ \mathrm{vec}(\mathbf{C}_p - \tilde{\mathbf{C}}_p)\ \mathrm{vec}^H(\mathbf{C}_p - \tilde{\mathbf{C}}_p)(\mathbf{H}_j^n)^H\Big\} \\ &= \mathbb{E}\left\{\begin{bmatrix} \mathbf{c}_p^T(0)\big(\mathbf{H}_i^m(0)\big)^T \\ \vdots \\ \mathbf{c}_p^T(N_c-1)\big(\mathbf{H}_i^m(N_c-1)\big)^T \end{bmatrix}\Big[\big(\mathbf{H}_j^n(0)\big)^*\mathbf{c}_p^*(0), \right. \\ &\qquad \left. \cdots, \big(\mathbf{H}_j^n(N_c-1)\big)^*\mathbf{c}_p^*(N_c-1)\Big]\right\}.\end{aligned} \tag{E.3}$$

In (E.3), $\mathbb{E}\Big\{\big(\mathbf{H}_i^m(u)\big)^T\big(\mathbf{H}_j^n(s)\big)^*\Big\}$ can be computed as follows:

$$\mathbb{E}\Big\{\big(\mathbf{H}_i^m(u)\big)^T\big(\mathbf{H}_j^n(s)\big)^*\Big\} = \sum_{l=0}^{L-1} e^{-j2\pi(u-s)\Delta f(\tau_{l,i}-\tau_{l,j})}\mathbb{E}\Big\{\big(\mathbf{h}_i^m(l)\big)^T\big(\mathbf{h}_j^n(l)\big)^*\Big\}. \tag{E.4}$$

By replacing (E.4) in (E.3), we get (E.5) as

$$\mathbb{E}\Big\{\boldsymbol{y}_i^m(\boldsymbol{y}_j^n)^H\Big\} = \sum_{l=0}^{L-1}\mathbb{E}\left\{\begin{bmatrix} \mathbf{c}_p^T(0)\big(\mathbf{h}_i^m(l)\big)^T \\ \vdots \\ \omega^{(N_c-1)\tau_{l,i}}\mathbf{c}_p^T(N_c-1)\big(\mathbf{h}_i^m(l)\big)^T \end{bmatrix}\right.$$
$$\left.\big[\big(\mathbf{h}_j^n(l)\big)^*\mathbf{c}_p^*(0),\cdots,\big(\mathbf{h}_j^n(l)\big)^*\mathbf{c}_p^*(N_c-1)\omega^{-(N_c-1)\tau_{l,i}}\big]\right\}$$
$$= \sum_{l=0}^{L-1}\boldsymbol{\Omega}^{\tau_{l,i}}(\mathbf{C}_i-\tilde{\mathbf{C}}_i)^T\,\mathbb{E}\Big\{\big(\mathbf{h}_i^m(l)\big)^T\big(\mathbf{h}_j^n(l)\big)^*\Big\}\,(\mathbf{C}_j-\tilde{\mathbf{C}}_j)^*(\boldsymbol{\Omega}^{\tau_{l,j}})^* \qquad \text{(E.5)}$$

where $\boldsymbol{\Omega}$ is defined in (6.29).